

# The North American Cordilleran Anatectic Belt

1  
2  
3  
4  
5  
6  
7  
8  
9  
10  
11  
12  
13  
14  
15  
16  
17  
18  
19  
20  
21  
22  
23

James B. Chapman<sup>1</sup>, Simone E. Runyon<sup>1</sup>, Jessie Shields<sup>1</sup>, Brandi L. Lawler<sup>1</sup>, Cody J. Pridmore<sup>1</sup>,  
Shane H. Scoggin<sup>1</sup>, Nathan T. Swaim<sup>1</sup>, Adam E. Trzinski<sup>1</sup>, Hannah N. Wiley<sup>1</sup>, Andrew P.  
Barth<sup>2</sup>, Gordon B. Haxel<sup>3</sup>

<sup>1</sup>University of Wyoming, Department of Geology and Geophysics, Laramie, WY 82071

<sup>2</sup>Indiana University–Purdue University Indianapolis, Department of Earth Sciences, Indianapolis,  
IN 46202

<sup>3</sup>Northern Arizona University, School of Earth and Sustainability, Division of Geosciences,  
Flagstaff, AZ 86011

## **Abstract**

The North American Cordilleran Anatectic Belt (CAB) is a ~3,000 km long region in the hinterland of the Cordillera that comprises numerous exposures of Late Cretaceous to Eocene intrusive rocks and anatectic rocks associated with crustal melting. As such, it is comparable in size and volume to major anatectic provinces including the Himalayan leucogranite belt. The CAB rocks are chiefly peraluminous, muscovite-bearing leucogranite produced primarily by anatexis of Proterozoic to Archean metasedimentary rocks. The CAB rocks lack extrusive equivalents and were typically emplaced as thick sheets, laccoliths, and dike/sill complexes. The extent, location, and age of the CAB suggests that it is integral to understanding the tectonic

---

This is the author's manuscript of the article published in final edited form as:

Chapman, J. B., Runyon, S. E., Shields, J. E., Lawler, B. L., Pridmore, C. J., Scoggin, S. H., Swaim, N. T., Trzinski, A. E., Wiley, H. N., Barth, A. P., & Haxel, G. B. (2021). The North American Cordilleran Anatectic Belt. *Earth-Science Reviews*, 215, 103576. <https://doi.org/10.1016/j.earscirev.2021.103576>

24 evolution of North America, however, the belt is rarely considered as a whole. This paper  
25 reviews localities associated with crustal melting in the CAB and compiles geochemical,  
26 geochronologic, and isotopic data to evaluate the melt conditions and processes that generated  
27 these rocks. The geochemistry and partial melting temperatures (ca. 675-775 °C) support water-  
28 absent muscovite dehydration melting and/or water-deficient melting as the primary melt  
29 reactions and are generally inconsistent with water-excess melting and high-temperature (biotite  
30 to amphibole) dehydration melting. The CAB rocks are oldest in the central U.S. Cordillera and  
31 become younger towards both the north and south. At any single location, partial melting  
32 appears to have been a protracted process ( $\geq 10$  Myr) and evidence for re-melting and  
33 remobilization of magmas is common. End-member hypotheses for the origin of the CAB  
34 include decompression, crustal thickening, fluid-flux melting, and increased heat flux from the  
35 mantle. Different parts of the CAB support different hypotheses and no single model may be  
36 able to explain the entirety of the anatectic event. Regardless, the CAB is a distinct component  
37 of the Cordilleran orogenic system.

38

39 **Keywords:** two-mica granite, peraluminous, crustal melting, anatexis, metamorphic core  
40 complex, decompression, fluid-flux, leucogranite, orogenic plateau, magmatism

41

## 42 **1. Introduction**

43 The North American Cordillera is an archetypal Cordilleran (ocean-continent subduction)  
44 orogenic system and has been the foundation for many tectonic and geodynamic concepts  
45 (Burchfiel and Davis, 1975; DeCelles, 2004; Dickinson, 2004; Yonkee and Weil, 2015; Fritz-  
46 Díaz et al., 2018). One of the fundamental components of the North American Cordillera is a

47 belt of Mesozoic to Cenozoic, peraluminous, muscovite-bearing granite (*sensu lato*) exposures in  
48 the orogenic hinterland, stretching from southern British Columbia, Canada to northern Sonora,  
49 Mexico (Miller and Bradfish, 1980; Miller and Barton, 1990) (Fig. 1). These rocks are located  
50 landward, or cratonward, of the Mesozoic Cordilleran coastal batholiths (e.g., the Sierra Nevada,  
51 Coast Mountains, and Peninsular Ranges batholiths) and are colloquially called the belt of two-  
52 mica (biotite + muscovite) granites. The belt of peraluminous, muscovite-bearing granite is  
53 generally considered to have formed by crustal melting (anatexis) (Miller and Bradfish, 1980;  
54 Lee et al., 1981; Farmer and DePaolo, 1983; Haxel et al., 1984; Miller and Barton, 1990; Patiño-  
55 Douce et al., 1990; Wright and Wooden, 1991). However, detailed experimental and field  
56 studies suggest that a variety of processes could have created these peraluminous compositions  
57 and mineral assemblages, including crustal anatexis, fractional crystallization, crustal  
58 assimilation, hydrothermal alteration, high-pressure differentiation, and localized melting of  
59 country rock during the emplacement of mantle-derived magmas (see review in Patiño-Douce,  
60 1999 and Clarke, 2019). Likewise, depending on the source rock, crustal melting may not  
61 always produce strongly peraluminous compositions (see review in Gao et al., 2016).

62         The primary goal of this review is to update the classic compilation of Miller and  
63 Bradfish (1980) and to distinguish igneous bodies and suites related to crustal melting from  
64 peraluminous, muscovite-bearing rocks generated by other processes. Crustal melting is defined  
65 here as *partial melting of pre-existing crustal rocks that does not directly involve the formation,*  
66 *crystallization, and differentiation of mantle-derived mafic magmas* (cf., Clemens, 2020). We  
67 refer to these rocks as the North American Cordilleran Anatectic Belt (CAB). Anatectic belts are  
68 generally associated with continental collisional orogens including the Himalayan (e.g., Kohn,  
69 2014; Weinberg, 2016), Grenville (Rivers et al., 2002), and Alpine orogens (Burri et al., 2005).

70 The CAB is one of the best examples of an anatectic province related to Cordilleran-style  
71 orogenesis and may provide an analog for deep crustal processes in other Cordilleran orogenic  
72 systems. With an along-strike length of ~3,000 km, the scale of the CAB rivals or exceeds the  
73 size of major continental collision-related anatectic belts, making it one of the largest anatectic  
74 provinces globally, regardless of tectonic setting (Fig. 2). Thinking about this belt in terms of  
75 process (crustal anatexis) rather than composition (aluminosity) or mineralogy (presence of  
76 muscovite) yields insight into the tectonic and thermal evolution of the North American  
77 Cordillera (Miller and Gans, 1989; Hodges and Walker, 1992; Foster et al., 2001; Vanderhaeghe  
78 and Teysier, 2001; Whitney et al., 2004; Wells and Hoisch, 2008; Bendick and Baldwin, 2009;  
79 Gervais and Brown, 2011; Konstantinou and Miller, 2015).

80 First, we describe how CAB rocks produced by crustal melting are distinguished from  
81 granitic bodies produced by other processes with an emphasis on locations previously included in  
82 the compilation by Miller and Bradfish (1980). Next, we document locations of crustal melting in  
83 the CAB and compile geologic, geochronologic, geochemical, and isotopic data for each  
84 occurrence. This information is summarized and the shared characteristics and commonalities  
85 among the CAB rocks are presented. Then, melt conditions and processes are evaluated, including  
86 water-absent dehydration melting, water-deficient melting, and water-excess (fluid-flux) melting.  
87 Finally, we evaluate the various tectonic mechanisms that have been proposed to have caused  
88 crustal melting.

89

## 90 **2. Geologic Setting**

91 The North American Cordillera was constructed as a result of prolonged eastward  
92 subduction of the oceanic Farallon and Kula plates beneath the North American plate during

93 Triassic to Eocene time and the accretion of various terranes during this interval of time  
94 (Dickinson, 2006). This paper focuses on the Cordillera between 53° N and 29° N, which is the  
95 range of latitudes where the CAB is exposed. The orogenic system comprises several key  
96 fundamental tectonic components including a retroarc thrust belt, orogenic hinterland, and a  
97 continental arc (Fig. 1).

98

### 99 ***2.1. The retroarc and orogenic interior***

100 The thin-skinned Sevier retroarc thrust belt extends from northernmost Canada to the  
101 Mojave region of southeast California (Fig. 1) and was active during the Early Cretaceous to  
102 Paleogene (Yonkee and Weil., 2015). The thrust belt records up to 350 km of horizontal  
103 shortening (DeCelles and Coogan, 2006) and precursor thrust belts like the Luning-Fencemaker,  
104 Central Nevada, and Eastern Sierra thrust belts accommodated another ~100 km of shortening  
105 during early Mesozoic time (Wyld, 2002). To the east (cratonward) of the Sevier thrust belt is  
106 the Laramide foreland belt that was most active from 80 to 40 Ma and temporally overlaps with  
107 the end of Sevier deformation (Copeland et al., 2017). The Laramide foreland belt is  
108 characterized by thick-skinned, basement-involved deformation with limited horizontal  
109 shortening (<50 km) (Yonkee and Weil, 2015).

110 Pre-Sevier, Sevier, and Laramide-related shortening thickened the crust in the orogenic  
111 hinterland and created a high-elevation plateau, called the Nevadaplano in the central U.S.  
112 Cordillera (DeCelles, 2004) and the Arizonaplano in the southern U.S. and northern Mexican  
113 Cordillera (Chapman et al., 2020). Maximum crustal thickness estimates range from 50 to 65 km  
114 in the U.S. and Mexican Cordillera (Coney and Harms, 1984; Chapman et al., 2015; 2020) and  
115 may have been as high as 80 km in southeastern British Columbia (Hinchey and Carr, 2006).

116 Exposures of recumbently folded and stacked nappes in metamorphic core complexes like the  
117 Ruby-East Humboldt Mountains suggest that upper crustal shortening was balanced by middle to  
118 lower crustal shortening and thickening (McGrew et al., 2000).

119         The regions of thickest crust in the orogenic hinterland during the Cretaceous to early  
120 Paleogene are thought to roughly coincide with the current position of the Cordilleran  
121 metamorphic core complexes (Coney and Harms, 1984), which were most active from 60 Ma to  
122 10 Ma (Bendick and Baldwin, 2009; Konstantinou and Miller, 2015; Gottardi et al., 2020).  
123 There is also a close spatial correlation between the CAB and the Cordilleran metamorphic core  
124 complexes (Fig. 1). We adopt the terminology of Whitney et al. (2013) who divided the  
125 Cordilleran core complexes into northern, central, and southern belts. The northern belt  
126 encompasses core complexes from the Shuswap complex (British Columbia, Canada) to the  
127 Pioneer Mountains (Idaho, USA). The central belt extends from the Raft River-Albion-Grouse  
128 Creek complex (Utah-Idaho, USA) to the Black Mountains (California, USA). The southern belt  
129 stretches from the Sacramento Mountains (California, USA) to Sierra Mazatán (Sonora,  
130 Mexico). We use the same geographic divisions when referring to the northern, central, and  
131 southern CAB hereafter.

132

## 133 ***2.2. Cordilleran magmatism***

134         The North American Cordillera has a rich magmatic history related to subduction and  
135 extension that overlaps with the CAB in both time and space. The North American Cordilleran  
136 continental arc is chiefly preserved as the belt of giant Mesozoic Cordilleran coastal batholiths  
137 including the Peninsular Ranges, Sierra Nevada, Idaho, and Coast Mountains batholiths located  
138 west of the CAB (Fig. 1). However, magmatism extended into the orogenic interior, particularly

139 during the Jurassic, and some Jurassic igneous rocks were originally included in the belt of  
140 muscovite-bearing granite of Miller and Bradfish (1980). In southern British Columbia, the  
141 Jurassic Kootenay arc overlaps spatially with the CAB and includes units such as the Kuskanax  
142 and Nelson suites that range in composition from diorite to peraluminous two-mica  $\pm$  garnet  
143 granite (Armstrong, 1988; Ghosh, 1995). In the Great Basin region, Jurassic igneous rocks  
144 located in a hinterland/back-arc position spatially overlap with the CAB and range in  
145 composition from gabbro to peraluminous, two-mica granite (e.g., Dawley Canyon granite;  
146 Kistler et al., 1981; Barton et al., 2011). Subsequent to Miller and Bradfish's (1980) study of  
147 muscovite-bearing granite, petrologic and isotopic studies indicated that Jurassic to Early  
148 Cretaceous magmatism that spatially overlaps with the CAB was chiefly produced from  
149 subduction-related (mantle-involved) melting and overwhelmingly tends to be metaluminous or  
150 weakly peraluminous (Farmer and DePaolo, 1983; Miller and Barton, 1990; Wright and Wooden  
151 1991; Brandon and Smith, 1994). Strongly peraluminous, Jurassic-age rocks, like the Dawley  
152 Canyon granite, may be related to localized crustal melting associated with the intrusion of mafic  
153 magmas at depth (Jones, 1999). In the eastern Great Basin, Jurassic magmatism has also been  
154 linked to mantle upwelling during back-arc extension (Elison, 1995; Miller and Hoisch, 1995;  
155 Miller and Barton, 1990) as well as a slab break-off event (Dickinson, 2006). We do not include  
156 any Jurassic or older rocks in the CAB.

157

### 158 *2.2.1. Laramide magmatism*

159 Subduction-related, calc-alkaline, metaluminous magmatism ended in the Mesozoic  
160 coastal batholiths during the Late Cretaceous (Chen and Moore, 1982; Silver and Chappell,  
161 1988; Gehrels et al., 2009; Gaschnig et al., 2010; Cecil et al., 2012). In the U.S. and Mexican

162 Cordillera, subduction-related magmatism then migrated eastward, sometimes referred to as the  
163 “magmatic sweep,” as the subduction angle shallowed during the Laramide Orogeny (Coney and  
164 Reynolds, 1977; Constenius et al., 2003; Yonkee and Weil, 2015; Fitz-Díaz et al., 2018). This  
165 eastward sweep was most pronounced to the north and south of the central U.S. Cordillera - the  
166 Great Basin region today. The central U.S. Cordillera contains only scattered evidence for  
167 magmatic activity during the Laramide Orogeny and has been referred to as a magmatic gap that  
168 is associated with low-angle subduction (Dickinson and Snyder, 1978). We refer to igneous  
169 rocks produced during this eastward sweep of magmatism as “Laramide magmatism” or the  
170 “Laramide arc,” as it is referred to in the southern U.S. and northern Mexican Cordillera (Lang  
171 and Titley, 1998; González-León et al., 2011; Leveille and Stegen, 2012; Seedorf et al., 2019).  
172 Laramide magmatism is compositionally distinct from rocks in the CAB and is generally  
173 characterized as calc-alkaline, quartz-poor to intermediate, metaluminous, containing biotite +  
174 hornblende ± clinopyroxene, and is more isotopically juvenile than rocks associated with the  
175 CAB (Barton, 1990; 1996). The eastward migration of subduction-related, Laramide magmatism  
176 reached or passed through the future position of the CAB during the Late Cretaceous to early  
177 Paleogene. Magmatism associated with the Laramide magmatic sweep is generally older than  
178 anatectic intrusive rocks in the CAB, but in some cases the two igneous suites overlap both  
179 spatially and temporally (e.g., Wright and Haxel, 1982; Miller and Barton, 1990).

180

### 181 *2.2.2. Mid-Cenozoic ignimbrite flare-up*

182         Soon after Laramide magmatism reached its most eastward extent during the Laramide  
183 orogeny, magmatism rapidly swept back westward toward the trench, producing the mid-  
184 Cenozoic (*née* mid-Tertiary) ignimbrite flare-up and several large-volume volcanic eruptive



185 centers (Ferrari et al., 2002; Best et al., 2009). The mid-Cenozoic ignimbrite flare-up is related  
186 to the foundering or rapid roll-back of the previously shallowly-dipping Farallon plate  
187 (Humphreys et al., 2003). The majority of mid-Cenozoic flare-up magmatism has been  
188 interpreted to have originated by melting of hydrated mantle lithosphere to produce mafic  
189 magmas that then experienced various degrees of fractional crystallization and assimilation  
190 within the crust to produce a range of compositions (basaltic to rhyolitic) (Farmer et al., 2008;  
191 Henry and John, 2013). In some locations, intrusion of mantle-derived mafic magmas into the  
192 crust locally caused crustal melting and produced magmas with similar geochemical and isotopic  
193 compositions to the CAB rocks (e.g., Watts et al., 2016). In the northern and central U.S.  
194 Cordillera, the mid-Cenozoic flare-up migrated southward while in the southern U.S. and  
195 Mexican Cordillera, the flare-up migrated west-northwestward (Armstrong and Ward, 1991;  
196 Humphreys, 1995). The oldest flare-up related rocks in the Canadian and northern U.S.  
197 Cordillera are the Eocene Kamloops-Challis-Absaroka volcanics (Moye et al., 1988;  
198 Breitsprecher et al., 2003) and the oldest related rocks in the southern U.S. and Mexican  
199 Cordillera are the Eocene volcanic rocks in the Big Bend National Park region in Texas, USA  
200 (Barker, 1987; Parker et al., 2012). Igneous rocks related to the mid-Cenozoic ignimbrite flare-  
201 up (including intrusive rocks) are generally younger than rocks in the CAB (Konstantinou and  
202 Miller, 2015). There is a close temporal association between the migration or passage of the  
203 ignimbrite flare-up and the onset of extension in the Cordilleran metamorphic core complexes  
204 (Gans, 1989; Best and Christiansen, 1991). Closely following the mid-Cenozoic ignimbrite  
205 flare-up, widespread magmatism associated with lithospheric extension commenced and  
206 continues to the present in the Basin and Range province (Best and Brimhall, 1974;  
207 Hawkesworth et al., 1995).

208

### 209 **3. Examples of peraluminous, muscovite-bearing rocks not produced by crustal melting**

210 In our review of North American Cordilleran magmatism, we identified many examples  
211 of Mesozoic to Cenozoic peraluminous, muscovite-bearing granites that were produced by  
212 processes other than crustal melting, including fractional crystallization, crustal assimilation,  
213 hydrothermal alteration, and localized crustal melting associated with mantle-derived mafic  
214 intrusions. Below, we provide a few examples with an emphasis on locations previously  
215 included in the compilation by Miller and Bradfish (1980).

216

#### 217 ***3.1. Fractional Crystallization and Crustal Assimilation***

218 Fractional crystallization of pyroxene or subaluminous amphibole (aluminum saturation  
219 index [ASI] =  $\sim 0.5$ ) can lead to peraluminous compositions during magmatic differentiation  
220 (Cawthorn and Brown, 1976; Zen, 1986). Throughout this contribution, we use ASI = molecular  
221  $\text{Al}_2\text{O}_3 / [\text{CaO} - (3.33 * \text{P}_2\text{O}_5) + \text{Na}_2\text{O} + \text{K}_2\text{O}]$  (Frost et al., 2001). Assimilation of aluminous  
222 sedimentary country rock during differentiation may also result in peraluminous compositions  
223 (Barbarin, 1996). In both cases, the simplest way to recognize these processes is to examine  
224 whether or not the felsic peraluminous rocks in question are part of a co-magmatic suite that  
225 ranges in composition and exhibits chemical or isotopic evidence for fractional crystallization or  
226 assimilation (e.g., decreasing  $\epsilon\text{Nd}_i$  with increasing  $\text{SiO}_2$ ) (DePaolo, 1981).

227 An example of peraluminous granite created by fractional crystallization is the Late  
228 Cretaceous (ca. 90 Ma) Chemehuevi Mountains plutonic suite in California, USA, which is part  
229 of the Chemehuevi metamorphic core complex (John, 1988; John and Mukasa, 1990). The  
230 Chemehuevi Mountains plutonic suite has evolved Pb and Sr isotopic values, similar to nearby

231 Proterozoic-age crust, and is compositionally and temporally zoned with older, metaluminous to  
232 weakly peraluminous biotite granodiorite on the margins and younger, peraluminous two-mica  $\pm$   
233 garnet granite in the center, forming a “bullseye” map pattern (John and Wooden, 1990) (Fig. 3).  
234 The occurrence of cogenetic magmas of variable composition as well as the nested geometry  
235 suggest that the strongly peraluminous granite differentiated from a more mafic, metaluminous  
236 magma and the evolved isotopic compositions suggest that the magma assimilated significant  
237 amounts of Proterozoic crust (John, 1988; John and Wooden, 1990). In contrast, igneous suites  
238 in the CAB generally have a comparatively limited compositional range, usually lacking  
239 intermediate to low SiO<sub>2</sub> and metaluminous members (Fig. 3). The Chemehuevi Mountains  
240 plutonic suite and similarly aged suites nearby have been interpreted to be part of the Cordilleran  
241 (Laramide) arc and to have formed by (mantle-derived) mafic magma influx, hybridization, and  
242 partial remelting of the lower crust (Miller and Wooden, 1994; Economos et al., 2010).

243

### 244 ***3.2. Hydrothermal Alteration***

245 Hydrothermal alteration can also influence the apparent peraluminosity of an intrusive  
246 rock unit (Luth et al., 1964; Miller et al., 1981; Zen, 1988; Clarke et al., 2005). There are many  
247 different forms of hydrothermal alteration, broadly categorized by the elements gained in  
248 comparison to the original protolith composition (e.g., Seedorff et al., 2005; 2008). Greisen  
249 alteration and coarse muscovite alteration are characterized by the dominant hydrothermal  
250 mineral assemblage muscovite-quartz  $\pm$  albite  $\pm$  K-feldspar with or without additional accessory  
251 minerals. Coarse muscovite alteration is commonly formed during fluid exsolution from a  
252 metaluminous intrusion and results in a relative increase in Al and Rb and relative decrease in Ca  
253 and Sr as muscovite  $\pm$  end-member albite replaces plagioclase (Runyon et al., 2019). As a result,

254 peraluminosity for coarse muscovite altered rocks is commonly higher than the original igneous  
255 composition (Fig. 4). Another form of hydrothermal alteration that may affect peraluminosity is  
256 hydrolytic (acidic) alteration, which strips cations from the host rock. In hydrolytic alteration,  
257 feldspar is commonly altered to fine-grained muscovite (sericite) or clay and original mafic  
258 minerals may be altered to chlorite with or without accessory minerals. In these cases, cations  
259 like Na, Ca, and K are more easily mobilized into the fluid than Al, resulting in an apparent  
260 increase in peraluminosity (Fig. 4). These two examples are among the more well-known types  
261 of hydrothermal alteration that could increase peraluminosity, however, there are many factors  
262 including fluid composition, intensity of alteration, host rock composition, and  
263 pressure/temperature conditions that will all influence the apparent changes in peraluminosity  
264 during hydrothermal alteration of a given rock.

265         In coarse muscovite alteration, muscovite is commonly found as dispersed, euhedral  
266 booklets, replaces igneous minerals (e.g., biotite, feldspars, amphibole), and occurs in veins, and  
267 fractures, and small “vugs” or open space that can develop in areas of pervasive wall-rock  
268 replacement (Runyon et al., 2019). Hydrothermal versus magmatic muscovite can be  
269 distinguished both chemically (e.g., Ti content) and texturally (Miller et al., 1981).  
270 Hydrothermally altered rocks may also be hyperaluminous, with an aluminum saturation index  
271 (ASI) > 1.3 (Clarke, 2019) and have very high Rb/Sr ratios – with values significantly higher  
272 than unaltered anatectic rocks (Fig. 4).

273         Many of the muscovite-bearing granite locations originally documented in Miller and  
274 Bradfish (1980) have been hydrothermally altered (e.g., Barton, 1987). An example of  
275 hydrothermal alteration creating an apparently strongly peraluminous, muscovite granite is the  
276 Texas Canyon stock in the Little Dragoon Mountains, Arizona (Cooper and Silver, 1964).

277 Unaltered samples of the Texas Canyon stock are commonly biotite  $\pm$  muscovite quartz  
278 monzonite in composition and metaluminous to weakly peraluminous. Coarse muscovite  
279 alteration is strongly developed within the Texas Canyon quartz monzonite, ranging from  
280 incomplete replacement of biotite by hydrothermal muscovite to pervasive wall-rock  
281 replacement by muscovite-albite-K-feldspar  $\pm$  fluorite mineral assemblages (Runyon et al.,  
282 2019). The alteration is well-developed over large areal extents (Cooper and Silver, 1964) and  
283 samples of the coarse muscovite altered Texas Canyon quartz monzonite have a significantly  
284 higher ASI than unaltered samples (Fig. 4).

285

### 286 ***3.3. Localized Melting from Mantle-Derived Intrusions***

287 Another way to create peraluminous granite is to locally melt the crust by underplating or  
288 intrusion of mantle-derived (basaltic) magmas (Barbarin, 1996). The majority of Phanerozoic  
289 granite suites in the North American Cordillera are hybrids with both mantle and crustal inputs,  
290 however, added heat or exsolved fluids from basaltic rocks can generate crustal melts with little  
291 to no geochemical or isotopic mantle signature (Patiño-Douce, 1999; Annen et al., 2006). As a  
292 result, peraluminous granite generated in this fashion is particularly difficult to distinguish from  
293 instances of crustal melting that does not involve the intrusion of mantle-derived mafic magmas.  
294 Recognition of a mantle-derived, basaltic precursor is mainly achieved through thermal  
295 arguments (e.g., a regional heating event) or by exposure of the basaltic intrusions themselves  
296 (including as mafic enclaves) and/or igneous rocks derived from these intrusions (e.g., Ireteba  
297 pluton, Eldorado Mountains, Nevada; Kapp et al., 2002).

298 An example of this process to create peraluminous granite comes from the Raft River-  
299 Albion-Grouse Creek metamorphic core complex. When examined in isolation, the 32-25 Ma

300 Cassia plutonic complex in the Albion Range and northern Grouse Creek Mountains is a good  
301 candidate for a crust-derived magma. The Cassia plutonic complex is 1) silica rich (> 70 wt. %  
302 SiO<sub>2</sub>), 2) peraluminous (ASI=1.0-1.2), 3) isotopically very evolved ( $\epsilon\text{Nd}_i < -25$ ;  $^{87}\text{Sr}/^{86}\text{Sr}_i >$   
303 0.71), 4) was emplaced into amphibolite-grade metamorphic rocks during or close to peak  
304 pressure-temperature conditions (4 kbar, 650°C), and 5) is syn-kinematic with early core  
305 complex extension (Egger et al., 2003; Strickland et al., 2011; Konstantinou et al., 2013).  
306 However, emplacement of the Cassia plutonic complex was immediately preceded by the  
307 intrusion of the 42-31 Ma Emigrant Pass plutonic complex, which ranges from mafic to felsic  
308 compositions (55-75 wt. % SiO<sub>2</sub>), is more isotopically primitive, and ranges from metaluminous  
309 to peraluminous compositions (Egger et al., 2003; Strickland et al., 2011; Konstantinou et al.,  
310 2013). In addition, both the Emigrant Pass and Cassia plutonic complexes have mantle-like,  
311 autocrystic (not inherited) zircon  $\delta^{18}\text{O}$  compositions (Strickland et al., 2011). Added heat from  
312 the mantle-derived Emigrant Pass magmatic event has been interpreted to have locally melted  
313 the crust to produce the Cassia plutonic suite (Strickland et al., 2011; Konstantinou et al., 2013).  
314 Rocks of the Cassia plutonic complex were included in the belt of muscovite-bearing granite of  
315 Miller and Bradfish (1980) but are excluded from our compilation of rocks in the CAB.

316 In the compilation and summary of CAB rocks presented below, locations that involved  
317 mantle-derived magmas were excluded. We omitted locations that contain cogenetic igneous  
318 rocks interpreted as primitive magmas or products of assimilation and/or fractional  
319 crystallization from primitive magmas. This distinction follows previous classification schemes  
320 that suggest only peraluminous leucogranite represents crustal melts with no mantle-input and  
321 that all other granitic rocks are crust-mantle hybrids, including the Cordilleran coastal batholiths  
322 (Collins, 1996; Patiño-Douce, 1999; Annen et al., 2006; Kemp et al., 2007). Alternative models

323 for producing metaluminous granite of intermediate composition (representative of the  
324 Cordilleran coastal batholiths) by crustal anatexis include restite unmixing (Chappell et al., 1987)  
325 and peritectic assemblage entrainment (Clemens and Stevens, 2012).

326

#### 327 **4. The North American Cordilleran Anatectic Belt**

328         The CAB includes most of the anatectic rocks in the Omineca Crystalline Belt in  
329 southern British Columbia, Canada (Monger et al., 1982; Parrish et al., 1988; Nelson et al.,  
330 2013), the “Late Cretaceous-Cenozoic plutonic suite” of Wright and Wooden (1991) and “S-type  
331 subzone” of Solomon and Taylor (1989) in the eastern Great Basin region of the United States,  
332 the “strongly peraluminous suite” of “Cordilleran Interior plutonism” of Miller and Barton  
333 (1990) in the U.S. Cordillera, the “compositionally restricted granites” of Haxel et al. (1984) in  
334 southern Arizona, U.S.A., and the “Aconchi granitic suite” in Mexico (Grijalva-Noriega and  
335 Roldan-Quintana, 1998). In the following section, we list and briefly describe all main  
336 exposures of anatectic rocks that collectively form the CAB. A summary of this information is  
337 presented in Table 1. We acknowledge that there are likely additional locations we are unaware  
338 of that were unintentionally omitted from the compilation. Following the descriptions, some of  
339 the shared characteristics of the CAB rocks are discussed.

340

#### 341 ***4.1. The Northern Belt***

##### 342 ***4.1.1. The Shuswap Complex***

343         The Shuswap is the largest Cordilleran metamorphic core complex and contains several  
344 migmatite-cored gneiss domes that are often treated as core complexes individually, including  
345 the Matton, Frenchman’s Cap, Thor-Odin, Valhalla, Okanagan, and Grand Forks-Kettle

346 complexes (Vanderhaege et al., 1999) (Fig. 1). Peraluminous granites interpreted as anatectic  
347 melts are found throughout the Shuswap complex as leucosome in migmatite and as numerous  
348 intrusive bodies (plutons, dikes, sills, laccoliths, and veins). Among the more well-known  
349 intrusive bodies are the large, sheet-like Ladybird, Airy, and Adams River leucogranites, which  
350 have been interpreted to be derived from partial melting in migmatite (Sevigny and Parrish,  
351 1993; Hinchey and Carr, 2006). The ages of Shuswap migmatite and leucogranite range from 61  
352 to 49 Ma and exhibit a wide range of ages ( $\geq 10$  Myr) in most individual locations (Vanderhaege  
353 et al., 1999; Hinchey et al., 2006; Gordon et al., 2008; Kruckenberg et al., 2008; Cubley et al.,  
354 2013). Metamorphic rocks and migmatite in the Shuswap complex record prograde  
355 metamorphism from ca. 85 to 55 Ma, with peak pressure and temperature conditions of 8-12  
356 kbar and 700-850 °C ca. 60 to 55 Ma (see review in Bendick and Baldwin, 2009), coincident  
357 with or slightly older than the age of crustal melting.

358

#### 359 *4.1.2. Mid-Cretaceous Kootenay Arc*

360 Partly overlapping and east of the Shuswap metamorphic core complex is the Kootenay  
361 arc, which contains a suite of mid-Cretaceous (117-95 Ma; Leclair et al., 1993) intrusions that  
362 have been associated with crustal melting (Brandon and Lambert, 1993; 1994; Brandon and  
363 Smith, 1994) and were included in the belt of muscovite-bearing granite of Miller and Bradfish  
364 (1980). These rocks include the White Creek, Fry Creek, Horsethief Creek, Battle Range,  
365 Bugaboo, and Bayonne batholiths (Fig. 1). The batholiths are typically zoned or nested and  
366 contain a wide range of compositions (60-78 wt. % SiO<sub>2</sub>) from metaluminous quartz  
367 monzodiorite to biotite-hornblende granodiorite to strongly peraluminous two-mica granite  
368 (Brandon and Lambert, 1993; 1994; Brandon and Smith, 1994). Whole rock  $\delta^{18}\text{O}$  (7.1-11.2 ‰)



369 increases and radiogenic isotope ratios become more evolved (-5 to -20  $\epsilon$ Nd; 0.707-0.74  
370  $^{87}\text{Sr}/^{86}\text{Sr}$ ) with increasing differentiation of the magmatic suite with the most evolved values  
371 represented by the two-mica granite (Brandon and Lambert, 1993; 1994; Brandon and Smith,  
372 1994). These compositional trends are consistent with crustal contamination of a basaltic  
373 precursor during differentiation. However, Brandon and Lambert (1994) note that there are no  
374 nearby exposures of basalt, that low Cr and Ni contents and weak negative Eu anomalies are  
375 inconsistent with fractional crystallization of plagioclase from a basaltic source, and that the  
376 more mafic mid-Cretaceous igneous rock compositions are similar to experimental melt  
377 compositions of amphibolite (Rapp et al., 1991; Beard and Lofgren, 1991). The mid-Cretaceous  
378 Kootenay arc rocks were interpreted to form by dehydration melting as a zone of anatexis  
379 migrated upward through the crust; initially melting Proterozoic amphibolite to tonalitic gneiss to  
380 produce the quartz monzodiorite and biotite-amphibole granodiorite and then melting  
381 Proterozoic metapelites to produce the two-mica granite (Brandon and Lambert, 1993; 1994;  
382 Brandon and Smith, 1994). The mid-Cretaceous suite was emplaced at 2-4 kbar and postdates  
383 Early Cretaceous (144-134 Ma) regional Barrovian metamorphism that records peak pressures  
384 and temperatures of 6-7 kbar and 650-700 °C (Moynihan and Pattison, 2013; Webster et al.,  
385 2017). The mid-Cretaceous Kootenay arc is significantly older (20-80 Myr) than the rest of the  
386 CAB (Table 1) and crustal melting has been associated with accretion events on the plate margin  
387 specific to this longitude (ca. 50 °N) that may not be relevant to other parts of the CAB (Monger  
388 et al., 1982; Brandon and Lambert, 1993; 1994).

389

#### 390 *4.1.3. Priest River-Clearwater Complexes*

391 Prograde metamorphism occurred from ca. 75 to 64 Ma in the Priest River metamorphic

392 core complex, with peak pressure and temperature conditions of 10 kbar and 790 °C, followed by  
393 nearly isothermal decompression ca. 60-57 Ma (Stevens et al., 2015) (Fig. 1). Migmatite  
394 exposures are estimated to contain 25-45% leucosome and are classified as metatexite (Stevens  
395 et al., 2016). Crustal anatexis, via dehydration melting, occurred during both prograde  
396 metamorphism and decompression with a majority of melt crystallization occurring ca. 54-44 Ma  
397 (Stevens et al., 2015). Intrusive rocks in the Priest River complex are generally Late Cretaceous  
398 or Eocene in age. The Late Cretaceous intrusive rocks (e.g., Spokane granite) partly precede  
399 prograde metamorphism, span a range of compositions including two-mica granite, and have  
400 radiogenic isotopic compositions that may require the involvement of a mantle-derived juvenile  
401 component (Whitehouse et al., 1992), which suggests that they are not crustal melts and are not  
402 included in the CAB. The Eocene intrusive rocks (e.g., Silver Point, Wrencoë, Rathdrum  
403 plutons) overlap in age (50-45 Ma) with leucosome in migmatite and include biotite-hornblende-  
404 bearing and biotite-bearing granite (Miller et al., 1975; Stevens et al., 2016) that have been  
405 interpreted to be crustal melts of Proterozoic basement (metapelite to orthogneiss) based on their  
406 highly evolved isotopic composition (zircon  $\epsilon\text{Hf}_i = -22$  to  $-27$ ;  $\epsilon\text{Nd}_i = -19$  to  $-21$ ; Whitehouse et  
407 al., 1992; Stevens et al., 2016) and are included in the CAB. Eocene magmatism also occurs  
408 outside (in the hanging wall) of the complex including the peraluminous two-mica granite in the  
409 Loon Lake batholith that has been attributed to crustal melting (Asmerom et al., 1988).

410         The Clearwater metamorphic core complex experienced peak metamorphism at 8-11 kbar  
411 and 650-750 °C during ca. 64-56 Ma, followed by the onset of decompression at ca. 59 Ma  
412 (Doughty and Chamberlain, 2007). Migmatite is absent, but intrusion of muscovite-bearing  
413 granite (e.g., Roundtop, Beaver Creek, Bungalow plutons) during the early Eocene (ca. 50-45  
414 Ma) may record crustal melting at depth (Marvin et al., 1984; Foster et al., 2007). Undated

415 pegmatitic two-mica leucogranite dikes and sills also intrude and cross-cut Proterozoic  
416 metasedimentary units (Guevara, 2012).

417

#### 418 *4.1.4. The Idaho Batholith & Bitterroot Complex*

419 Unlike the other large Mesozoic coastal arc batholiths, the Idaho batholith was emplaced  
420 entirely into Proterozoic basement and is dominated by peraluminous granite including the 83-67  
421 Ma peraluminous Atlanta suite in the Atlanta lobe and the 66-53 Ma (mostly 55-53 Ma; e.g.,  
422 Bear Creek and Paradise plutons) peraluminous Bitterroot suite in the Bitterroot lobe (Hyndman,  
423 1983; Johnson et al., 1988; Foster et al., 2007; Gaschnig et al., 2010) (Fig. 1). Whether the  
424 peraluminous suites represent crustal melts or extensive crustal assimilation has been a topic of  
425 debate for the last half-century (see review in Gaschnig et al., 2011). Emplacement of both  
426 peraluminous suites was immediately preceded by cogenetic metaluminous arc magmatism and  
427 the batholith generally exhibits increasingly evolved radiogenic isotopes through time (Gaschnig  
428 et al., 2011). These patterns, along with the presence of mafic igneous rocks that overlap in age  
429 with the Bitterroot suite (Hyndman and Foster, 1988) and mantle-like zircon  $\delta^{18}\text{O}$  (King and  
430 Valley, 2001), support models linking the formation of the Idaho batholith to injection of mantle-  
431 derived magmas that eventually led to melting of continental crust. However, the highly evolved  
432 isotopic compositions and limited compositional range of the peraluminous suites suggest that if  
433 mantle-derived magmas were involved in petrogenesis of the suites, they likely provided heat  
434 and not mass input (Gaschnig et al., 2011). Gaschnig et al. (2011) interpreted the Atlanta  
435 peraluminous suite to have formed by dehydration melting of greywacke or biotite-bearing  
436 granitic rocks and the Bitterroot suite to have formed by dehydration melting of orthogneiss,  
437 both at relatively high pressure.

438           The Bitterroot peraluminous suite is located within the Bitterroot metamorphic core  
439 complex and has been interpreted in terms of core complex formation as well as part of the  
440 Cordilleran coastal batholith system. The region experienced crustal thickening and prograde  
441 metamorphism during the Sevier-Laramide orogeny (80-50 Ma) and the intrusion of the  
442 Bitterroot peraluminous suite (“main phase” plutons) as a series of thick (3-4 km) sills and  
443 laccoliths has been interpreted to be related to anatexis of Proterozoic basement gneisses (Foster  
444 et al., 2001; 2010). Migmatite is locally exposed in the Bitterroot metamorphic core complex  
445 and records anatectic melting (leucosome and pegmatite intrusions) at ~53 Ma and peak  
446 metamorphic pressures and temperatures of 7-8 kbar and 650-750 °C, resulting in muscovite  
447 breakdown (Foster et al., 2001).

448

#### 449 *4.1.5. Anaconda-Pioneer Complexes*

450           The Anaconda metamorphic core complex shares many similarities with the Priest River,  
451 Clearwater, and Bitterroot complexes and they are linked by the dextral Lewis and Clark fault  
452 zone (Foster et al., 2007) (Fig. 1). The footwall of the Anaconda complex exposes recumbently  
453 folded nappes that record deformation and metamorphism related to crustal thickening during the  
454 Late Cretaceous (80-75 Ma) with peak pressures and temperatures of 4-6 kbar and 600-700 °C  
455 (Grice, 2006; Haney, 2008). Eocene plutons and abundant pegmatite and aplite dikes and sills  
456 intrude Proterozoic host rocks, which are locally migmatitic (Foster et al., 2007). The Eocene  
457 (53-50 Ma) intrusive rocks include the Hearst Lake pluton, a peraluminous, two-mica  
458 leucogranite (Wallace et al., 1992; Foster et al., 2007).

459           The footwall of the Pioneer metamorphic core complex locally contains migmatite and is  
460 pervasively intruded by leucogranite dikes and sills with crystallization ages of 52-46 Ma, which

461 overlap in age with the Pioneer Intrusive Suite (50-48 Ma) (Silverberg, 1990; Vogl et al., 2012).

462

## 463 **4.2. The Central Belt**

### 464 *4.2.1. Ruby-East Humboldt Core Complex*

465 Fold nappes exposed in the core of the Ruby-East Humboldt metamorphic core complex  
466 and thrust faults in nearby mountain ranges record crustal thickening and prograde  
467 metamorphism, starting during the mid-Cretaceous (ca. 100-95 Ma) and peaking during the Late  
468 Cretaceous (ca. 85-80 Ma) (Camilleri and Chamberlain, 1997; McGrew et al., 2000; Hallet and  
469 Spear, 2015) (Fig. 1). Metamorphic rocks indicate that the complex experienced decompression  
470 from ca. 85-55 Ma, although the amount of decompression (1-6 kbar) varies and there is little to  
471 no upper crustal or basinal record of this event (Hodges et al., 1992; McGrew et al., 2000; Henry  
472 et al., 2011; Hallet and Spear, 2014; 2015). Some authors have related decompression to vertical  
473 ductile thinning (Hallet and Spear, 2014; Long and Kohn, 2020). Migmatite is exposed at deep  
474 structural levels in the complex (Howard, 1980) and partial melting in these migmatites has been  
475 linked to pervasive intrusion of leucogranite at higher structural levels during the Late  
476 Cretaceous (Lee et al., 2003; Premo et al., 2008). Late Cretaceous pegmatitic leucogranite is the  
477 dominant intrusive component of the Ruby-East Humboldt complex and forms an injection  
478 complex of innumerable dikes and sills (Howard et al., 2011). The pegmatitic leucogranite has  
479 been interpreted to have formed by muscovite dehydration melting of Proterozoic metapelite and  
480 to be related to crustal anatexis during both prograde metamorphism and decompression (Wright  
481 and Snoke, 1993; McGrew et al., 2000; Lee et al., 2003; Howard et al., 2011; Hallet and Spear,  
482 2014; 2015). A younger population (46-29 Ma) of leucogranite bodies is also present in the  
483 Ruby-East Humboldt complex and overlaps in age with a compositionally expanded suite of

484 igneous rocks (e.g., Harrison Pass pluton) ranging from gabbro to two-mica granite that involve  
485 a mantle-derived component (Barnes et al., 2001; Lee et al., 2003; Howard et al., 2011). These  
486 younger rocks are volumetrically less significant and geochemically and isotopically distinct  
487 from the Late Cretaceous pegmatitic granite (Barnes et al., 2001; Lee et al., 2003). Howard et al.  
488 (2011) suggested that mafic underplating during the younger phase of magmatism (Eocene-  
489 Oligocene) provided heat  $\pm$  fluids that resulted in additional crustal melting and re-melting and  
490 remobilization of the Late Cretaceous pegmatitic granite. Regionally, Eocene-Oligocene  
491 magmatism is related to the mid-Cenozoic ignimbrite flare-up and rollback of the Farallon slab  
492 (Humphreys, 1995; Konstantinou and Miller, 2015) and is not included in the CAB.

493 East of the Ruby-East Humboldt complex, Late Cretaceous two-mica  $\pm$  garnet  
494 leucogranite, pegmatite, and aplite dikes interpreted to have formed by crustal melting are  
495 present in the Wood Hills, Pequop Mountains, and Toano Range (Lee and Marvin, 1981; Miller  
496 et al., 1990; Camilleri and Chamberlain, 1997; Milliard et al., 2015). The 77-72 Ma Toano  
497 Springs pluton in the Toano Range marks the northeastern extent of Late Cretaceous crustal  
498 anatexis in the Great Basin as interpreted by Wright and Wooden (1991).

499

#### 500 *4.2.2. Snake Range-Kern Mountains-Deep Creek Range*

501 The Snake Range, Kern Mountains, and Deep Creek Range are part of a single  
502 metamorphic core complex/extensional fault system (Miller et al., 1999), herein referred to as the  
503 Snake Range complex (Fig. 1). No migmatite is exposed in the Snake Range complex, but the  
504 region experienced peak metamorphism during the Late Cretaceous (90-70 Ma) associated with  
505 the Sevier orogeny (Miller and Gans, 1989). Metamorphic rocks in the footwall record  
506 maximum pressures and temperatures of 6-8 kbar and 500-650 °C (Cooper et al., 2010). Late

507 Cretaceous (ca. 86-70 Ma), strongly peraluminous, two-mica granite (e.g., Lexington Creek, Pole  
508 Canyon-Can Young Canyon, Tungstonia plutons) in the Snake Range complex have been  
509 interpreted to be crustal melts formed by dehydration melting of Proterozoic metapelite (Lee et  
510 al. 1981, Lee et al., 1986; Farmer and DePaolo et al., 1983; Lee and Christiansen 1983; Wright  
511 and Wooden, 1991; Gottlieb, 2017). Eocene peraluminous, muscovite-bearing granite (e.g.,  
512 Young Canyon-Kious Basin plutons; ~37 Ma) is also present in the Snake Range complex (Lee  
513 and Christiansen 1983) and may have formed in a similar way to the Eocene peraluminous rocks  
514 in the Ruby-Humboldt Mountains (i.e., associated with the mid-Cenozoic ignimbrite flare-up).  
515 The Eocene intrusive rocks have more juvenile  $^{87}\text{Sr}/^{86}\text{Sr}$  ratios, are more oxidized, and have  
516 lower  $\delta^{18}\text{O}$  ratios compared to the strongly peraluminous Cretaceous intrusions (Lee and  
517 Christiansen 1983; King et al., 2004).

518         Swarms of pegmatitic leucogranite sills and dikes are common in the Snake Range  
519 complex as well as in neighboring ranges (e.g., Schell Creek Range) and may also be associated  
520 with crustal anatexis (Lee et al., 1981; Miller and Gans, 1989). Miller et al. (1999) reported an  
521 age of 82 Ma on a leucogranite dike in the Smith Creek region, Kern Mountains. Two-mica  
522 granite, potentially equivalent with the strongly peraluminous Cretaceous intrusions in the Snake  
523 Range, is also exposed in some surrounding ranges, including the ca. 84 Ma Troy Granite in the  
524 Grant Range (Fryxell, 1988; Lund et al., 2014) and the ca. 84 Ma McCullough Butte and Rocky  
525 Canyon plutons in the Fish Creek Range (Barton, 1987).

526

#### 527 *4.2.3. Central Great Basin Two-Mica Granite*

528         All the rocks in the central CAB described in the preceding sections (Sections 4.2.1 and  
529 4.2.2) occur east of the  $^{87}\text{Sr}/^{86}\text{Sr} = 0.708$  isopleth and east of the Roberts Mountain thrust, which

530 marks a suture zone separating accreted (para)allochthonous terranes to the west from North  
531 American cratonic basement to the east (Kistler and Peterman, 1973; Stewart, 1980). Small  
532 exposures of Late Cretaceous, peraluminous, two-mica granite occur throughout the Great Basin  
533 region west of the  $^{87}\text{Sr}/^{86}\text{Sr} = 0.708$  isopleth (Fig. 1). These granites are interpreted to have a  
534 significant sedimentary input and were included in previous compilations of strongly  
535 peraluminous rocks (Miller and Bradfish, 1980; Barton, 1987; 1990; Miller and Barton, 1990;  
536 Barton and Trim, 1991). In Nevada, these granites include the Pipe Springs (80 Ma) and Round  
537 Mountain plutons (95 Ma) in the Toiyabe Range (Shawe et al., 1986), the Birch Creek pluton  
538 (89 Ma) in the Toiyabe Range (Stewart et al., 1977), and the New York Canyon and Rocky  
539 Canyon plutons (73-71 Ma) in the Humboldt and Stillwater Ranges (Johnson et al., 1977;  
540 McFarlane, 1981; Barton and Trim, 1991). In eastern California, these include the Birch Creek  
541 and Papoose Flat plutons (83-82 Ma) in the White and Inyo Mountains (Sylvester et al., 1978;  
542 Barton, 2000). Two-mica granite intrusions in the central Great Basin are generally considered  
543 to be satellites of the Sierra Nevada batholith and occur along with more common Late  
544 Cretaceous metaluminous intrusive rocks (Sylvester et al., 1978; McFarlane, 1981; Barton, 1987;  
545 2000; Brown et al., 2018). Besides slightly more juvenile radiogenic isotopic compositions  
546 (compared to the eastern Great Basin), these rocks have lower zircon  $\delta^{18}\text{O}$  ratios (King et al.,  
547 2004) and, where studied in detail, are associated with rare mafic dikes and enclaves (e.g.,  
548 Barton, 2000). Late Cretaceous, two-mica granite in the central Great Basin has been interpreted  
549 to be an evolved, high-pressure equivalent to more metaluminous, calc-alkaline continental arc  
550 rocks (Patiño-Douce, 1999) or related to increased mantle heat flow (e.g., basaltic underplating  
551 or intrusion, mantle upwelling; Barton, 1990). Wright and Wooden (1991) suggested that none  
552 of the Late Cretaceous two-mica granite located west of  $^{87}\text{Sr}/^{86}\text{Sr} = 0.708$  isopleth are crustal



553 melts and they are not included in the CAB here.

554

### 555 **4.3. The Southern Belt**

#### 556 *4.3.1. Death Valley area, California*

557           The Funeral Mountains metamorphic core complex contains migmatite that record Late  
558 Cretaceous prograde metamorphism and maximum pressures and temperatures of 7-9 kbar and  
559 600-700 °C during ca. 90-70 Ma (Hodges and Walker, 1990; Hoisch and Simpson, 1993;  
560 Mattinson et al., 2007) (Fig. 1). The migmatite is cut by Paleocene (64-62 Ma) two-mica  
561 leucogranite dikes and sills that were emplaced syn-kinematically and have been interpreted to  
562 have formed by water-excess to water-deficient melting of muscovite-bearing metasedimentary  
563 rocks (Mattinson et al., 2007).

564           Leucogranite dikes and pegmatite (59-55 Ma) are also present in the Black Mountains  
565 metamorphic core complex in the Badwater, Mormon Point, and Copper Canyon turtlebacks  
566 (antiformal footwall corrugations) (Miller and Friedman, 1999; Lima et al., 2018) and in the  
567 Panamint Mountains (Mahood et al., 1996). The ~72 Ma Hall Canyon pluton, a two-mica  
568 granodiorite, in the Panamint Mountains was interpreted by Mahood et al. (1996) to be a product  
569 of water-absent biotite dehydration melting.

570           Late Cretaceous muscovite-garnet granite is found south and west of Death Valley in the  
571 western Mojave Desert region and is interpreted to have formed in part by partial melting and  
572 assimilation of Pelona-Orocopia-Rand Schist, which was underplated in this area during  
573 Laramide low-angle subduction (Miller et al., 1996; 2000; Grove et al., 2003). Despite  
574 significant involvement of the Pelona-Orocopia-Rand Schist in the source region, these  
575 muscovite-garnet granites are still interpreted to be subduction-related and to have originated in

576 the upper mantle (Miller et al., 1996; Saleeby, 2003). They are considered distinct from the  
577 Cordilleran interior belt of muscovite-granite (Miller and Barton, 1990; Miller et al., 1996), and  
578 are not included in the CAB.

579

#### 580 *4.3.2. Colorado River Extensional Corridor*

581 The Colorado River extensional corridor extends from southern Nevada to the Phoenix,  
582 Arizona area and consists of a series of top-to-the-northeast metamorphic core complexes and  
583 extensional fault systems (Howard and John, 1987). Numerous magmatic rocks occur  
584 throughout this corridor that have been or could be interpreted as crustally-derived magmas. The  
585 Ireteba pluton (~66 Ma) in the Eldorado Mountains, Nevada is a two-mica  $\pm$  garnet granite that  
586 was included in the belt of muscovite-bearing granite of Miller and Bradfish (1980). However,  
587 the Ireteba granite shows extensive interaction with mafic magmas and has been interpreted to be  
588 related to injection of juvenile basaltic magmas causing melting of the crust (Kapp et al., 2002).

589 Late Cretaceous peraluminous granite in the Sacramento and Chemehuevi core  
590 complexes, California has been interpreted to be related to fractional crystallization and crustal  
591 assimilation of mantle-derived magmas as discussed in Section 3.1 (John and Wooden, 1980).  
592 Likewise, Late Cretaceous (~89 Ma) peraluminous granite in the Whipple Mountains  
593 metamorphic core complex has been interpreted to have formed in a subduction setting and  
594 involved a mantle input (Anderson and Cullers, 1990).

595 Late Cretaceous (75-70 Ma), strongly peraluminous two-mica granite in the Old Woman-  
596 Piute batholith, California (e.g., Sweetwater Wash, Lazy Daisy, Painted Rock plutons) has been  
597 interpreted to represent crustal melts with limited mantle input (Foster et al., 1989; Miller et al.,  
598 1990b; Miller and Wooden, 1994). The strongly-peraluminous plutons were emplaced along

599 with metaluminous rocks of the same age, show a spectrum of major element and isotopic  
600 compositions, and in some cases are nested within the metaluminous rocks, similar to the  
601 peraluminous granite in the Chemehuevi Mountains (John and Wooden, 1990; Miller et al.,  
602 1990). However, the peraluminous stocks in the Old Woman-Piute batholiths have been  
603 interpreted to reflect anatexis of a hybridized lower crustal source consisting of older basement  
604 rocks and mantle-derived Jurassic arc igneous rocks (Miller et al., 1990; Miller and Wooden,  
605 1994). The nearby Iron Mountains, California also contain Late Cretaceous (ca. 75-70 Ma)  
606 strongly peraluminous two-mica  $\pm$  garnet granite equivalent to the Old Woman-Piute batholith  
607 (Wells et al., 2002; Wells and Hoisch, 2008). The Iron Mountains intrusive suite and nearby  
608 Coxcomb intrusive suite comprise the Cadiz Valley batholith, which has been interpreted to be  
609 subduction-related (Howard, 2002; Economos et al., 2010).

610         Widespread exposures of two-mica  $\pm$  garnet leucogranite occur in the Buckskin-  
611 Rawhide, Harcuvar, Harquahala, and White Tank metamorphic core complexes, Arizona,  
612 including the Tank Pass granite (ca. 80-78 Ma; DeWitt and Reynolds, 1990; Bryant and  
613 Wooden, 2008), the Brown's Canyon granite (ca. 72 Ma; Richard et al., 1990; Isachsen et al.,  
614 1998), and the White Tank granite (ca. 72 Ma; Reynolds et al., 2002; Prior et al., 2016) which  
615 intruded primarily as large sills, but also form dense networks of smaller dikes and sills.  
616 Locally, areas of particularly voluminous intrusions have been referred to as migmatitic injection  
617 complexes (Bryant and Wooden, 2008), although evidence for *in situ* melting during the Late  
618 Cretaceous is not documented in Arizona. Bryant and Wooden (2008) report a ~110 Ma  
619 mylonitized, "migmatitic" gneiss in the Harcuvar Mountains, and Knapp and Heizler (1990)  
620 report a ~67 Ma partially mylonitized, "migmatitic" gneiss in the Mesquite Mountains, Arizona.  
621

622 4.3.3. *Southern Arizona*

623 Strongly peraluminous, two-mica  $\pm$  garnet leucogranite is exposed throughout southern  
624 Arizona, primarily within the footwalls of metamorphic core complexes. The Paleocene to  
625 Eocene (ca. 60-45 Ma) Wilderness Suite in the Catalina-Rincon metamorphic core complex was  
626 emplaced as series of thick ( $\leq 2$  km) sills and has been interpreted to have formed by crustal  
627 melting of Proterozoic Oracle granite (Keith, 1980; Farmer and DePaolo, 1984; Force, 1997;  
628 Fornash et al., 2013; Davis et al., 2019) or from other unexposed lithologies (Ketcham, 1996).  
629 Equivalent rocks (e.g., Fresno Canyon granite) are exposed in the Picacho and Tortolita  
630 Mountains core complexes as well (Banks, 1980; Spencer et al., 2003; Ferguson et al., 2003).  
631 The Wilderness suite was estimated to have been emplaced at 3-4 kbar and ca. 625-725 °C  
632 (Anderson et al., 1988).

633 The Pan Tak granite in the Coyote Mountains core complex and the Presumido Peak  
634 granite in the Pozo Verde Mountains core complex are both  $\sim 58$  Ma, two-mica  $\pm$  garnet  
635 leucogranites that have been interpreted to have formed by crustal anatexis of Proterozoic  
636 basement, potentially the Pinal schist (Wright and Haxel, 1982; Goodwin and Haxel, 1990).  
637 Haxel et al. (1984) report similar peraluminous granite in the Kupuk Hills, Sierra Blanca, and  
638 Comobabi core complexes. Apart from the southern Arizona metamorphic core complexes,  
639 peraluminous two-mica leucogranite occurrences include the Texas Canyon stock ( $\sim 55$  Ma),  
640 Senita Basin granite, and Artesa Mountains granite (Cooper and Silver, 1964; May and Haxel,  
641 1980; Shafiqullah et al., 1980; Haxel et al., 1984; Chapman et al., 2018). Arnold (1986)  
642 interpreted the Gunnery Range batholith and Texas Canyon stock (Fig. 1) to represent crustal  
643 melting of a deep granulitic source terrane, although the strongly peraluminous compositions of  
644 the Texas Canyon stock may be related to hydrothermal alteration as discussed in Section 3.2

645 (Runyon et al., 2019).

646

#### 647 *4.3.4. Northern Sonora*

648         The Aconchi suite in northern Sonora comprises Late Cretaceous to Paleogene two-mica  
649  $\pm$  garnet leucogranite that has been interpreted as crustal melts and has been mapped throughout  
650 the region, primarily within the footwalls of metamorphic core complexes, including in the  
651 Mesquital (59-51 Ma), Tubutama, Carnero (ca. 55 Ma), Tortuga, Guacomea (78 Ma),  
652 Magdalena, Madera, Aconchi (58-55 Ma), Puerta del Sol (68-59 Ma), and Mazatán (58 Ma)  
653 complexes (Anderson et al., 1980; Hayama et al., 1984; Nourse et al. 1994; Nourse, 1995;  
654 Grijalva-Noriega and Roldan-Quintana, 1998; González-León et al., 2011; González-Becuar et  
655 al., 2017; Mallery et al., 2018). Relatively little information is available on many of these  
656 localities, although the intrusions are often described as laterally extensive sills, laccoliths, small  
657 plutons, and networks of small dikes and sills. The largest exposure is the Aconchi-El Jaralito  
658 batholith located between the Mazatán and Aconchi complexes, which contains the Huépac (58-  
659 55 Ma) and El Babizo leucogranites (71 Ma) among others (Roldán-Quintana, 1991; González-  
660 León et al., 2011). Late Cretaceous to Paleocene (68-59 Ma) orthogneiss migmatite is reported  
661 from the Puerta del Sol complex and has been interpreted as the source for the El Pajarito (68  
662 Ma) garnet-bearing leucogranite (González-Becuar et al., 2017). The youngest leucogranite in  
663 the Puerta del Sol complex is the ~42 Ma El Oquimonis granite, a two-mica + garnet  
664 leucogranite (González-Becuar et al., 2017).

665

### 666 **5. Common Characteristics of the Cordilleran Anatectic Belt**

667         The most straightforward way to recognize igneous rocks produced by crustal anatexis is

668 to observe them in situ – leucosome in migmatite. Leucosome often represents the initial stages  
669 of crustal anatexis and has been interpreted to feed larger-scale intrusive bodies or represent  
670 crystal fractionation from these bodies (Solar and Brown, 2001; Johannes et al., 2003).  
671 Migmatite (of similar age to the CAB) is common in the northern CAB, but rare to absent in the  
672 central and southern CAB. In some locations, leucosomes have been shown to be the source for  
673 more voluminous CAB magmas (e.g., Ladybird Suite in the Shuswap complex; Hinchey and  
674 Carr, 2006). However, in most instances a direct relationship between migmatitic leucosomes  
675 and CAB magmas has not been demonstrated. Most exposures of migmatite associated with the  
676 CAB record mid-crustal (5-10 kbar), amphibolite facies conditions (Table 1). In rare cases,  
677 evidence is present suggesting that significant leucosome accumulation  $\pm$  melt extraction took  
678 place at these conditions (e.g., Priest River complex; Stevens et al., 2015; 2016). In the majority  
679 of locations, however, CAB igneous rocks were derived from deep structural levels not exposed  
680 at the surface.

681         The emplacement geometry of CAB igneous rocks varies greatly, but commonly forms  
682 dike and sill networks, injection complexes, or large sheets and laccoliths (e.g., Ruby-East  
683 Humboldt complex and Catalina-Rincon complex; Howard et al., 2011; Fornash et al., 2013).  
684 This is similar to the geometry of igneous bodies in other major anatectic provinces (e.g.,  
685 Manaslu laccolith in the Himalaya leucogranite belt, LeFort et al., 1987). Where CAB rocks are  
686 exposed as stocks or plutons, they are commonly pervasively intruded by late-phase pegmatite  
687 and aplite dikes that are generally interpreted to have been derived from closed-system  
688 crystallization of water-bearing felsic magmas (e.g., Coyote Mountains complex; Wright and  
689 Haxel, 1982). To our knowledge, there are no extrusive rocks equivalent to the intrusive rocks  
690 of the CAB. The inferred high water contents of the CAB melts likely caused them to reach their

691 solidus and freeze at moderate pressure (depth) during ascent (Miller, 1985; Clemens and Droop,  
692 1998), which may explain the lack of extrusive equivalents.

693

### 694 ***5.1. Geochemistry, Isotopic Composition, and Protoliths***

695 The CAB igneous rocks are silica-rich ( $\geq 70$  wt. % SiO<sub>2</sub>; Fig. 3; Table 1), consistent with  
696 experimentally produced melts from a wide range of crustal protoliths (e.g., greywacke, schist,  
697 gneiss; Patiño-Douce, 1999). The paucity of anatectic rocks of intermediate composition ( $< 70$   
698 wt. % SiO<sub>2</sub>) suggest that crustal melting of more mafic source rocks (e.g., basaltic amphibolite)  
699 is less common (Beard and Lofgren, 1991; Patiño-Douce and Beard, 1995; Rapp and Watson,  
700 1995; Gao et al., 2016). CAB rocks are usually identified in the field as leucogranite and are  
701 geochemically and mineralogically classified as granite or rarely, as trondhjemite (Fig. 5).

702 Potassium feldspar is common, but always significantly less abundant than plagioclase.

703 Compositions range from alkalic to calcic on modified alkali–lime index (MALI; Na<sub>2</sub>O + K<sub>2</sub>O –  
704 CaO) diagrams, consistent with global compilations of leucogranites (Frost et al., 2001). CAB  
705 rocks are weakly to moderately peraluminous (ASI = 1.0-1.3; Fig. 3; Table 1) and are corundum  
706 normative with modal minerals more aluminous than biotite, chiefly muscovite and garnet,  
707 characteristic of crustal melting of metasedimentary protoliths (Castro et al., 1999; Chappell et  
708 al., 2012). Biotite is generally more abundant than muscovite and cordierite is very rare, which  
709 is one of the reasons why the CAB rocks are not strictly classified as S-type granites (White et  
710 al., 1986; Chappell and White, 2001). Another difference between the CAB and classic S-type  
711 granites is that magnetite, rather than ilmenite, is the dominant opaque oxide in CAB rocks  
712 (White et al., 1986), which suggests that the CAB magmas may be more oxidized. Crustal melts  
713 originating from (meta)sedimentary protoliths containing small amounts of organic material tend

714 to be reduced ( $fO_2 < FMQ$ ) (Nabelek, 2019). However, there has been no comprehensive  
715 investigation of the oxidation state of CAB rocks. Peraluminous S-type granites as well as  
716 peraluminous, calc-alkaline Cordilleran (subduction-related) granite are enriched in FeO, MgO,  
717 and TiO<sub>2</sub> compared to CAB rocks (Patiño-Douce, 1999; Fig. 6). Despite their geochemical and  
718 mineralogical differences, CAB rocks have been informally referred to as S-type granites  
719 because the large majority have been interpreted to have formed from melting of  
720 metasedimentary protoliths (Miller and Bradfish, 1980; Patiño-Douce et al., 1990; Wright and  
721 Wooden, 1991). Additional geochemical data for CAB rocks is presented below in Section 6,  
722 focusing on melt processes.

723         The CAB rocks exhibit highly evolved radiogenic isotopic compositions (e.g., low  $\epsilon Nd_{(t)}$ ,  
724  $\epsilon Hf_{(t)}$ , high  $^{87}Sr/^{86}Sr_i$ ; Table 1) that reflect the composition and age of local basement rocks. In  
725 North America, the  $^{87}Sr/^{86}Sr_i = 0.706$  isopleth (“0.706 line”) is often interpreted to represent the  
726 western edge of autochthonous, North American crystalline basement (Kistler and Peterman,  
727 1973) and the CAB is almost everywhere located east (cratonward) of this isopleth (Fig. 1). For  
728 the Great Basin region, Wright and Wooden (1991) suggested that Mesozoic to Cenozoic crustal  
729 melting was limited to areas east of the  $^{87}Sr/^{86}Sr_i = 0.708$  isopleth and east of the  $\epsilon Nd_i = -7$   
730 isopleth (Farmer and DePaolo, 1983), although the relationship between these isopleths and the  
731 CAB is less clear to the north and south (Fig. 1). The CAB crosses multiple Archean to  
732 Proterozoic basement/lithospheric provinces including, from north to south, the Rae craton,  
733 Hearne craton, Medicine Hat block, Selway terrane, Grouse Creek block, Mojave province,  
734 Yavapai province, Mazatzal province, and Caborca block (Whitmeyer and Karlstrom, 2007; Fig.  
735 7).

736         CAB rocks generally have high  $\delta^{18}O$  ratios (2-5 ‰ above mantle array values) as



737 reflected in whole rock and single mineral (e.g., quartz, zircon) analyses (Table 1). The high  
738  $\delta^{18}\text{O}$  ratios have been interpreted to reflect crustal melting of metasedimentary rocks, rather than  
739 (meta)igneous rocks (Solomon and Taylor, 1989; King et al., 2004; Gottlieb, 2017). In the  
740 northern and central CAB, upper Proterozoic metasedimentary rocks are present as part of the  
741 Cordilleran passive margin sequence (Cordilleran Miogeocline) and are often cited as a possible  
742 protolith (e.g., Neoproterozoic McCoy Creek Group, Ruby-East Humboldt complex; Lee et al.,  
743 2003). Metasedimentary members of the Mesoproterozoic Belt-Purcell Supergroup and the  
744 overlying Neoproterozoic Windermere Supergroup have also been suggested as potential  
745 protoliths in the northern CAB (e.g., Shuswap complex; Norlander et al., 1992). The southern  
746 CAB does not contain metasedimentary rocks associated with the Mesoproterozoic basins or  
747 Neoproterozoic metasedimentary rocks associated the Cordilleran passive margin sequence  
748 (Stewart et al., 1984) (Fig. 7). Paleoproterozoic metasedimentary rocks in the Pinal Basin in  
749 southern Arizona and northern Sonora (Meijer., 2014; Bickford et al., 2019) have been proposed  
750 as a potential source for the southern CAB (e.g., Pinal Schist; Haxel et al., 1984). Proterozoic  
751 (meta)igneous rocks and Jurassic arc rocks in the southern CAB have also been mentioned as  
752 possible protoliths (Miller and Wooden, 1994; Fornash et al., 2013; Mallery et al., 2018).

753

## 754 ***5.2. Melt Temperature Estimates***

755 Zircon saturation temperatures were calculated using the calibration of Watson and  
756 Harrison (1983) for CAB rocks that meet the compositional criteria for this thermometer (Table  
757 1). The dataset indicates an average temperature of  $724 \pm 48$  °C ( $1\sigma$ ) (Fig. 8). The calibration of  
758 Watson and Harrison (1983) results in higher calculated zircon saturation temperatures than  
759 other recently revised calibrations (Boehnke et al., 2013; Gervasoni et al., 2016; Borisov and

760 Aranovich, 2019) and can be considered a maximum estimate. For intrusive rocks, zircon  
761 saturation temperature has been used as a proxy for the temperature of partial melting or magma  
762 temperature (e.g., Collins et al., 2016). Zircon saturation temperature is a dynamic variable that  
763 predicts when zircon saturation begins in a cooling magma and increases during crystallization  
764 (Clemens et al., 2020). Siegel et al. (2018) suggest that magma temperature and zircon  
765 saturation temperature are only approximately equal when SiO<sub>2</sub> contents increase to a certain  
766 value, which was determined to be 64-74 wt. % based on a limited dataset. For higher SiO<sub>2</sub>  
767 values, calculated zircon saturation temperatures may overestimate the magma temperature.  
768 Because CAB rocks have SiO<sub>2</sub> > 70 wt. %, we interpret the calculated zircon saturation  
769 temperatures to be close to or a slight overestimate of the partial melting temperature. In  
770 addition, almost all zircon U-Pb analyses of CAB rocks report inherited (antecrystic or  
771 xenocrystic) zircon components (Applegate et al., 1992; Wright and Snoke, 1993; Vanderhaege  
772 et al., 1999; Vogl et al., 2012; Gaschnig et al., 2013; Stevens et al., 2016; Davis et al., 2019).  
773 Intrusions with abundant inherited zircon indicate saturation at the source and suggest that  
774 calculated zircon saturation temperatures are a maximum since part of the bulk Zr concentration  
775 is from inherited crystals rather than the melt (Miller et al., 2003; Barth and Wooden, 2006).  
776 Our compilation of CAB rocks also contains some analyses of late-stage, highly fractionated  
777 melts (chiefly aplite and pegmatite dikes). Zircon saturation temperatures of these rocks can be  
778 interpreted as minimum estimates of magma temperature at the time of melt segregation (Miller  
779 et al., 2003).

780 Peak metamorphic temperature estimates from migmatite in the central and northern  
781 CAB are plotted in Figure 8 and show a broad maxima from 650-825 °C that overlaps with the  
782 average CAB zircon saturation temperature. For individual localities, zircon saturation

783 temperatures are consistently 50-100 °C lower than estimates of peak metamorphic temperatures  
784 obtained using equilibria thermobarometry or pseudosection analysis (Table 1). Kohn (2014)  
785 made a similar observation in his review of the Himalayan leucogranite belt.

786

### 787 *5.3. Age Relationships*

788 A compilation of crystallization or emplacement ages of rocks in the CAB are presented  
789 in Figure 9 and Table 1. Ages range from 92 to 42 Ma, with the majority of ages between 80 and  
790 50 Ma. Ages are youngest in the northern and southern CAB and oldest in the central CAB. The  
791 age pattern suggests that anatectic magmatism started in the central U.S. Cordillera and  
792 simultaneously migrated (or “swept”) northward and southward with crustal melting shutting  
793 down in its wake. Many locations in the CAB only have a few dated samples, but where  
794 sufficient geochronologic data are available, the duration of anatexis is typically protracted,  
795 lasting 10 Myr or more. Examples of well-studied locations with a wide range of ages include  
796 the Shuswap complex (60-50 Ma; Vanderhaege et al., 1999; Hinchey et al., 2006; Gordon et al.,  
797 2008; Kruckenberg et al., 2008), the Ruby-East Humboldt complex (70-40 Ma; Howard et al.,  
798 2011), and the Catalina-Rincon complex (65-45 Ma; Fornash et al., 2013; Davis et al., 2019).  
799 Similar observations have been made in the Himalayan leucogranite belt with anatectic  
800 magmatism lasting ~10 Myr in any single location (Lederer et al., 2013; Weinberg, 2016). The  
801 reasons for protracted anatexis in the CAB are unclear but may be related to fluid and/or magma  
802 pulses, magma mixing and age hybridization, slow fractionation and cooling, evolving  
803 metamorphic and thermal conditions, or combinations of these. Despite the uncertainty,  
804 prolonged remobilization and reworking of melts appears to have been a common feature of  
805 CAB intrusive rocks. Protracted periods of crustal melting imply that either the source region

806 was not completely melted (fusible components remain to be melted later) or that conditions  
807 changed throughout the melt process (e.g., increasing temperature) so that melting could  
808 proceed. Apart from the Kootenay arc (Brandon and Lambert, 1993; 1994; Brandon and Smith,  
809 1994) (e.g., White Creek batholith; Figs. 3 and 6), there is no geochemical evidence that more  
810 refractory minerals or restitic components were melted during later stages of crustal melting in  
811 the CAB.

812 Figure 9 also shows the timing for the onset of extension and the period of most rapid  
813 cooling for the Cordilleran metamorphic core complexes (see Supplementary File 1 for the data  
814 compilation). The period of most rapid cooling is generally constrained by thermochronological  
815 data and represented by the steepest segment of time-temperature cooling histories (Fig. 10).  
816 The onset of extension is constrained by thermochronological data as well as by other geologic  
817 data (e.g., timing of normal faulting, extensional basins, P-T-t modelling, etc.). The period of  
818 rapid cooling/exhumation occurred shortly after ( $\leq 5$  Myr) the onset of extension for most core  
819 complexes, except for the central belt of core complexes where it may have been delayed by up  
820 to ca. 30 Myr (Fig. 9). Extension and exhumation in these areas is thought to have occurred in  
821 two or more stages (Miller et al., 1999; Henry et al., 2011; Konstantinou et al., 2012). The  
822 younger stage is generally associated with extensional tectonics, whereas the older stage of  
823 extension has been related to gravitational collapse of tectonically thickened crust and/or heating,  
824 magmatism, and uplift accompanying delamination/roll-back of the Farallon slab (McGrew and  
825 Snee, 1994; Humphreys, 1995; Constenius, 1996; Dickinson et al., 2009; Konstantinou et al.,  
826 2013; Cassel et al., 2018). The timing of core complex extension and the age of CAB  
827 magmatism overlap in the northern CAB, however, extension/exhumation is up to 50 Myr  
828 younger than crustal melting in the central and southern CAB.

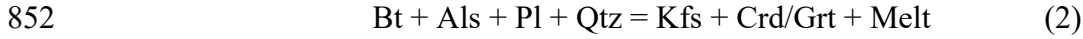
829

## 830 **6. Melting Conditions and Processes**

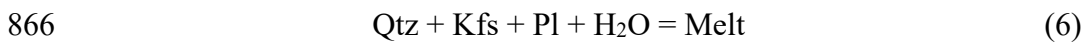
831         The following section explores melting conditions, processes, and sources using  
832 compiled geochemical compositions of the CAB rocks (Supplementary File 2). One of the  
833 fundamental questions we seek to address is the role of water in the production of the CAB. We  
834 refer to water regardless of its state (vapor or liquid) and use water as a more general term for  
835 mixed-fluid solutions (e.g., containing CO<sub>2</sub>). We distinguish three types of partial melting based  
836 on the amount of available water; water-absent melting, water-excess melting, and water-  
837 deficient melting (cf., Clemens et al., 2020).

838         We use the term water-absent melting synonymously with dehydration melting to  
839 describe conditions in which the water present is entirely structurally bound in hydrous minerals,  
840 chiefly mica and amphibole. Water released from these minerals during dehydration melting is  
841 dissolved into the melt, which is water-undersaturated. Water-absent melting is buffered by the  
842 amount and type of hydrous minerals. Muscovite dehydration melting occurs at the lowest  
843 temperatures (ca. 700 °C at 5 kbar), followed by biotite dehydration melting (ca. 800 °C at 5  
844 kbar) and then amphibole dehydration melting (ca. 900 °C at 5 kbar) (Patiño-Douce and Harris,  
845 1998) (Fig. 11). Amphibole dehydration melting is relatively uncommon in orogenic anatectic  
846 terranes because of the high temperatures (>850 °C) required (Thompson and Connolly, 1995).  
847 For metapelitic rocks, muscovite dehydration melting reactions (Reaction 1; Peto, 1976) produce  
848 K-feldspar and sillimanite (or kyanite) as peritectic products and biotite dehydration melting  
849 reactions (Reaction 2; Le Breton and Thompson, 1988) produce peritectic K-feldspar and  
850 cordierite (or garnet at high-pressure).





853 Water-excess melting describes melting in water-saturated conditions where water  
854 remains present in the protolith above the (wet) solidus and the melt is water-saturated. Most  
855 experimental studies with added water are water-excess experiments and for most studies water-  
856 excess, water-flux, and fluid-flux melting are synonymous (e.g., Patiño Douce, 1996). Water-  
857 excess melting requires an external source of water to sustain melting and is buffered by the  
858 amount of available water. Water-excess melting of metasedimentary protoliths, including  
859 muscovite- and/or biotite-bearing schist (Reactions 3-5; Yardley and Barber, 1991; Patiño-Douce  
860 and Harris, 1998; Vielzeuf and Schmidt, 2001) and metagreywacke (Reaction 6; Genier et al.,  
861 2008) occurs at relatively low temperatures (ca. 650 °C at 5 kbar) and may or may not produce  
862 an aluminosilicate (including garnet) peritectic phase.



867 Water-deficient melting describes an intermediate condition (between water-absent and  
868 water-excess melting) where a free water phase is present (e.g., pore-space fluid), but limited. In  
869 this case, the protolith is water-undersaturated and excess water is consumed at or just above the  
870 wet solidus. Melting continues along a dehydration path after the excess water is exhausted.  
871 Water-deficient melting is generally rock-buffered and produces water-undersaturated melts  
872 ( $a_{\text{H}_2\text{O}} < 1$ ) above the wet solidus (Nabelek, 2019). Water-absent and water-excess melting are  
873 end-members and can be distinguished geochemically (see review in Weinberg and Hasalová,  
874 2015), however, water-deficient melting is considered geochemically indistinguishable from

875 dehydration melting and is generally only inferred based on melt volumes and temperature  
876 (Schwindinger et al., 2018; 2019).

877

### 878 ***6.1. Water-Absent Melting vs. Water-Excess Melting***

879 In this section, we use CAB geochemistry to evaluate the roles of water-absent and  
880 water-excess melting in generating these rocks. Although there are various hypotheses  
881 concerning the tectonic mechanisms involved (see discussion in Section 7 below), the large  
882 majority of anatectic rocks in the CAB have been previously interpreted to have formed by  
883 dehydration melting (Coney and Harms, 1984; Haxel et al., 1984; Armstrong, 1988; Miller and  
884 Gans, 1989; Barton, 1990; Patiño-Douce et al., 1990; Wright and Wooden, 1991; Brandon and  
885 Lambert, 1993; Mahood et al., 1996; Vanderhaege et al., 1999; Foster et al., 2001; Norlander et  
886 al., 2002; Teyssier and Whitney, 2002; Lee et al., 2003; Hinchey et al., 2006; Mattinson et al.,  
887 2007; Gaschnig et al., 2011; Stevens et al., 2015). An exception is the Big Maria Mountains,  
888 California that contain field and petrographic evidence for widespread fluid infiltration during  
889 Late Cretaceous metamorphism (Hoisch, 1987). The metamorphic rocks in the Big Maria  
890 Mountains are not migmatitic but are intruded by numerous pegmatitic leucogranite dikes that  
891 have been interpreted to result from water-excess/fluid-flux melting (Hamilton, 1987; Hoisch,  
892 1987). The fluid source in the Big Maria Mountains could be metamorphic reactions within the  
893 crust, crystallizing magmas at depth (Hoisch, 1987), or the dehydrating Farallon slab (Wells and  
894 Hoisch, 2008).

895 Micas have high Rb and low Sr concentrations, whereas plagioclase has the opposite –  
896 low Rb and high Sr concentrations. Water-absent melting, involving the breakdown of  
897 muscovite and biotite, enriches the melt in Rb. Restitic feldspar increases during muscovite

898 dehydration melting, depleting the melt in Sr, but does not increase during (relatively higher  
899 temperature) biotite dehydration melting, causing little change in Sr concentrations in the melt  
900 (Harris and Inger, 1992). As a result, mica dehydration melting is often associated with  
901 geochemical trends showing increasing Rb/Sr and decreasing Sr (muscovite dehydration) or near  
902 constant Sr (biotite dehydration) concentrations (Inger and Harris, 1993). Conversely, water-  
903 excess melting breaks down plagioclase before mica, resulting in increased Sr in the melt and  
904 low Rb/Sr that remains relatively constant during melt evolution (Conrad et al., 1988; Harris and  
905 Inger, 1992; Inger and Harris, 1993). There is no absolute value of Rb/Sr that can be used to  
906 discriminate water-absent melting from water-excess melting, but Harris et al. (1993) suggested  
907 that water-excess melting was unlikely for granite with Rb/Sr >3.5 for most metasedimentary  
908 protoliths. Figure 12A shows that the rocks of the CAB have a wide range of Rb/Sr values (4  
909 orders of magnitude) and follow Rb/Sr geochemical trends consistent with muscovite  
910 dehydration melting. However, this trend is also consistent with fractional crystallization of  
911 feldspar (particularly plagioclase) and could be produced by strongly differentiated rocks with  
912 high Rb/Sr and cumulates with low Rb/Sr.

913         Melting of feldspar during water-excess melting has also been linked to positive Eu  
914 anomalies. Prince et al. (2001) used strongly positive (> 3) Eu anomalies in Eocene Himalayan  
915 leucogranites to identify water-excess melting. Negative Eu anomalies are generally produced  
916 by fractional crystallization of feldspar and positive Eu anomalies may record a complementary  
917 feldspar-rich cumulate (Sawyer, 1987; Rudnick, 1992). Cumulates may also be recognized by  
918 low total REE, which increases for more strongly fractionated melts. Fig. 12B plots Eu anomaly  
919 vs. total REE for CAB rocks and shows that rocks with weak positive Eu anomalies (1-3) also  
920 have low total REE and are probably cumulates. Removal of trivalent REE during



921 crystallization of accessory phases can also produce low total REE and positive Eu anomalies  
922 (Bea and Montero, 1999). Few CAB rocks have strong positive Eu anomalies associated with  
923 water-excess melting or other processes (Fig. 12B).

924 Potassium concentration relative to Na and Ca (or normative orthoclase relative to albite  
925 and anorthite) in melts produced from crustal anatexis is another method used to qualitatively  
926 assess the role of water-excess melting. The melting of plagioclase prior to mica, particularly  
927 biotite, during water-excess melting results in melts with tonalite to trondhjemite compositions  
928 (Conrad et al. 1988; Scaillet et al. 1995; Patiño-Douce, 1996). Conversely, the preferential  
929 melting of mica prior to plagioclase during water-absent melting results in more potassic  
930 compositions and rocks with significant modal K-feldspar. With few exceptions, CAB intrusive  
931 rocks have normative Ab/Or (albite/orthoclase) ratios  $< 2$  and do not have the tonalite or  
932 trondhjemite compositions produced experimentally by water-excess melting of  
933 metasedimentary protoliths (Patiño-Douce and Beard, 1996; Patiño-Douce, 1996; Patiño-Douce  
934 and Harris, 1998) (Fig. 5). Studies have also proposed that ferromagnesian contents increase  
935 during water-excess melting (e.g.,  $\text{FeO}_{\text{total}} > 2$  wt. %; Weinberg and Hasalová, 2015), but are  
936 sequestered by refractory residual mineral phases during water-absent melting of  
937 metasedimentary protoliths (Naney, 1983; Holtz and Johannes, 1991; Patiño-Douce, 1996). The  
938 majority of CAB rocks have low total FeO ( $< 2$  wt. %), consistent with water-absent melting.

939 The geochemistry and magma temperature estimates (Fig. 8) for the CAB are most  
940 consistent with muscovite dehydration (water-absent) melting at middle to lower crustal  
941 pressures ( $\geq 5$  kbar) (Fig. 11) and the composition of the CAB rocks compare favorably to  
942 experimental studies of muscovite dehydration melting (e.g., Patiño-Douce, 1999). Textural  
943 heterogeneity and numerous pegmatite and aplite dikes/sills associated with the CAB indicate

944 exsolution of water throughout the crystallization processes from relatively hydrous melts.  
945 These observations further support muscovite dehydration melting over biotite dehydration  
946 melting. Biotite dehydration melting at higher temperature requires less water to stabilize the  
947 melt and produces relatively dry melts that are more texturally homogenous (Clemens and  
948 Vielzeuf 1987; Villaros et al., 2018; Nabelek, 2019). Muscovite dehydration melting of  
949 metasedimentary protoliths at 750 °C and 5 kbar results in ca. 6 wt. % H<sub>2</sub>O in the melt compared  
950 to ca. 2 wt. % H<sub>2</sub>O at 850 °C for biotite breakdown at the same pressure (Patiño Douce and  
951 Beard, 1995; Patiño Douce and Harris, 1998; Castro, 2013).

952

## 953 ***6.2. Water-Deficient Melting***

954         There are two main problems with invoking water-absent, muscovite dehydration melting  
955 as the dominant processes to produce the CAB rocks. Both problems can potentially be resolved  
956 if water-deficient melting is involved. The first problem is that muscovite dehydration melting  
957 may not produce enough melt volume to initiate melt migration and accumulation (Clemens and  
958 Vielzeuf, 1987; Barton, 1990; Patiño Douce et al., 1990; Wells and Hoisch, 2008). Melt  
959 extraction is thought to be limited by a melt-connectivity threshold (~7 % melt), at which point  
960 melt/solid segregation can occur if the solid residue is able to deform and/or compact (Rosenberg  
961 and Handy, 2005; Vanderhaeghe, 2009). Under inefficient melt extraction conditions, a  
962 migmatite may accumulate large amounts of leucosome/melt (diatexite) until the solid-liquid  
963 threshold (20-40% melt) is reached and the migmatite starts to behave as a crystal mush (van der  
964 Molen and Paterson, 1979). A very muscovite-rich (20-30 %) schistose protolith could generate  
965 ca. 10 % melt during muscovite dehydration melting (Wyllie, 1977), but most metasedimentary  
966 compositions are estimated to produce <5 % melt by volume (Patiño Douce et al., 1990;

967 Johannes and Holtz, 1996; Droop and Brodie, 2012). Biotite dehydration melting of common  
968 metasedimentary protoliths can produce up to 40 % melt (Miller et al., 1985; Clemens and  
969 Vielzeuf, 1987; Patiño Douce et al., 1990; Stevens et al., 1997), but the geochemical data and  
970 melting temperature estimates discussed above do not appear to support biotite dehydration  
971 melting.

972 Many locations in the CAB expose significant (approaching batholith-scale) volumes of  
973 muscovite-bearing peraluminous granite related to crustal melting that suggest relatively large  
974 melt fractions. For example, ~600 km<sup>3</sup> of CAB rocks are exposed in the Lamoille Canyon area  
975 in the Ruby-East Humboldt core complex and several times that amount is estimated to be  
976 present in the subsurface (Howard et al., 2011). Unless melt is being drained laterally from areas  
977 beyond the Ruby-East Humboldt Mountains, 5-10 % melting cannot produce the observed rock  
978 volumes. Water-deficient melting that incorporates small amounts of externally-derived water  
979 (~1 wt. % added) can result in large increases in melt fractions, 2-3 times larger than by  
980 dehydration melting alone – resulting in a 10-20 % increase in melt volume (Sola et al., 2017;  
981 Nabelek, 2019; Schwindinger et al., 2019).

982 To illustrate this issue, we constructed an isobaric (5 kbar) temperature-X<sub>H2O</sub> assemblage  
983 diagram for a muscovite-rich metasedimentary protolith (Fig. 13). The whole rock starting  
984 composition was modeled after a muscovite-bearing quartz wacke from the Pinal Schist in  
985 Arizona (sample “B” in Copeland and Condie, 1986). This composition is comparable to other  
986 muscovite-bearing metasedimentary rocks from the Neoproterozoic Cordilleran passive margin  
987 sequence (e.g., McCoy Creek Group in Nevada; Misch and Hazzard, 1962) and comparable to  
988 generic metasedimentary rocks compositions used in modeling partial melting of other anatectic  
989 provinces (cf., Nabelek, 2019), but is more quartz-rich than the most melt-fertile rocks (e.g.,

990 muscovite schist). Closed-system phase assemblages and melt volumes were calculated with  
991 `Perple_X` version 6.8.7. (Connolly, 1990; 2005; Connolly and Petrini, 2002) in the  
992 NCKMASHTO model system ( $\text{Na}_2\text{O}$ ,  $\text{CaO}$ ,  $\text{K}_2\text{O}$ ,  $\text{Al}_2\text{O}_3$ ,  $\text{SiO}_2$ ,  $\text{H}_2\text{O}$ ,  $\text{TiO}_2$ ,  $\text{O}_2$ ,  $\text{FeO}_t$ , and  $\text{MgO}$ ),  
993 using a quartz-fayalite-magnetite assemblage for  $f\text{O}_2$  buffering and thermodynamic data from  
994 Holland and Powell (2011). One way to read the assemblage diagram in Fig. 13 is to consider  
995 the average zircon saturation temperature estimate for the CAB and examine changes in melt  
996 content (shown as volume percent) as the amount of water in the protolith is increased (moving  
997 to the right along the x-axis). Muscovite dehydration melting occurs at  $\sim 0.7$  wt. %  $\text{H}_2\text{O}$ , which  
998 is the amount of structurally bound water in mica in the protolith, not a free fluid phase. Water-  
999 absent muscovite dehydration melting produces  $< 5$  % melt. Water-excess melting occurs above  
1000  $\sim 2.3$  wt. %  $\text{H}_2\text{O}$ , at which point free water remains in the protolith above the solidus (pink line  
1001 labeled “melt in”) and  $> 20$  % melt is produced. Water-deficient melting (ca. 0.7-2.3 wt. %  $\text{H}_2\text{O}$ )  
1002 consumes all free water at the solidus and produces water-undersaturated melts but results in  
1003 significant increases of melt volume. For example, 1 wt. % of free water in the protolith (1.7 wt.  
1004 %  $\text{H}_2\text{O}$  in Fig. 13) increases melt volume from 1.2 % (water-absent, muscovite dehydration  
1005 melting) to 16.9 % at 725 °C. Debate continues about whether any amount of free water is  
1006 reasonable to expect in the middle to lower crust (Thompson, 1983; Weinberg and Hasalová,  
1007 2015).

1008         The second problem with muscovite dehydration melting is that, despite relatively low  
1009  $\text{FeO}$  and  $\text{MgO}$  values in CAB rocks, biotite is very common, which requires partial melting of a  
1010 phase more mafic than muscovite. Additional Fe and Mg can be added to the melt with added  
1011 water (water-deficient or water-excess) melting (Holtz and Johannes, 1991; Patiño-Douce,  
1012 1996). Water-deficient melting is one possible mechanism to increase ferromagnesian

1013 components in CAB melts, although our modeling (Fig. 13) as well as other studies of water-  
1014 deficient melting (Schwindinger et al., 2018) have indicated relatively small to insignificant  
1015 increases in FeO and MgO ( $\leq 0.5$  wt. %) from water-absent melting. Other processes such as  
1016 restite/peritectic mineral entrainment have also been proposed to increase Fe and Mg in crustal  
1017 melts (Stevens et al., 2007). The importance of water-deficient melting has only recently been  
1018 emphasized globally (e.g., Nabelek, 2019) and it has not been previously considered for intrusive  
1019 suites in the CAB, but it deserves future investigation.

1020

## 1021 **7. Tectonic Causes of Crustal Melting**

1022       There is no consensus on the underlying causes of Late Cretaceous to Paleogene crustal  
1023 anatexis in the CAB, but hypotheses can be generally grouped into four categories: 1)  
1024 decompression melting, 2) melting resulting from radiogenic heating and thermal relaxation  
1025 following crustal thickening, 3) melting resulting from the introduction of slab-derived fluids,  
1026 and 4) melting associated with increased heat flux from the mantle. These hypotheses are not all  
1027 mutually exclusive and there is no requirement for a single process to explain the entire CAB.  
1028 However, the CAB occupies a relatively narrow time interval and appears to be a coherent  
1029 spatial feature, which supports treating it as a distinct component of the North American  
1030 Cordilleran orogenic system, on par with other components such as the continental arc and  
1031 retroarc thrust belt. Previous researchers have favored different hypotheses in the northern,  
1032 central, and southern CAB, but it is instructive to consider how hypotheses favored in one region  
1033 may be extended or extrapolated into other areas.

1034

## 1035 ***7.1. Decompression Melting Related to Exhumation***

1036           There is a close spatial association between the CAB and the Cordilleran metamorphic  
1037 core complexes (Fig. 1), suggesting a possible petrogenetic relationship as well (Armstrong,  
1038 1982). One possible scenario is that core complex extension and exhumation caused  
1039 decompression melting. Decompression melting is a form of dehydration melting and is  
1040 commonly invoked when melting and exhumation of the crust are contemporaneous (Harris and  
1041 Massey, 1994). Decompression melting has received the most attention in the northern CAB,  
1042 particular within the Shuswap complex, where anatectic crystallization ages, cooling ages,  
1043 extension timing, and the timing of near-isothermal decompression in reconstructed P-T paths all  
1044 overlap (Vanderhaeghe et al., 1999; Norlander et al., 2002; Teyssier and Whitney, 2002;  
1045 Whitney et al, 2004b; Gordon et al., 2008; Stevens et al., 2016) (Fig. 9). The Shuswap complex  
1046 is cored by several migmatitic gneiss domes that display structural fabrics and geometries  
1047 supporting vertical motion within the domes and flattening above the domes – consistent with  
1048 diapiric-like rise of the deep crust (e.g., Duncan, 1984; Whitney et al., 2004). Relatively hot,  
1049 ductile middle-to-lower crust is a prerequisite for diapirism although a variety of processes could  
1050 trigger initial ascent, including a density inversion resulting from underthrusting of  
1051 (meta)sedimentary rocks into the deep crust, low-degrees of partial melting causing density  
1052 reduction, focused erosion at the surface, localized crustal thickening or buckling, and rapid  
1053 tectonic denudation (Teyssier and Whitney, 2002). Estimates for diapir-related exhumation rates  
1054 from migmatitic gneiss domes in the Shuswap complex are ca. 20 km/Myr, which is significantly  
1055 faster than tectonic exhumation associated with extension (Whitney et al., 2004; 2013). Rapid  
1056 decompression should produce a narrow range of ages, which is at odds with the wide range of  
1057 ages ( $\geq 10$  Myr) and the remobilization of melts prior to emplacement observed in some CAB

1058 localities. Furthermore, (re)melting events related to repeated or prolonged decompression are  
1059 difficult to reconcile with dehydration melting as the protolith becomes increasingly refractory  
1060 and requires increasingly high temperatures to make new melts. Regardless, once upward  
1061 movement and decompression is initiated, there is a positive feedback between melting, viscosity  
1062 reduction, and exhumation resulting in relatively large volumes ( $\geq 20\%$ ) of dehydration-related  
1063 leucocratic melt (Whitney et al., 2004b; Rey et al., 2009), consistent with some locations in the  
1064 northern CAB (e.g., Priest River complex, Stevens et al., 2015; 2016). The positive P-T slope of  
1065 dehydration melting solidi suggests that melting can occur throughout the decompression process  
1066 and that emplacement in the middle-to-upper crust is efficient.

1067         Decompression melting is considered less likely in the central and southern CAB, in part  
1068 because the timing of extension and exhumation is younger than crustal melting (Fig. 9).  
1069 However, P-T paths from metamorphic rocks in many Cordilleran core complexes suggest that  
1070 decompression is a near-isothermal process that would not be expected to be recorded by  
1071 thermochronometers. For example, by some estimates, the Ruby-East Humboldt complex  
1072 experienced  $\sim 4$  kbar ( $\sim 15$  km) decompression at ca. 750-650 °C from ca. 85-55 Ma (McGrew et  
1073 al., 2000; Henry et al., 2011) (Fig. 10), which largely overlaps with the crystallization ages of  
1074 CAB rocks in the complex (Howard et al., 2011). How this period of decompression occurred is  
1075 unclear because the complex exposes a series of stacked and folded nappes, rather than discrete  
1076 gneiss domes or evidence for diapirism (Howard, 1980). Deep structural levels within the Ruby-  
1077 East Humboldt complex show some evidence for lateral crustal flow (MacCready et al., 1997)  
1078 and numerical models suggest that relatively slow extension rates may have kept the complex  
1079 from developing more defined migmatitic gneiss domes (Rey et al., 2009). Another possibility is  
1080 that the recumbently folded nappes in the Ruby Mountains record flattening strain during Late

1081 Cretaceous to Eocene decompression and that they sit above an even deeper structural level (not  
1082 exposed) that records vertical, diapir-like exhumation. Regardless, diapiric exhumation of the  
1083 lower crust has not been seriously proposed to have generated anatectic melting in North  
1084 America outside of the northern CAB.

1085         There is also evidence for syn-convergent, Late Cretaceous extension (prior to core  
1086 complex extensional faulting) in the central and southern CAB (Carl et al., 1991; Wells and  
1087 Hoisch, 2008; Druschke et al., 2009; Wells et al., 2012; Long et al., 2015). In some cases, this  
1088 extension has been proposed to have caused decompression melting. Examples include the Iron  
1089 Mountains and Old Woman Mountains in southeast California (Wells and Hoisch, 2008) and the  
1090 Death Valley region (Hodges and Walker, 1990; Applegate et al., 1992; Applegate and Hodges,  
1091 1995). However, the amount of Late Cretaceous extension documented in the U.S Cordillera is  
1092 limited (Miller et al., 2012; Lund-Snee et al., 2016) and it is uncertain whether there was enough  
1093 extension to cause widespread decompression melting.

1094         Relating anatectic melting to near-isothermal decompression in the central and northern  
1095 CAB is possible because migmatite and metamorphic rocks are exposed, enabling P-T-t paths to  
1096 be reconstructed and deep crustal strain to be evaluated. These types of rocks are generally not  
1097 exposed in the southern CAB, specifically in Arizona and Sonora, and as a result, decompression  
1098 melting has not been seriously proposed or evaluated in that region. However, one end-member  
1099 interpretation is that intrusive rocks in the southern CAB signify a period of decompression in  
1100 the deep crust that is otherwise inscrutable. As such, the northern core complexes and CAB may  
1101 provide a template for understanding deep crustal process in the southern U.S. and northern  
1102 Mexican Cordillera.

1103



## 1104 **7.2. Radiogenic Heat and Thermal Relaxation**

1105 Radiogenic heating and relaxation of isotherms following crustal thickening has also  
1106 been proposed to account for CAB rocks (Haxel et al., 1984; Miller and Gans, 1989; Patiño-  
1107 Douce et al., 1990; Wright and Wooden, 1991). The Laramide orogeny (ca. 80-40 Ma) overlaps  
1108 in age with the CAB, however, Laramide deformation is chiefly characterized by slip on high-  
1109 angle reverse faults that produced limited horizontal shortening and hence limited crustal  
1110 thickening (Yonkee and Weil, 2015). In addition, thermal models suggest that maximum  
1111 temperatures in the middle to lower crust are attained 40-60 Myr after (instantaneous) crustal  
1112 thickening (England and Thompson, 1984; 1986; Clark et al., 2011), ruling out Laramide-age  
1113 crustal thickening as a cause of crustal anatexis in the CAB. In contrast, the Sevier orogeny  
1114 caused significant crustal thickening and the time elapsed between the end of shortening (ca.  
1115 100-80 Ma) and the onset of crustal melting in the CAB is ca. 10-50 Myr, consistent with the  
1116 thermal models. These models implicitly assume that the crust, perhaps in the form of an  
1117 orogenic plateau, remained thick after the end of crustal thickening. Anatexis resulting from  
1118 crustal thickening was modelled explicitly for the North American Cordillera by Patiño-Douce et  
1119 al. (1990) who suggested that a 10-15 km thick migmatite layer at 30-40 km depth would  
1120 develop by the end of the Sevier orogeny if the crust was thickened to 50-55 km, consistent with  
1121 estimates of crustal thickness for the Nevadaplano (Coney and Harms, 1984; Chapman et al.,  
1122 2015). Modeling by both Patiño-Douce et al. (1990) and England and Thompson (1984, 1986)  
1123 assumed that free water was not present in the melt source region and that relatively high  
1124 temperatures ( $> 850$  °C) were required to produce biotite dehydration melting in order to  
1125 generate the melt volumes (20-40%) observed. To generate these high temperatures, the models  
1126 required mid-crustal layers with moderately high radiogenic heat production ( $>2$   $\mu\text{W}/\text{m}^3$ ). The

1127 high temperatures required for biotite-dehydration melting are one of the main arguments against  
1128 crustal thickening as a primary mechanism to generate the CAB rocks (e.g., Wells and Hoisch,  
1129 2008; 2012; Wells et al., 2012). If water-excess or water-deficient melting are important  
1130 processes in the origin of the CAB, then melting at lower temperatures and the production of  
1131 large melt volumes is less problematic for hypotheses relating anatexis to crustal thickening (Fig.  
1132 13).

1133         Much of the southern CAB is located southeast of the deformational limit of the Sevier  
1134 thrust belt (Fig. 1) and southeast of the Maria contractional belt in western Arizona and southeast  
1135 California (Spencer and Reynolds, 1990; Boettcher et al., 2002). This region (southern Arizona  
1136 and Sonora) experienced limited shortening during the Laramide orogeny, but the amount of  
1137 documented shortening (ca. 30 km; Davis et al., 1979; Haxel et al., 1984) is not enough to  
1138 significantly thicken the crust. Nonetheless, geochemical data suggest that the crust in southern  
1139 Arizona and northern Sonora was relatively thick (55-60 km) during Late Cretaceous to early  
1140 Paleogene time (Chapman et al., 2020), which may be related to magmatic thickening (Erdman  
1141 et al., 2016). If the southern CAB is related to crustal thickening and radiogenic heating, then  
1142 the age of the intrusive rocks could be interpreted as the age of peak metamorphism in the deep  
1143 crust, which is otherwise unconstrained.

1144         Total horizontal shortening in the Sevier thrust belt is greatest (~350 km) in the central  
1145 U.S. Cordillera (DeCelles and Coogan, 2006) and decreases to the north (e.g., Fuentes et al.,  
1146 2012) and to the south (e.g., Giallorenzo et al., 2018). This fact may help explain why the  
1147 central CAB is older than the northern and southern CAB – because the crust was thickened  
1148 more and/or faster and reached peak metamorphic conditions earlier. The wide range of ages  
1149 and evidence for melt remobilization in the CAB (e.g., Catalina-Rincon complex, Davis et al.,

1150 2019; Ducea et al., 2020) is consistent with melts formed during prograde metamorphism that  
1151 remained at high temperature and pressure, existing at near-solidus or partially-molten conditions  
1152 until melt extraction or exhumation.

1153

### 1154 **7.3. *Water Present Melting***

1155 Melting involving free water in the parent rock has not received much attention as a  
1156 significant cause for anatexis in the CAB. As mentioned in Section 6, Hoisch (1987) suggested  
1157 that fluids exsolved from crystallizing magmas at depth resulted in water-flux melting in the Big  
1158 Maria Mountains, California and hypothesized that crustal melting in the nearby Old Woman  
1159 Mountains, California may be analogous. Wells and Hoisch (2008) proposed that delamination  
1160 and mantle upwelling was a primary cause of crustal melting throughout the CAB (see next  
1161 section), but they also suggested that dehydration of the Farallon slab could have played a role.  
1162 The timing of low-angle subduction of the Farallon slab beneath the CAB matches closely with  
1163 the age of CAB intrusive rocks. Many studies have suggested that the mantle lithosphere was  
1164 hydrated during the Laramide orogeny (Dumitru et al., 1991; Humphreys et al., 2003; Farmer et  
1165 al., 2008) and several studies in the last decade have suggested that the lower crust was hydrated  
1166 as well (Jones et al., 2015; Butcher et al., 2017; Porter et al., 2017; Levandowski et al., 2018).  
1167 Other potential sources of free water include metamorphic reactions within the crust (e.g.,  
1168 underthrusting of crustal lithologies) and small amounts of relict water in pore spaces.

1169 The geochemistry of the CAB rocks does not support water-excess melting (Fig. 12), but  
1170 it is consistent with water-deficient melting, which is difficult to distinguish from water-absent  
1171 melting by geochemistry alone. The relatively low calculated zircon saturation temperatures for  
1172 the CAB may even require some degree of water-added melting because some temperature

1173 estimates are below the solidus for muscovite dehydration melting (Fig. 11). Melts produced by  
1174 water-absent and water-deficient melting are both water-undersaturated and are more likely to  
1175 ascend through the crust to form intrusive bodies. Periodic fluid influx could also explain the  
1176 wide range of crystallization ages at individual CAB locations.

1177

#### 1178 **7.4. Mantle Heat Flux**

1179 The two main hypotheses proposed for CAB rocks that involve increased mantle heat  
1180 flow are 1) asthenospheric upwelling following delamination and 2) mantle upwelling above a  
1181 subducting slab. The delamination hypothesis suggests that upwelling following delamination of  
1182 the mantle lithosphere resulted in decompression melting of the asthenosphere and basaltic  
1183 underplating/intrusion that provided additional heat to melt the overlying crust (Wells and  
1184 Hoisch, 2008; 2012; Wells et al., 2012). Delamination is common in areas of thickened crust  
1185 (e.g., England and Houseman, 1989), consistent with the position of the CAB and  
1186 reconstructions of the orogenic interior and the Nevadaplano (Coney and Harms, 1984; DeCelles  
1187 et al., 2004). The delamination model has been applied specifically in the Great Basin and  
1188 Mojave regions where melting is generally Late Cretaceous in age (Wells and Hoisch, 2008).  
1189 The model could be extended to the northern and southern CAB, where melting is generally  
1190 early to middle Paleogene in age, if delamination migrated spatially through time or if there were  
1191 separate delamination events. However, geophysical studies suggest that many parts of the  
1192 northern and southern CAB have intact, ancient, cratonic (or peri-cratonic) mantle lithosphere  
1193 preserved, which suggests delamination has not occurred (e.g., Li et al., 2007).

1194 The subduction hypothesis suggests that the upwelling arm of corner flow (also called  
1195 counterflow or induced mantle flow) in the mantle wedge above a subducting slab may steadily

1196 heat up the base of the lithosphere and could eventually cause crustal melting (Armstrong, 1982;  
1197 Farmer and DePaolo, 1983; Barton, 1990). A variation of this model was proposed for the Death  
1198 Valley region and suggests that asthenospheric upwelling above steepened portions of the  
1199 Farallon slab may have caused crustal melting (Lima et al., 2018). Some studies have suggested  
1200 that thermal convection or other processes in (non-extending) back-arc regions may produce  
1201 temperatures high-enough to cause crustal melting (Currie and Hyndman, 2006; Wolfram et al.,  
1202 2019). But most studies indicate that corner-flow and normal subduction processes (including  
1203 changes in slab dip) do not provide enough heat to cause (water-absent) crustal melting in the  
1204 upper plate, particularly during periods of low-angle to flat-slab subduction when the upper  
1205 mantle and lithosphere are cooled by the slab (English et al., 2003; Liu and Currie, 2016). The  
1206 timing and progression direction of Farallon slab roll-back in the U.S. Cordillera is also at odds  
1207 with the timing and progression direction of the CAB. Flare-up magmatism related to slab roll-  
1208 back is oldest in the northern and southern U.S. Cordillera and youngest in the central U.S.  
1209 Cordillera (Humphreys, 1995), whereas the CAB is oldest in the central U.S. Cordillera and  
1210 becomes younger to the north and south (Fig. 9). Nonetheless, individual parts of the CAB  
1211 coincide with the timing of Farallon slab roll-back and have been interpreted to be related to  
1212 mantle upwelling or mantle-derived magmatic intrusion (e.g., Konstantinou and Miller, 2015).

1213 Both the delamination and subduction hypotheses suggest that mantle processes are  
1214 required to produce temperatures high enough ( $> 800\text{ }^{\circ}\text{C}$ ) to cause biotite dehydration melting to  
1215 explain the large volumes of CAB rocks (Wells and Hoisch, 2012; Barton, 1990). This is not  
1216 supported by the zircon saturation temperatures (Fig. 8), assuming that those temperatures are  
1217 representative of partial melting temperatures (see Section 5.2). The rarity of mantle-derived  
1218 magmatic products in CAB locations is another argument against a significant role for the mantle

1219 in the formation of the CAB (e.g., Wright and Wooden, 1991).

1220

## 1221 **8. Conclusions**

1222         The North American Cordilleran Anatectic Belt (CAB) is a chain of Late Cretaceous to  
1223 Eocene intrusive rocks and anatectic rocks produced by crustal melting that is exposed from  
1224 southern British Columbia, Canada to northern Sonora, Mexico in the interior, or hinterland, of  
1225 the North American Cordilleran orogenic system. The duration of melting at any given location  
1226 was often protracted, lasting ~10 Myr, and characterized by repeated melt remobilization and  
1227 reworking. The CAB rocks are generally leucocratic ( $\text{SiO}_2 > 70$  wt. %), peraluminous ( $\text{ASI} >$   
1228 1.0), contain igneous muscovite  $\pm$  garnet, have evolved radiogenic isotopic compositions  
1229 ( $^{87}\text{Sr}/^{86}\text{Sr}_i > 0.706$ ), and have elevated (crustal-like)  $\delta^{18}\text{O}$ . The CAB was chiefly produced by  
1230 partial melting of metasedimentary rocks (e.g., schist, greywacke) and has no little or no mantle-  
1231 derived component, including partial melting of basalt/amphibolite. Geochemically, the CAB  
1232 rocks are consistent with muscovite dehydration melting and/or water-deficient melting, but not  
1233 water-excess melting. Zircon saturation temperatures for the CAB cluster between 600-800 °C  
1234 with an average of  $724 \pm 48$  °C, which is too low for biotite or amphibole dehydration melting.  
1235 CAB rocks were primarily emplaced as sills, dikes, laccoliths, or large sheeted complexes and  
1236 lack extrusive equivalents. Late aplite and pegmatite dikes are common and suggest relatively  
1237 hydrous melts, which is also consistent with muscovite dehydration melting or water-added  
1238 melting. A small amount of free water during melting may be required by the relatively large  
1239 melt volumes within the CAB, supporting water-deficient conditions. The source of this free  
1240 water is unknown, but may have been in relict pore fluids, exsolved from magmas, produced by  
1241 metamorphic reactions, or liberated by dehydration of the Farallon slab. Crystallization ages of

1242 rocks in the CAB overlap with the timing of the Laramide orogeny and many of these rocks were  
1243 emplaced during a period of low-angle to flat-slab subduction when the Farallon slab was located  
1244 beneath the CAB.

1245         There is a close spatial correlation between the CAB and the belt of Cordilleran  
1246 metamorphic core complexes, and a large majority of the rocks in the CAB are found in the  
1247 footwalls of core complexes. Only in a few locations, however, have CAB intrusive rocks been  
1248 demonstrated to have originated from melting of the rocks (i.e., migmatite) exposed at the  
1249 surface in the core complexes. An unanswered question in the CAB is whether the prevalence of  
1250 crustal melting in core complexes is related to the core complexes themselves or is an artifact of  
1251 core complexes exposing middle to lower crust, where the CAB magmas appear to have been  
1252 commonly emplaced. In the northern CAB, the timing for core complex extension/exhumation  
1253 and anatexis overlap, supporting a shared origin between the two and emphasizing the role of  
1254 decompression melting. This overlap in ages is not observed in the central and southern CAB  
1255 where core complex extension/exhumation is up to 50 Myr younger than crustal melting,  
1256 suggesting that mechanisms other than decompression melting are required there.

1257         The CAB formed in a region of previously thickened crust, interpreted as an orogenic  
1258 plateau. Radiogenic heating and relaxation of isotherms following crustal thickening during the  
1259 Sevier orogeny may explain crustal melting, particularly in the central CAB where horizontal  
1260 shortening in the retroarc thrust belt is the greatest. Horizontal shortening during the Laramide  
1261 orogeny was not large enough to significantly thicken the crust structurally. In addition, the  
1262 oldest rocks in the CAB occur in the central CAB and are younger to the north and to the south.  
1263 Melting associated with crustal thickening may not be applicable to the southern CAB because  
1264 the Sevier thrust belt did not extend that far south and crustal shortening was limited.

1265           A prominent role of delamination, mantle upwelling, or other mechanisms that increase  
1266 mantle heat flux in producing the CAB is difficult to assess but appears unlikely. Most locations  
1267 in the CAB do not contain mantle-derived, co-genetic igneous rocks and those that do have been  
1268 interpreted to reflect processes other than crustal anatexis. Arguments that a component of  
1269 elevated mantle heat flow is required to produce temperatures high enough to initiate biotite  
1270 dehydration melting to account for large melt volumes are not supported by thermometry or  
1271 geochemistry, and estimated melt volumes can best be reconciled with water-deficient melting.

1272

### 1273 **Acknowledgements**

1274           Chapman acknowledges support from U.S. National Science Foundation grant EAR-  
1275 1928312. Comments from three anonymous reviewers helped improved the manuscript.

1276

### 1277 **References**

1278 Anderson, J.L., and Cullers, R.L., 1990, Middle to upper crustal plutonic construction of a  
1279 magmatic arc; An example from the Whipple Mountains metamorphic core complex, *in*,  
1280 Anderson, J.L., ed., The Nature and Origin of Cordilleran Magmatism: Geological  
1281 Society of America Memoir 174, p. 47-69.

1282 Anderson, J.L., Barth, A.P. and Young, E.D., 1988, Mid-crustal Cretaceous roots of Cordilleran  
1283 metamorphic core complexes: *Geology*, v. 16, p. 366-369.

1284 Anderson, T.H., Silver, L.T., and Salas, G.A., 1980, Distribution and U-Pb isotope ages of some  
1285 lineated plutons, northwestern Mexico, *in*, Crittenden, M.D., Coney, P.J., and Davis,  
1286 G.H., Cordilleran Metamorphic Core Complexes, Geological Society of America  
1287 Memoir, v. 153, p. 269–283.



- 1288 Annen, C., Blundy, J.D., and Sparks, R.S.J., 2006, The genesis of intermediate and silicic  
1289 magmas in deep crustal hot zones: *Journal of Petrology*, v. 47, p. 505-539.
- 1290 Applegate, J.D.R. and Hodges, K.V., 1995, Mesozoic and Cenozoic extension recorded by  
1291 metamorphic rocks in the Funeral Mountains, California: *Geological Society of America*  
1292 *Bulletin*, v. 107, p. 1063-1076.
- 1293 Applegate, J.D.R., Walker, J.D. and Hodges, K.V., 1992, Late Cretaceous extensional unroofing  
1294 in the Funeral Mountains metamorphic core complex, California: *Geology*, v. 20, p. 519-  
1295 522.
- 1296 Armstrong, R.L. and Ward, P., 1991, Evolving geographic patterns of Cenozoic magmatism in  
1297 the North American Cordillera: The temporal and spatial association of magmatism and  
1298 metamorphic core complexes: *Journal of Geophysical Research: Solid Earth*, v. 96, p.  
1299 13201-13224.
- 1300 Armstrong, R.L., 1982, Cordilleran metamorphic core complexes-From Arizona to southern  
1301 Canada: *Annual Review of Earth and Planetary Sciences*, v. 10, p. 129-154.
- 1302 Armstrong, R.L., 1988, Mesozoic and early Cenozoic magmatic evolution of the Canadian  
1303 Cordillera, in, Clark, S.P., Burchfiel, B.C., and Suppe, J., eds., *Processes in continental*  
1304 *lithospheric deformation: Geological Society of America Special Paper*, v. 218, p. 55-91.
- 1305 Arnold, A.H., 1986, Geologic implications of a geochemical study of three two-mica granites in  
1306 Southern Arizona: University of Arizona, MS thesis.
- 1307 Asmerom, Y., Ikramuddin, M. and Kinart, K., 1988, Geochemistry of Late Cretaceous granitoids  
1308 from northeastern, Washington: Implication for genesis of two-mica, Cordilleran  
1309 granites: *Geology*, v. 16, p. 431-435.
- 1310 Banks, N.G., 1980, Geology of a zone of metamorphic core complexes in southeastern Arizona,

- 1311 *in*, Crittenden, M. D., Jr., Coney, P. J., and Davis, G. H., eds., Cordilleran metamorphic  
1312 core complexes: Geological Society of America Memoir 153, p. 177-215.
- 1313 Barbarin, B., 1996, Genesis of the two main types of peraluminous granitoids: *Geology*, v. 24, p.  
1314 295-298.
- 1315 Barker, D.S., 1987, Tertiary alkaline magmatism in Trans-Pecos Texas: Geological Society,  
1316 London, Special Publications, v. 30, p. 415-431.
- 1317 Barnes, C.G., Burton, B.R., Burling, T.C., Wright, J.E. and Karlsson, H.R., 2001, Petrology and  
1318 geochemistry of the late Eocene Harrison Pass pluton, Ruby Mountains core complex,  
1319 northeastern Nevada: *Journal of Petrology*, v. 42, p. 901-929.
- 1320 Barth, A.P. and Wooden, J.L., 2006, Timing of magmatism following initial convergence at a  
1321 passive margin, southwestern US Cordillera, and ages of lower crustal magma sources:  
1322 *Journal of Geology*, v. 114, p. 231-245.
- 1323 Barton, M.D. and Trim, H.E., 1991, Late Cretaceous two-mica granites and lithophile-element  
1324 mineralization in the Great Basin, *in*, Raines, G.L., Lisle, R.E., Schafer, R.W., and  
1325 Wilkinson, W.H., eds., *Geology and ore deposits of the Great Basin*, p 529–538.
- 1326 Barton, M.D., 1987, Lithophile-element mineralization associated with Late Cretaceous two-  
1327 mica granites in the Great Basin; *Geology*, v. 15, p. 337-340.
- 1328 Barton, M.D., 1990, Cretaceous magmatism, metamorphism, and metallogeny in the east-central  
1329 Great Basin. The nature and origin of Cordilleran magmatism: Geological Society of  
1330 America Memoir, 174, p. 283-302.
- 1331 Barton, M.D., 1996, Granitic magmatism and metallogeny of southwestern North America:  
1332 *Transactions of the Royal Society of Edinburgh: Earth Sciences*, v. 87, p. 261-280.
- 1333 Barton, M.D., 2000, Overview of the lithophile element-bearing magmatic-hydrothermal system

1334 at Birch Creek, White Mountains, California, *in*, Dilles, J.H., Barton, M.D., Johnson,  
1335 D.A., Proffett, J.M., Einaudi, M.T., and Crafford, E.J., eds., *Contrasting Styles of*  
1336 *Intrusion Associated Hydrothermal Systems: Society of Economic Geologists Guide*  
1337 *Book*, v. 32, p. 9-26.

1338 Barton, M.D., Girardi, J.D., Kreiner, D.C., Seedorff, E., Zurcher, L., Dilles, J.H., Haxel, G.B.,  
1339 Johnson, D.A., Steininger, R.C., and Pennell, W.M., 2011, Jurassic igneous-related  
1340 metallogeny of southwestern North America: Great Basin Evolution and Metallogeny,  
1341 *Proceedings of the Geological Society of Nevada Symposium*, p. 373-396.

1342 Bea, F. and Montero, P., 1999, Behavior of accessory phases and redistribution of Zr, REE, Y,  
1343 Th, and U during metamorphism and partial melting of metapelites in the lower crust: an  
1344 example from the Kinzigite Formation of Ivrea-Verbano, NW Italy: *Geochimica et*  
1345 *Cosmochimica Acta*, v. 63, p. 1133-1153.

1346 Beard, J.S. and Lofgren, G.E., 1991, Dehydration melting and water-saturated melting of basaltic  
1347 and andesitic greenstones and amphibolites at 1, 3, and 6. 9 kb: *Journal of Petrology*, v.  
1348 32, p. 365-401.

1349 Bendick, R. and Baldwin, J., 2009, Dynamic models for metamorphic core complex formation  
1350 and scaling: The role of unchanneled collapse of thickened continental crust:  
1351 *Tectonophysics*, v. 477, p. 93-101.

1352 Best, M.G. and Brimhall, W.H., 1974, Late Cenozoic alkalic basaltic magmas in the western  
1353 Colorado Plateaus and the Basin and Range transition zone, USA, and their bearing on  
1354 mantle dynamics; *Geological Society of America Bulletin*, v. 85, p. 1677-1690.

1355 Best, M.G. and Christiansen, E.H., 1991, Limited extension during peak Tertiary volcanism,  
1356 Great Basin of Nevada and Utah: *Journal of Geophysical Research, Solid Earth*, v. 96, p.

1357 13509-13528.

1358 Best, M.G., Barr, D.L., Christiansen, E.H., Gromme, S., Deino, A.L. and Tingey, D.G., 2009,  
1359 The Great Basin Altiplano during the middle Cenozoic ignimbrite flareup: Insights from  
1360 volcanic rocks: *International Geology Review*, v. 51, p. 589-633.

1361 Beyene, M.A., 2011, Mesozoic burial, Mesozoic and Cenozoic exhumation of the Funeral  
1362 Mountains core complex, Death Valley, Southeastern California: University of Nevada  
1363 Las Vegas, MS thesis.

1364 Boehnke, P., Watson, E.B., Trail, D., Harrison, T.M. and Schmitt, A.K., 2013, Zircon saturation  
1365 re-revisited: *Chemical Geology*, v. 351, p. 324-334.

1366 Boettcher, S.S., Mosher, S., and Tosdal, R.M., 2002, Structural and tectonic evolution of  
1367 Mesozoic basement-involved fold nappes and thrust faults in the Dome Rock Mountains,  
1368 Arizona, *in*, Barth, A., ed., *Contributions to Crustal Evolution of the Southwestern United*  
1369 *States*: Boulder, Colorado, Geological Society of America Special Paper 365, p. 73–97.

1370 Borisov, A. and Aranovich, L., 2019, Zircon solubility in silicate melts: New experiments and  
1371 probability of zircon crystallization in deeply evolved basic melts: *Chemical Geology*, v.  
1372 510, p. 103-112.

1373 Brandon, A.D. and Lambert, R.S., 1993, Geochemical characterization of mid-Cretaceous  
1374 granitoids of the Kootenay Arc in the southern Canadian Cordillera: *Canadian Journal of*  
1375 *Earth Sciences*, v. 30, p. 1076-1090.

1376 Brandon, A.D. and Lambert, R.S., 1994, Crustal melting in the Cordilleran Interior: the mid-  
1377 Cretaceous White Creek batholith in the southern Canadian Cordillera: *Journal of*  
1378 *Petrology*, v. 35, p. 239-269.

1379 Brandon, A.D. and Smith, A.D., 1994, Mesozoic granitoid magmatism in southeast British

1380 Columbia: implications for the origin of granitoid belts in the North American Cordillera:  
1381 Journal of Geophysical Research: Solid Earth, v. 99, p. 11879-11896.

1382 Breitsprecher, K., Thorkelson, D.J., Groome, W.G., and Dostal, J., 2003, Geochemical  
1383 confirmation of the Kula-Farallon slab window beneath the Pacific Northwest in Eocene  
1384 time: Geology, v. 31, p. 351-354.

1385 Brown, K.L., Hart, W.K. and Stuck, R.J., 2018, Temporal and geochemical signatures in  
1386 granitoids of northwestern Nevada: Evidence for the continuity of the Mesozoic  
1387 magmatic arc through the western Great Basin: Lithosphere, v. 10, p. 327-350.

1388 Bryant, B., and Wooden, J.L., 2008, Geology of the Northern Part of the Harcuvar Complex,  
1389 West-Central Arizona: U.S. Geological Survey Professional Paper 1752, 52p.

1390 Burchfiel, B.C. and Davis, G.A., 1975, Nature and controls of Cordilleran orogenesis, western  
1391 United States: Extensions of an earlier synthesis: American Journal of Science, v. 275, p.  
1392 363-396.

1393 Burri, T., Berger, A., and Engi, M., 2005, Tertiary migmatites in the Central Alps: regional  
1394 distribution, field relations, conditions of formation, and tectonic implications:  
1395 Schweizerische Mineralogische und Petrographische Mitteilungen, v. 85, p. 215-232.

1396 Butcher, L.A., Mahan, K.H. and Allaz, J.M., 2017, Late Cretaceous crustal hydration in the  
1397 Colorado Plateau, USA, from xenolith petrology and monazite geochronology:  
1398 Lithosphere, v. 9, p. 561-578.

1399 Camilleri, P.A. and Chamberlain, K.R., 1997, Mesozoic tectonics and metamorphism in the  
1400 Pequop Mountains and Wood Hills region, northeast Nevada: Implications for the  
1401 architecture and evolution of the Sevier orogen: Geological Society of America Bulletin,  
1402 v. 109, p. 74-94.

- 1403 Campbell-Stone, E., John, B.E., Foster, D.A., Geissman, J.W. and Livaccari, R.F., 2000,  
1404 Mechanisms for accommodation of Miocene extension: Low-angle normal faulting,  
1405 magmatism, and secondary breakaway faulting in the southern Sacramento Mountains,  
1406 southeastern California: *Tectonics*, v. 19, p. 566-587.
- 1407 Carl, B.S., Miller, C.F., and Foster, D.A., 1991, Western Old Woman Mountains shear zone:  
1408 Evidence for late ductile extension in the Cordilleran orogenic belt: *Geology*, v. 19, p.  
1409 893-896.
- 1410 Carlson, D.H., Fleck, R., Moye, F.J., and Fox, K.F., 1991, Geology, geochemistry, and isotopic  
1411 character of the Colville Igneous Complex, northeastern Washington: *Journal of*  
1412 *Geophysical Research: Solid Earth*, v. 96, p. 13313-13333.
- 1413 Carter, T.J., Kohn, B.P., Foster, D.A., Gleadow, A.J. and Woodhead, J.D., 2006, Late-stage  
1414 evolution of the Chemehuevi and Sacramento detachment faults from apatite (U-Th)/He  
1415 thermochronometry—Evidence for mid-Miocene accelerated slip: *Geological Society of*  
1416 *America Bulletin*, v. 118, p. 689-709.
- 1417 Cassel, E.J., Smith, M.E., and Jicha, B.R., 2018, The impact of slab rollback on earth's surface:  
1418 uplift and extension in the hinterland of the North American Cordillera: *Geophysical*  
1419 *Research Letters*, v. 45.
- 1420 Castro, A., 2013, Tonalite–granodiorite suites as cotectic systems: a review of experimental  
1421 studies with applications to granitoid petrogenesis: *Earth-Science Reviews*, v. 124, p. 68-  
1422 95.
- 1423 Castro, A., Douce, A.E.P., Corretgé, L.G., Jesús, D., El-Biad, M., and El-Hmidi, H., 1999,  
1424 Origin of peraluminous granites and granodiorites, Iberian massif, Spain: an experimental  
1425 test of granite petrogenesis: *Contributions to Mineralogy and Petrology*, v. 135, p. 255-

1426 276.

1427 Cawthorn, R.G. and Brown, P.A., 1976, A model for the formation and crystallization of  
1428 corundum-normative calc-alkaline magmas through amphibole fractionation: *The Journal*  
1429 *of Geology*, v. 84, p. 467-476.

1430 Cecil, M.R., Rotberg, G.L., Ducea, M.N., Saleeby, J.B., and Gehrels, G.E., 2012, Magmatic  
1431 growth and batholithic root development in the northern Sierra Nevada, California:  
1432 *Geosphere*, v. 8, p. 592-606.

1433 Chapman, J.B., Dafon, M.N., Gehrels, G., Ducea, M.N., Valley, J.W. and Ishida, A., 2018,  
1434 Lithospheric architecture and tectonic evolution of the southwestern US Cordillera:  
1435 Constraints from zircon Hf and O isotopic data: *Geological Society of America Bulletin*,  
1436 v. 130, p. 2031-2046.

1437 Chapman, J.B., Ducea, M.N., DeCelles, P.G. and Profeta, L., 2015, Tracking changes in crustal  
1438 thickness during orogenic evolution with Sr/Y: An example from the North American  
1439 Cordillera; *Geology*, v. 43, p. 919-922.

1440 Chapman, J.B., Greig, R. and Haxel, G.B., 2020, Geochemical evidence for an orogenic plateau  
1441 in the southern US and northern Mexican Cordillera during the Laramide orogeny:  
1442 *Geology*, v. 48, p. 164-168.

1443 Chappell, B.W. and White, A.J., 2001, Two contrasting granite types: 25 years later: *Australian*  
1444 *Journal of Earth Sciences*, v. 48, p. 489-499.

1445 Chappell, B.W., Bryant, C.J. and Wyborn, D., 2012, Peraluminous I-type granites: *Lithos*, v.  
1446 153, p. 142-153.

1447 Chappell, B.W., White, A.J.R., and Wyborn, D., 1987, The importance of residual source  
1448 material (restite) in granite petrogenesis: *Journal of Petrology* v. 28, p. 11–38.

- 1449 Chen, J.H. and Moore, J.G., 1982, Uranium-lead isotopic ages from the Sierra Nevada batholith,  
1450 California: *Journal of Geophysical Research: Solid Earth*, v. 87, p. 4761-4784.
- 1451 Clark, C., Fitzsimons, I.C., Healy, D. and Harley, S.L., 2011, How does the continental crust get  
1452 really hot?: *Elements*, v. 7, p. 235-240.
- 1453 Clarke, D.B., 2019, The origins of strongly peraluminous granitoid rocks: *The Canadian*  
1454 *Mineralogist*, v. 57, p. 529-550.
- 1455 Clarke, G.L., Daczko, N.R., Klepeis, K.A. and Rushmer, T., 2005, Roles for fluid and/or melt  
1456 advection in forming high-P mafic migmatites, Fiordland, New Zealand: *Journal of*  
1457 *Metamorphic Geology*, v. 23, p. 557-567.
- 1458 Clemens, J.D. and Droop, G.T.R., 1998, Fluids, P–T paths and the fates of anatectic melts in the  
1459 Earth's crust: *Lithos*, v. 44, p. 21-36.
- 1460 Clemens, J.D. and Stevens, G., 2012, What controls chemical variation in granitic magmas?:  
1461 *Lithos*, v. 134–135, p. 317–329.
- 1462 Clemens, J.D. and Vielzeuf, D., 1987, Constraints on melting and magma production in the  
1463 crust: *Earth and Planetary Science Letters*, v. 86, p. 287-306.
- 1464 Collins, W.J., 1996, Lachlan Fold Belt granitoids: products of three-component mixing:  
1465 *Transactions of the Royal Society of Edinburgh: Earth Sciences* v. 87, p. 171–181.
- 1466 Collins, W.J., Huang, H.Q. and Jiang, X., 2016, Water-fluxed crustal melting produces  
1467 Cordilleran batholiths: *Geology*, v. 44, p. 143-146.
- 1468 Coney, P.J. and Harms, T.A., 1984, Cordilleran metamorphic core complexes: Cenozoic  
1469 extensional relics of Mesozoic compression: *Geology*, v. 12, p. 550-554.
- 1470 Coney, P.J. and Reynolds, S.J., 1977, Cordilleran Benioff zones: *Nature*, v. 270, p. 403-406.
- 1471 Connolly, J.A.D. and Pettrini, K., 2002, An automated strategy for calculation of phase diagram



1472 sections and retrieval of rock properties as a function of physical conditions: *Journal of*  
1473 *Metamorphic Geology*, v. 20, p. 697-708.

1474 Connolly, J.A.D., 1990, Multivariable phase diagrams; an algorithm based on generalized  
1475 thermodynamics: *American Journal of Science*, v. 290, p. 666-718.

1476 Connolly, J.A.D., 2005, Computation of phase equilibria by linear programming: A tool for  
1477 geodynamic modeling and its application to subduction zone decarbonation: *Earth and*  
1478 *Planetary Science Letters*, v. 236, p. 524-541.

1479 Conrad, W.K., Nicholls, I.A. and Wall, V.J., 1988, Water-saturated and-undersaturated melting  
1480 of metaluminous and peraluminous crustal compositions at 10 kb: evidence for the origin  
1481 of silicic magmas in the Taupo Volcanic Zone, New Zealand, and other occurrences:  
1482 *Journal of Petrology*, v. 29, p. 765-803.

1483 Constenius, K.N., 1996, Late Paleogene extensional collapse of the Cordilleran foreland fold and  
1484 thrust belt: *Geological Society of America Bulletin*, v. 108, p. 20-39.

1485 Constenius, K.N., Esser, R.P., and Layer, P.W., 2003, Extensional collapse of the Charleston-  
1486 Nebo salient and its relationship to space-time variations in Cordilleran orogenic belt  
1487 tectonism and continental stratigraphy, *in*, Reynolds, R.G. and Flores, R.M., eds.,  
1488 *Cenozoic Systems of the Rocky Mountain Region: SEPM Rocky Mountain Section*, p.  
1489 303-353.

1490 Cooper, F.J., Platt, J.P., Anczkiewicz, R. and Whitehouse, M.J., 2010, Footwall dip of a core  
1491 complex detachment fault: Thermobarometric constraints from the northern Snake Range  
1492 (Basin and Range, USA): *Journal of Metamorphic Geology*, v. 28, p. 997-1020.

1493 Cooper, J.R. and Silver, L.T., 1964, *Geology and ore deposits of the Dragoon quadrangle,*  
1494 *Cochise County, Arizona: U.S. Geological Survey Professional Paper*, v. 416, p. 165-168.

- 1495 Copeland, P. and Condie, K.C., 1986, Geochemistry and tectonic setting of lower Proterozoic  
1496 supracrustal rocks of the Pinal Schist, southeastern Arizona: Geological Society of  
1497 America Bulletin, v. 97, p. 1512-1520.
- 1498 Crowley, J.L., Brown, R.L. and Parrish, R.R., 2001, Diachronous deformation and a strain  
1499 gradient beneath the Selkirk allochthon, northern Monashee complex, southeastern  
1500 Canadian Cordillera: Journal of Structural Geology, v. 23, p. 1103-1121.
- 1501 Crowley, J.L., Brown, R.L., Gervais, F. and Gibson, H.D., 2008, Assessing inheritance of zircon  
1502 and monazite in granitic rocks from the Monashee Complex, Canadian Cordillera:  
1503 Journal of Petrology, v. 49, p. 1915-1929.
- 1504 Cubley, J.F., Pattison, D.R., Tinkham, D.K., and Fanning, C.M., 2013, U–Pb geochronological  
1505 constraints on the timing of episodic regional metamorphism and rapid high-T  
1506 exhumation of the Grand Forks complex, British Columbia: Lithos, v. 156, p. 241-267.
- 1507 Currie, C.A. and Hyndman, R.D., 2006, The thermal structure of subduction zone back arcs:  
1508 Journal of Geophysical Research: Solid Earth, v. 111.
- 1509 Davis, G.H., 1979, Laramide folding and faulting in southeastern Arizona: American Journal of  
1510 Science, v. 279, p. 543-569.
- 1511 Davis, G.H., Spencer, J.E., and Gehrels, G.E., 2019, Field-trip guide to the Catalina-Rincon  
1512 metamorphic core complex, Tucson, Arizona: Geologic Excursions in Southwestern  
1513 North America, Geological Society of America Field Trip Guide, v. 55.
- 1514 DeCelles, P.G. and Coogan, J.C., 2006, Regional structure and kinematic history of the Sevier  
1515 fold-and-thrust belt, central Utah: Geological Society of America Bulletin, v. 118, p. 841-  
1516 864.
- 1517 DeCelles, P.G., 2004, Late Jurassic to Eocene evolution of the Cordilleran thrust belt and

1518 foreland basin system, western USA: *American Journal of Science*, v. 304, p. 105-168.

1519 DePaolo, D.J., 1981, Trace element and isotopic effects of combined wallrock assimilation and  
1520 fractional crystallization: *Earth and Planetary Science Letters*, v. 53, p. 189-202.

1521 Dewey, J.F., 1988, Extensional collapse of orogens: *Tectonics*, v. 7, p. 1123-1139.

1522 Dewitt, Ed, and Reynolds, S.J., 1990, Late Cretaceous plutonism and cooling in the Maria fold  
1523 and thrust belt, west-central Arizona: *Geological Society of America Abstracts with*  
1524 *Programs*, v. 22, n. 3, p. 18.

1525 Dickinson, W.R. and Snyder, W.S., 1978, Plate tectonics of the Laramide orogeny, *in*, Matthews,  
1526 V., ed., *Laramide Folding Associated with Basement Block Faulting in the Western*  
1527 *United States: Geological Society of America Memoir 151*, p. 355-366.

1528 Dickinson, W.R., 2004, Evolution of the North American Cordillera: *Annual Review of Earth*  
1529 *and Planetary Sciences*, v. 32, p. 13-45.

1530 Dickinson, W.R., 2006, Geotectonic evolution of the Great Basin: *Geosphere*, v. 2, p. 353-368.

1531 Dickinson, W.R., Kay, S.M., and Ramos, V.A., 2009, Anatomy and global context of the North  
1532 American Cordillera. Backbone of the Americas: Shallow subduction, plateau uplift, and  
1533 ridge and terrane collision: *Geological Society of America Memoir*, v. 204, p. 1-29.

1534 Doughty, P.T., and Chamberlain, K.R., 2007, Age of Paleoproterozoic basement and related  
1535 rocks in the Clearwater complex, northern Idaho, U.S.A., *in*, Link, P.K., and Lewis, R.L.,  
1536 eds., *Proterozoic geology of western North America and Siberia: Society of Economic*  
1537 *Paleontologists and Mineralogists Special Publication 86*, p. 9–35.

1538 Droop, G.T.R. and Brodie, K.H., 2012, Anatectic melt volumes in the thermal aureole of the  
1539 Etive Complex, Scotland: The roles of fluid-present and fluid-absent melting: *Journal of*  
1540 *Metamorphic Geology*, v. 30, p. 843–864.

1541 Druschke, P., Hanson, A.D., Wells, M.L., Rasbury, T., Stockli, D.F. and Gehrels, G., 2009,  
1542 Synconvergent surface-breaking normal faults of Late Cretaceous age within the Sevier  
1543 hinterland, east-central Nevada: *Geology*, v. 37, p. 447-450.

1544 du Bray, E.A., Ressel, M.W., and Barnes, C.G., 2007, Geochemical database for intrusive rocks  
1545 of north-central and northeast Nevada: U.S. Geological Survey Data Series 244.

1546 Dumitru, T.A., Gans, P.B., Foster, D.A. and Miller, E.L., 1991, Refrigeration of the western  
1547 Cordilleran lithosphere during Laramide shallow-angle subduction: *Geology*, v. 19, p.  
1548 1145-1148.

1549 Duncan, I.J., 1984, Structural evolution of the Thor-Odin gneiss dome: *Tectonophysics*, v. 101,  
1550 p. 87-130.

1551 Economos, R.C., Barth, A.P., Wooden, J.L., Howard, K.A., and Wiegand, B.A., 2010,  
1552 Comparing batholith-source connections for the Cadiz Valley Batholith and a deeper  
1553 sheeted intrusive complex in the Mojave Desert, CA through whole rock and pre-  
1554 magmatic zircon geochemistry: Abstract V51E-02, 2010 AGU Annual Fall Meeting, San  
1555 Francisco, California.

1556 Egger, A.E., Dumitru, T.A., Miller, E.L., Savage, C.F., and Wooden, J.L., 2003, Timing and  
1557 nature of Tertiary plutonism and extension in the Grouse Creek Mountains, Utah:  
1558 *International Geology Review*, v. 45, p. 497-532.

1559 Elison, M.W., 1995, Causes and consequences of Jurassic magmatism in the northern Great  
1560 Basin: Implications for tectonic development, *in*, Miller, D.M. and Busby, C., eds.,  
1561 Jurassic Magmatism and Tectonics of the North American Cordillera, Geological Society  
1562 of America Special Paper, v. 299, p. 249-265.

1563 England, P. and Houseman, G., 1989, Extension during continental convergence, with

1564 application to the Tibetan Plateau: *Journal of Geophysical Research: Solid Earth*, v. 94, p.  
1565 17561-17579.

1566 England, P.C. and Thompson, A., 1984, Pressure-temperature-time paths of regional  
1567 metamorphism I. Heat transfer during the evolution of regions of thickened continental  
1568 crust: *Journal of Petrology*, v. 25, p. 894-928.

1569 England, P.C. and Thompson, A., 1986, Some thermal and tectonic models for crustal melting in  
1570 continental collision zones: *Geological Society, London, Special Publications*, v. 19, p.  
1571 83-94.

1572 English, J.M., Johnston, S.T., and Wang, K., 2003, Thermal modelling of the Laramide orogeny:  
1573 testing the flat-slab subduction hypothesis: *Earth and Planetary Science Letters*, v. 214, p.  
1574 619-632.

1575 Erdman, M.E., Lee, C.T.A., Levander, A., and Jiang, H., 2016, Role of arc magmatism and  
1576 lower crustal foundering in controlling elevation history of the Nevadaplano and  
1577 Colorado Plateau: A case study of pyroxenitic lower crust from central Arizona, USA:  
1578 *Earth and Planetary Science Letters*, v. 439, p. 48-57.

1579 Evans, S.L., Styron, R.H., van Soest, M.C., Hodges, K.V. and Hanson, A.D., 2015, Zircon and  
1580 apatite (U-Th)/He evidence for Paleogene and Neogene extension in the Southern Snake  
1581 Range, Nevada, USA: *Tectonics*, v. 34, p. 2142-2164.

1582 Farmer, G.L. and DePaolo, D.J., 1983, Origin of Mesozoic and Tertiary granite in the western  
1583 United States and implications for Pre-Mesozoic crustal structure: 1. Nd and Sr isotopic  
1584 studies in the geocline of the Northern Great Basin: *Journal of Geophysical Research:*  
1585 *Solid Earth*, v. 88, p. 3379-3401.

1586 Farmer, G.L. and DePaolo, D.J., 1984, Origin of Mesozoic and Tertiary granite in the western

1587 United States and implications for Pre-Mesozoic crustal structure: 2. Nd and Sr isotopic  
1588 studies of unmineralized and Cu-and Mo-mineralized granite in the Precambrian Craton:  
1589 Journal of Geophysical Research: Solid Earth, v. 89, p. 10141-10160.

1590 Farmer, G.L., Bailey, T., and Elkins-Tanton, L.T., 2008, Mantle source volumes and the origin  
1591 of the mid-Tertiary ignimbrite flare-up in the southern Rocky Mountains, western US:  
1592 Lithos, v. 102, p. 279-294.

1593 Fayon, A.K., Peacock, S.M., Stump, E. and Reynolds, S.J., 2000, Fission track analysis of the  
1594 footwall of the Catalina detachment fault, Arizona: Tectonic denudation, magmatism, and  
1595 erosion: Journal of Geophysical Research: Solid Earth, v. 105, p. 11047-11062.

1596 Ferguson, C.A., Johnson, B.J., Skotnicki, J.S., Maher, J.D., Spencer, J.E., Gilbert, W.G.,  
1597 Richard, S.M., Youberg, A., Demsey, K.A. and House, P.K., 2003, Geologic Map of the  
1598 Tortolita Mountains, Pinal and Pima Counties, Arizona: Arizona Geological Survey  
1599 Digital Geologic Map DGM-26.

1600 Ferrari, L., López-Martínez, M., and Rosas-Elguera, J., 2002, Ignimbrite flare-up and  
1601 deformation in the southern Sierra Madre Occidental, western Mexico: Implications for  
1602 the late subduction history of the Farallon plate: Tectonics, v. 21.

1603 Fitz-Díaz, E., Lawton, T.F., Juárez-Arriaga, E. and Chávez-Cabello, G., 2018. The Cretaceous-  
1604 Paleogene Mexican orogen: Structure, basin development, magmatism and tectonics:  
1605 Earth-Science Reviews, v. 183, p. 56-84.

1606 Fitzgerald, P.G., Reynolds, S.J., Stump, E., Foster, D.A. and Gleadow, A.J.W., 1993,  
1607 Thermochronologic evidence for timing of denudation and rate of crustal extension of the  
1608 South Mountains metamorphic core complex and Sierra Estrella, Arizona: Nuclear  
1609 Tracks and Radiation Measurements, v. 21, p. 555-563.

1610 Force, E.R., 1997, Geology and mineral resources of the Santa Catalina Mountains, Southeastern  
1611 Arizona: a cross-sectional approach: Mineral Resource Science Monograph, v. 1., Center  
1612 for Mineral Resources, University of Arizona, 135p.

1613 Fornash, K. F., Patchett, P. J., Gehrels, G. E., and Spencer, J.E., 2013, Evolution of granitoids in  
1614 the Catalina metamorphic core complex, southeastern Arizona: U-Pb, Nd, and Hf isotopic  
1615 constraints: Contributions to Mineralogy and Petrology, v. 165, p. 1295–1310.

1616 Foster, D.A. and Fanning, M.C., 1997, Geochronology of the northern Idaho batholith and the  
1617 Bitterroot metamorphic core complex: Magmatism preceding and contemporaneous with  
1618 extension: Geological Society of America Bulletin, v. 109, p. 379-394.

1619 Foster, D.A. and John, B.E., 1999, Quantifying tectonic exhumation in an extensional orogen  
1620 with thermochronology: examples from the southern Basin and Range Province:  
1621 Geological Society, London, Special Publications, v. 154, p. 343-364.

1622 Foster, D.A., Doughty, P.T., Kalakay, T.J., Fanning, C.M., Coyner, S., Grice, W.C., Vogl, J.,  
1623 Till, A.B., Roeske, S.M. and Sample, J.C., 2007, Kinematics and timing of exhumation of  
1624 metamorphic core complexes along the Lewis and Clark fault zone, northern Rocky  
1625 Mountains, USA, *in*, Till, A.B., ed., Exhumation associated with continental strike-slip  
1626 fault systems: Geological Society of America Special Paper, v. 434, p. 207-232.

1627 Foster, D.A., Grice, W.C. and Kalakay, T.J., 2010, Extension of the Anaconda metamorphic core  
1628 complex:  $^{40}\text{Ar}/^{39}\text{Ar}$  thermochronology and implications for Eocene tectonics of the  
1629 northern Rocky Mountains and the Boulder batholith: Lithosphere, v. 2, p. 232-246.

1630 Foster, D.A., Harrison, T.M. and Miller, C.F., 1989, Age, inheritance, and uplift history of the  
1631 Old Woman-Piute batholith, California and implications for K-feldspar age spectra; The  
1632 Journal of Geology, v. 97, p. 232-243.

- 1633 Foster, D.A., Harrison, T.M., Miller, C.F. and Howard, K.A., 1990, The  $^{40}\text{Ar}/^{39}\text{Ar}$   
1634 thermochronology of the eastern Mojave Desert, California, and adjacent western  
1635 Arizona with implications for the evolution of metamorphic core complexes: *Journal of*  
1636 *Geophysical Research: Solid Earth*, v. 95, p. 20005-20024.
- 1637 Foster, D.A., Schafer, C., Fanning, C.M. and Hyndman, D.W., 2001, Relationships between  
1638 crustal partial melting, plutonism, orogeny, and exhumation: Idaho–Bitterroot batholith:  
1639 *Tectonophysics*, v. 342, p. 313-350.
- 1640 Frost, B.R., Barnes, C.G., Collins, W.J., Arculus, R.J., Ellis, D.J. and Frost, C.D., 2001, A  
1641 geochemical classification for granitic rocks: *Journal of Petrology*, v. 42, p. 2033-2048.
- 1642 Fryxell, J.E., 1988, Geologic map and description of stratigraphy and structure of the west-  
1643 central Grant Range, Nye County, Nevada: Geological Society of America Map and  
1644 Chart Series MCH064, 16p.
- 1645 Fuentes, F., DeCelles, P.G. and Constenius, K.N., 2012, Regional structure and kinematic history  
1646 of the Cordilleran fold-thrust belt in northwestern Montana, USA: *Geosphere*, v. 8, p.  
1647 1104-1128.
- 1648 Gans, P.B. and Gentry, B.J., 2016, Dike emplacement, footwall rotation, and the transition from  
1649 magmatic to tectonic extension in the Whipple Mountains metamorphic core complex,  
1650 southeastern California: *Tectonics*, v. 35, p. 2564-2608.
- 1651 Gans, P.B., 1989, Synextensional magmatism in the Basin and Range province: A case study  
1652 from the eastern Great Basin: *Geological Society of America Special Paper*, v. 233, 53p.
- 1653 Gao, P., Zheng, Y.F. and Zhao, Z.F., 2016, Experimental melts from crustal rocks: a  
1654 lithochemical constraint on granite petrogenesis; *Lithos*, v. 266, p. 133-157.
- 1655 Gaschnig, R.M., Vervoort, J.D., Lewis, R.S. and Tikoff, B., 2011, Isotopic evolution of the Idaho



1656 batholith and Challis intrusive province, northern US Cordillera: *Journal of Petrology*, v.  
1657 52, p. 2397-2429.

1658 Gaschnig, R.M., Vervoort, J.D., Lewis, R.S. and Tikoff, B., 2013, Probing for Proterozoic and  
1659 Archean crust in the northern US Cordillera with inherited zircon from the Idaho  
1660 batholith: *Geological Society of America Bulletin*, v. 125, p. 73-88.

1661 Gaschnig, R.M., Vervoort, J.D., Lewis, R.S., and McClelland, W.C., 2010, Migrating  
1662 magmatism in the northern US Cordillera: in situ U–Pb geochronology of the Idaho  
1663 batholith: *Contributions to Mineralogy and Petrology*, v. 159, p. 863-883.

1664 Gehrels, G., Rusmore, M., Woodsworth, G., Crawford, M., Andronicos, C., Hollister, L.,  
1665 Patchett, J., Ducea, M., Butler, R., Klepeis, K., and Davidson, C., 2009, U-Th-Pb  
1666 geochronology of the Coast Mountains batholith in north-coastal British Columbia:  
1667 Constraints on age and tectonic evolution: *Geological Society of America Bulletin*, v.  
1668 121, p. 1341-1361.

1669 Genier, F., Bussy, F., Epard, J.L., and Baumgartner, L., 2008, Water-assisted migmatization of  
1670 metagraywackes in a Variscan shear zone, Aiguilles–Rouges massif, western Alps:  
1671 *Lithos*, v. 102, p. 575–597.

1672 Gervais, F. and Brown, R.L., 2011, Testing modes of exhumation in collisional orogens:  
1673 Synconvergent channel flow in the southeastern Canadian Cordillera: *Lithosphere*, v. 3,  
1674 p. 55-75.

1675 Gervasoni, F., Klemme, S., Rocha-Júnior, E.R., and Berndt, J., 2016, Zircon saturation in silicate  
1676 melts: a new and improved model for aluminous and alkaline melts: *Contributions to*  
1677 *Mineralogy and Petrology*, v. 171, n. 21.

1678 Ghosh, D.K. 1995, U–Pb geochronology of Jurassic to early Tertiary granitic intrusives from the

1679 Nelson-Castlegar area, southeastern British Columbia, Canada: *Canadian Journal of*  
1680 *Earth Sciences*, v. 32, p. 1668–1680.

1681 Giallorenzo, M.A., Wells, M.L., Yonkee, W.A., Stockli, D.F. and Wernicke, B.P., 2018, Timing  
1682 of exhumation, Wheeler Pass thrust sheet, southern Nevada and California: Late Jurassic  
1683 to middle Cretaceous evolution of the southern Sevier fold-and-thrust belt: *Geological*  
1684 *Society of America Bulletin*, v. 130, p. 558-579.

1685 González-Becuar, E., Pérez-Segura, E., Vega-Granillo, R., Solari, L., González-León, C.M.,  
1686 Solé, J. and Martínez, M.L., 2017, Laramide to Miocene syn-extensional plutonism in the  
1687 Puerta del Sol area, central Sonora, Mexico: *Revista Mexicana de Ciencias Geológicas*, v.  
1688 34, p. 45-61.

1689 González-León, C.M., Solari, L., Solé, J., Ducea, M.N., Lawton, T.F., Bernal, J.P., Becuar, E.G.,  
1690 Gray, F., Martínez, M.L. and Santacruz, R.L., 2011, Stratigraphy, geochronology, and  
1691 geochemistry of the Laramide magmatic arc in north-central Sonora, Mexico: *Geosphere*,  
1692 v. 7, p. 1392-1418.

1693 Goodwin, L.B. and Haxel, G.B., 1990, Structural evolution of the Southern Baboquivari  
1694 Mountains, south-central Arizona and north-central Sonora: *Tectonics*, v. 9, p. 1077-  
1695 1095.

1696 Gordon, S.M., Whitney, D.L., Teyssier, C., Grove, M. and Dunlap, W.J., 2008, Timescales of  
1697 migmatization, melt crystallization, and cooling in a Cordilleran gneiss dome: Valhalla  
1698 complex, southeastern British Columbia: *Tectonics*, v. 27.

1699 Gottardi, R., McAleer, R., Casale, G., Borel, M., Iriondo, A. and Jepson, G., 2020, Exhumation  
1700 of the Coyote Mountains metamorphic core complex (Arizona): implications for orogenic  
1701 collapse of the southern North American Cordillera: *Tectonics*, 2019TC006050.

- 1702 Gottlieb, E.S., 2017, Geologic insights from zircon inheritance, Ph.D. dissertation, Stanford  
1703 University, 354p.
- 1704 Grice, W.C., 2006, Exhumation and cooling history of the Middle Eocene Anaconda  
1705 metamorphic core complex, western Montana: University of Florida, PhD Dissertation.
- 1706 Grijalva-Noriega, F.J., and Roldan-Quintana, J, 1998, An overview of the Cenozoic tectonic and  
1707 magmatic evolution of Sonora, northwestern Mexico: *Revista Mexicana de Ciencias*  
1708 *Geológicas*, v. 15, p.145-156.
- 1709 Guevara, V., 2012, Structural, thermochronological, and stratigraphic constraints on the  
1710 evolution of the Clearwater metamorphic core complex, Idaho.; University of Montana,  
1711 MS Thesis.
- 1712 Hallett, B.W. and Spear, F.S., 2014, The P–T history of anatectic pelites of the Northern East  
1713 Humboldt Range, Nevada: Evidence for tectonic loading, decompression, and anatexis:  
1714 *Journal of Petrology*, v. 55, p. 3-36.
- 1715 Hallett, B.W. and Spear, F.S., 2015, Monazite, zircon, and garnet growth in migmatitic pelites as  
1716 a record of metamorphism and partial melting in the East Humboldt Range, Nevada:.  
1717 *American Mineralogist*, v. 100, p. 951-972.
- 1718 Hamilton, W., 1987, Mesozoic geology and tectonics of the Big Maria Mountains region,  
1719 southeastern California. *Mesozoic rocks of southern Arizona and adjacent areas: Arizona*  
1720 *Geological Society Digest*, v. 18, p. 33-47.
- 1721 Haney, E.M., 2008, Pressure-temperature evolution of metapelites within the Anaconda  
1722 metamorphic core complex, southwestern Montana: University of Montana, M.S. thesis.
- 1723 Harris, N. and Massey, J., 1994, Decompression and anatexis of Himalayan metapelites:  
1724 *Tectonics*, v. 13, p. 1537-1546.

- 1725 Harris, N., Massey, J. and Inger, S., 1993, The role of fluids in the formation of High Himalayan  
1726 leucogranites: Geological Society, London, Special Publications, v. 74, p. 391-400.
- 1727 Harris, N.B.W. and Inger, S., 1992, Trace element modelling of pelite-derived granites:  
1728 Contributions to Mineralogy and Petrology, v. 110, p. 46-56.
- 1729 Hawkesworth, C., Turner, S., Gallagher, K., Hunter, A., Bradshaw, T. and Rogers, N., 1995,  
1730 Calc-alkaline magmatism, lithospheric thinning and extension in the Basin and Range:  
1731 Journal of Geophysical Research: Solid Earth, v. 100, p. 10271-10286.
- 1732 Haxel, G.B., Tosdal, R.M., May, D.J. and Wright, J.E., 1984, Latest Cretaceous and early  
1733 Tertiary orogenesis in south-central Arizona: Thrust faulting, regional metamorphism,  
1734 and granitic plutonism: Geological Society of America Bulletin, v. 95, p. 631-653.
- 1735 Hayama, Y., Shibata, K. and Takeda, H., 1984, K-Ar ages of the low-grade metamorphic rocks  
1736 in the Altar massif, northwest Sonora, Mexico: Journal of the Geological Society of  
1737 Japan, v. 90, p. 589-596.
- 1738 Henry, C.D. and John, D.A., 2013, Magmatism, ash-flow tuffs, and calderas of the ignimbrite  
1739 flareup in the western Nevada volcanic field, Great Basin, USA: Geosphere, v. 9, p. 951-  
1740 1008.
- 1741 Henry, C.D., McGrew, A.J., Colgan, J.P., Snoke, A.W., Brueseke, M.E., Lee, J., and Evans, J.P.,  
1742 2011, Timing, distribution, amount, and style of Cenozoic extension in the northern Great  
1743 Basin. Geologic Field Trips to the Basin and Range, Rocky Mountains, Snake River  
1744 Plain, and Terranes of the US Cordillera: Geological Society of America Field Guide, v.  
1745 21, p. 27-66.
- 1746 Hinchey, A.M., and Carr, S.D., 2006, The S-type Ladybird leucogranite suite of southeastern  
1747 British Columbia: Geochemical and isotopic evidence for a genetic link with migmatite

1748 formation in the North American basement gneisses of the Monashee complex: *Lithos*, v.  
1749 90, p. 223-248

1750 Hinchey, A.M., Carr, S.D., McNeill, P.D., and Rayner, N., 2006, Paleocene–Eocene high-grade  
1751 metamorphism, anatexis, and deformation in the Thor–Odin dome, Monashee complex,  
1752 southeastern British Columbia: *Canadian Journal of Earth Sciences*, v. 43, p. 1341-1365.

1753 Hodges, K.V. and Walker, J.D., 1990, Petrologic constraints on the unroofing history of the  
1754 Funeral Mountain metamorphic core complex, California: *Journal of Geophysical  
1755 Research: Solid Earth*, v. 95, p. 8437-8445.

1756 Hodges, K.V. and Walker, J.D., 1992, Extension in the Cretaceous Sevier orogen, North  
1757 American Cordillera: *Geological Society of America Bulletin*, v. 104, p. 560-569.

1758 Hodges, K.V., Snoke, A.W. and Hurlow, H.A., 1992, Thermal evolution of a portion of the  
1759 Sevier hinterland: the northern Ruby Mountains-East Humboldt Range and Wood Hills,  
1760 northeastern Nevada: *Tectonics*, v. 11, p. 154-164.

1761 Hoisch, T.D. and Simpson, C., 1993, Rise and tilt of metamorphic rocks in the lower plate of a  
1762 detachment fault in the Funeral Mountains, Death Valley, California: *Journal of  
1763 Geophysical Research: Solid Earth*, v. 98, p. 6805-6827.

1764 Hoisch, T.D., 1987, Heat transport by fluids during Late Cretaceous regional metamorphism in  
1765 the Big Maria Mountains, southeastern California: *Geological Society of America  
1766 Bulletin*, v. 98, p. 549-553.

1767 Hoisch, T.D., Wells, M.L., Beyene, M.A., Styger, S. and Vervoort, J.D., 2014, Jurassic  
1768 Barrovian metamorphism in a western US Cordilleran metamorphic core complex,  
1769 Funeral Mountains, California: *Geology*, v. 42, p. 399-402.

1770 Holk, G.J. and Taylor Jr, H.P., 1997,  $^{18}\text{O}/^{16}\text{O}$  homogenization of the middle crust during

1771 anatexis: The Thor-Odin metamorphic core complex, British Columbia: *Geology*, v. 25,  
1772 p. 31-34.

1773 Holk, G.J. and Taylor Jr, H.P., 2000, Water as a petrologic catalyst driving  $^{18}\text{O}/^{16}\text{O}$   
1774 homogenization and anatexis of the middle crust in the metamorphic core complexes of  
1775 British Columbia: *International Geology Review*, v. 42, p. 97-130.

1776 Holland, T.J.B. and Powell, R., 2011, An improved and extended internally consistent  
1777 thermodynamic dataset for phases of petrological interest, involving a new equation of  
1778 state for solids: *Journal of Metamorphic Geology*, v. 29, p. 333-383.

1779 Holm, D.K. and Dokka, R.K., 1991, Major late Miocene cooling of the middle crust associated  
1780 with extensional orogenesis in the Funeral Mountains, California: *Geophysical Research*  
1781 *Letters*, v. 18, p. 1775-1778.

1782 Holtz, F. and Johannes, W., 1991, Genesis of peraluminous granites I. Experimental  
1783 investigation of melt compositions at 3 and 5 kb and various H<sub>2</sub>O activities: *Journal of*  
1784 *Petrology*, v. 32, p. 935-958.

1785 Howard, K.A. and John, B.E., 1987, Crustal extension along a rooted system of imbricate low-  
1786 angle faults: Colorado River extensional corridor, California and Arizona: *Geological*  
1787 *Society, London, Special Publications*, v. 28, p. 299-311.

1788 Howard, K.A., 1980, Metamorphic infrastructure in the northern Ruby Mountains, Nevada, *in*,  
1789 Crittenden, M.D., Coney, P.J., and Davis, G.H., eds., *Cordilleran metamorphic core*  
1790 *complexes: Geological Society of America Memoir*, v. 153, p. 335-347.

1791 Howard, K.A., 2002, *Geologic Map of the Sheep Hole Mountains 30'x 60'quadrangle, San*  
1792 *Bernardino and Riverside Counties, California: U.S. Geological Survey Geologic*  
1793 *Investigations Series I-2344.*

- 1794 Howard, K.A., Wooden, J.L., Barnes, C.G., Premo, W.R., Snoke, A.W. and Lee, S.Y., 2011,  
1795 Episodic growth of a Late Cretaceous and Paleogene intrusive complex of pegmatitic  
1796 leucogranite, Ruby Mountains core complex, Nevada, USA: *Geosphere*, v. 7, p. 1220-  
1797 1248.
- 1798 Humphreys, E., Hessler, E., Dueker, K., Farmer, G.L., Erslev, E. and Atwater, T., 2003, How  
1799 Laramide-age hydration of North American lithosphere by the Farallon slab controlled  
1800 subsequent activity in the western United States: *International Geology Review*, v. 45, p.  
1801 575-595.
- 1802 Humphreys, E.D., 1995, Post-Laramide removal of the Farallon slab, western United States:  
1803 *Geology*, v. 23, p. 987-990.
- 1804 Hyndman, D.W. and Foster, D.A., 1988, The role of tonalites and mafic dikes in the generation  
1805 of the Idaho batholith: *The Journal of Geology*, v. 96, p. 31-46.
- 1806 Hyndman, D.W., 1983. The Idaho Batholith and associated plutons, Idaho and western Montana,  
1807 *in*, Roddick, J.A., ed., *Circum-Pacific Plutonic Terranes*: Geological Society of America,  
1808 *Memoir*, v. 159, p. 213-240.
- 1809 Inger, S. and Harris, N., 1993, Geochemical constraints on leucogranite magmatism in the  
1810 Langtang Valley, Nepal Himalaya: *Journal of Petrology*, v. 34, p. 345-368.
- 1811 Isachsen, C., Gehrels, G., Ferguson, C., Skotnicki, S., Richard, S. M., and Spencer, J. E., 1998,  
1812 U-Pb zircon dates from nine granitic rocks in central and western Arizona: Arizona  
1813 Geological Survey Open-File Report 98, 35p.
- 1814 James, D.E., 1981, The combined use of oxygen and radiogenic isotopes as indicators of crustal  
1815 contamination: *Annual Review of Earth and Planetary Sciences*, v. 9, p. 311-344.
- 1816 Johannes, W., Ehlers, C., Kriegsman, L.M., and Mengel, K., 2003, The link between migmatites

1817 and S-type granites in the Turku area, southern Finland: *Lithos*, v. 68, p. 69-90.

1818 Johannes, W., Holtz, F., 1996, *Petrogenesis and Experimental Petrology of Granitic Rocks*,

1819 Springer, 335p.

1820 John, B.E. and Mukasa, S.B., 1990, Footwall rocks to the Mid-Tertiary Chemehuevi Detachment

1821 Fault: A window into the middle crust in the Southern Cordillera: *Journal of Geophysical*

1822 *Research: Solid Earth*, v. 95, p. 463-485.

1823 John, B.E. and Wooden, J., 1990, Petrology and geochemistry of the metaluminous to

1824 peraluminous Chemehuevi Mountains Plutonic Suite, southeastern California. *The Nature*

1825 *and Origin of Cordilleran Magmatism: Geological Society of America Memoir*, v. 174, p.

1826 71-98.

1827 John, B.E., 1988, Structural reconstruction and zonation of a tilted mid-crustal magma chamber:

1828 *The felsic Chemehuevi Mountains plutonic suite: Geology*, v. 16, p. 613-617.

1829 Johnson, K.M., Lewis, R.S., Bennett, E.H. and Kiilsgaard, T.H., 1988, Cretaceous and Tertiary

1830 intrusive rocks of south-central Idaho. *Guidebook to the geology of central and southern*

1831 *Idaho: Idaho Geological Survey Bulletin*, v. 27, p. 55-86.

1832 Johnson, M. G., 1977, *Geology and mineral deposits of Pershing County, Nevada: Nevada*

1833 *Bureau of Mines and Geology Bulletin*, 89p.

1834 Jones, C.H., Mahan, K.H., Butcher, L.A., Levandowski, W.B. and Farmer, G.L., 2015,

1835 *Continental uplift through crustal hydration: Geology*, v. 43, p. 355-358.

1836 Jones, J.V., 1999, Deformational, magmatic, and metamorphic history of the central Ruby

1837 *Mountains, Elko County, Nevada, M.S. thesis, University of Wyoming.*

1838 Kapp, J.D.A., Miller, C.F. and Miller, J.S., 2002, Ireteba pluton, Eldorado Mountains, Nevada:

1839 *Late, deep-source, peraluminous magmatism in the Cordilleran Interior: The Journal of*



1840 geology, v. 110, p. 649-669.

1841 Keith, S.B., S.J. Reynolds, P.E. Damon, M. Shafiqullah, D.E. Livingston and P.D. Pushkar,  
1842 1980, Evidence for multiple intrusion and deformation within the Santa Catalina Rincon-  
1843 Tortolita crystalline complex, southeastern Arizona, *in*, Crittenden, M.D., Coney, P.J.,  
1844 and Davis, G.H., eds., Cordilleran Metamorphic Core Complexes: Geological Society of  
1845 America Memoir 153, p. 217-267.

1846 Kemp, A.I., Hawkesworth, C.J., Foster, G.L., Paterson, B.A., Woodhead, J.D., Hergt, J.M.,  
1847 Gray, C.M., and Whitehouse, M.J., 2007, Magmatic and crustal differentiation history of  
1848 granitic rocks from Hf–O isotopes in zircon: *Science*, v. 315, p. 980–983.

1849 Ketcham, R.A., 1996, Thermal models of core-complex evolution in Arizona and New Guinea:  
1850 Implications for ancient cooling paths and present-day heat flow: *Tectonics*, v. 15, p.  
1851 933-951.

1852 King, E.M. and Valley, J.W., 2001, The source, magmatic contamination, and alteration of the  
1853 Idaho batholith: *Contributions to Mineralogy and Petrology*, v. 142, p. 72-88.

1854 King, E.M., Valley, J.W., Stockli, D.F. and Wright, J.E., 2004, Oxygen isotope trends of granitic  
1855 magmatism in the Great Basin: Location of the Precambrian craton boundary as reflected  
1856 in zircons: *Geological Society of America Bulletin*, v. 116, p. 451-462.

1857 Kistler, R.W. and Anderson, J.L., 1990, Two different lithosphere types in the Sierra Nevada,  
1858 California. The nature and origin of Cordilleran magmatism: *Geological Society of*  
1859 *America Memoir*, v. 174, p. 271-281.

1860 Kistler, R.W. and Peterman, Z.E., 1973, Variations in Sr, Rb, K, Na, and initial Sr87/Sr86 in  
1861 Mesozoic granitic rocks and intruded wall rocks in central California: *Geological Society*  
1862 *of America Bulletin*, v. 84, p. 3489-3512.

1863 Kistler, R.W., Ghent, E.D. and O'Neil, J.R., 1981, Petrogenesis of garnet two-mica granites in  
1864 the Ruby Mountains, Nevada: *Journal of Geophysical Research: Solid Earth*, v. 86, p.  
1865 10591-10606.

1866 Knapp, J.H. and Heizler, M.T., 1990, Thermal history of crystalline nappes of the Maria fold and  
1867 thrust belt, west central Arizona: *Journal of Geophysical Research: Solid Earth*, v. 95, p.  
1868 20049-20073.

1869 Kohn, M.J., 2014, Himalayan metamorphism and its tectonic implications. *Annual Review of*  
1870 *Earth and Planetary Sciences*, v. 42, p. 381-419.

1871 Konstantinou, A. and Miller, E., 2015, Evidence for a long-lived accommodation/transfer zone  
1872 beneath the Snake River Plain: A possible influence on Neogene magmatism?: *Tectonics*,  
1873 v. 34, p. 2387-2398.

1874 Konstantinou, A., Strickland, A., Miller, E., Vervoort, J., Fisher, C.M., Wooden, J., and Valley,  
1875 J., 2013, Synextensional magmatism leading to crustal flow in the Albion–Raft River–  
1876 Grouse Creek metamorphic core complex, northeastern Basin and Range: *Tectonics*, v.  
1877 32, p. 1384-1403.

1878 Konstantinou, A., Strickland, A., Miller, E.L. and Wooden, J.P., 2012, Multistage Cenozoic  
1879 extension of the Albion–Raft River–Grouse Creek metamorphic core complex:  
1880 *Geochronologic and stratigraphic constraints: Geosphere*, v. 8, p. 1429-1466.

1881 Kruckenberg, S.C., Whitney, D.L., Teyssier, C., Fanning, C.M. and Dunlap, W.J., 2008,  
1882 Paleocene-Eocene migmatite crystallization, extension, and exhumation in the hinterland  
1883 of the northern Cordillera: Okanogan dome, Washington, USA: *Geological Society of*  
1884 *America Bulletin*, v. 120, p. 912-929.

1885 Laberge, J.D. and Pattison, D.R.M., 2007, *Geology of the western margin of the Grand Forks*

1886 complex, southern British Columbia: high-grade Cretaceous metamorphism followed by  
 1887 early Tertiary extension on the Granby fault: *Canadian Journal of Earth Sciences*, v. 44,  
 1888 p. 199-228.

1889 Lang, J.R. and Titley, S.R., 1998, Isotopic and geochemical characteristics of Laramide  
 1890 magmatic systems in Arizona and implications for the genesis of porphyry copper  
 1891 deposits: *Economic Geology*, v. 93, p. 138-170.

1892 Le Breton, N. and Thompson, A.B., 1988, Fluid-absent (dehydration) melting of biotite in  
 1893 metapelites in the early stages of crustal anatexis: *Contributions to Mineralogy and  
 1894 Petrology*, v. 99, p. 226-237.

1895 Le Fort, P., Cuney, M., Deniel, C., France-Lanord, C., Sheppard, S.M.F., Upreti, B.N., and  
 1896 Vidal, P., 1987, Crustal generation of the Himalayan leucogranites: *Tectonophysics*, v.  
 1897 134, p. 39-57.

1898 Leclair, A.D., Parrish, R.R., and Archibald, D.A. 1993, Evidence for Cretaceous deformation in  
 1899 the Kootenay Arc on U-Pb and  $^{40}\text{Ar}/^{39}\text{Ar}$  dating, southeastern British Columbia.  
 1900 *Current Research, Part A: Geological Survey of Canada, Paper 93-1A*, p. 207–220.

1901 Lederer, G.W., Cottle, J.M., Jessup, M.J., Langille, J.M. and Ahmad, T., 2013, Timescales of  
 1902 partial melting in the Himalayan middle crust: insight from the Leo Pargil dome,  
 1903 northwest India: *Contributions to Mineralogy and Petrology*, v. 166, p. 1415-1441.

1904 Lee, D. E., Stacey, J. S. D., and Fisher, L., 1986, Muscovite phenocrystic two-mica granites of  
 1905 NE Nevada are Late Cretaceous in age, in *Shorter contributions to isotope research: U.S.  
 1906 Geological Survey Bulletin 1622*, p. 31–39.

1907 Lee, D.E. and Christiansen, E.H., 1983, The granite problem as exposed in the southern Snake  
 1908 Range, Nevada: *Contributions to Mineralogy and Petrology*, v. 83, p. 99-116.

- 1909 Lee, D.E., and Marvin, R.F., 1981, Markedly discordant K-Ar ages for coexisting biotite and  
1910 muscovite from a two-mica granite in the Toano Range, Elko County, Nevada:  
1911 Isochron/West, no. 32, p. 19.
- 1912 Lee, D.E., Kistler, R.W., Friedman, I. and Van Loenen, R.E., 1981, Two-mica granites of  
1913 northeastern Nevada: Journal of Geophysical Research: Solid Earth, v. 86, p. 10607-  
1914 10616.
- 1915 Lee, J. and Sutter, J.F., 1991, Incremental  $^{40}\text{Ar}/^{39}\text{Ar}$  thermochronology of mylonitic rocks from  
1916 the northern Snake Range, Nevada: Tectonics, v. 10, p. 77-100.
- 1917 Lee, J., Blackburn, T. and Johnston, S., 2017, Timing of mid-crustal ductile extension in the  
1918 northern Snake Range metamorphic core complex, Nevada: Evidence from U/Pb zircon  
1919 ages: Geosphere, v. 13, p. 439-459.
- 1920 Lee, S.Y., Barnes, C.G., Snoke, A.W., Howard, K.A. and Frost, C.D., 2003, Petrogenesis of  
1921 Mesozoic, peraluminous granites in the Lamoille Canyon area, Ruby Mountains, Nevada,  
1922 USA: Journal of Petrology, v. 44, p. 713-732.
- 1923 Levandowski, W., Jones, C.H., Butcher, L.A. and Mahan, K.H., 2018, Lithospheric density  
1924 models reveal evidence for Cenozoic uplift of the Colorado Plateau and Great Plains by  
1925 lower-crustal hydration: Geosphere, v. 14, p. 1150-1164.
- 1926 Leveille, R.A., and Stegen, R.J., 2012, The southwestern North America porphyry copper  
1927 province, *in*, Hedenquist, J.W., Harris, M.O., and Camus, F., eds., Geology and Genesis  
1928 of Major Copper Deposits and Districts of the World: A Tribute to Richard H. Sillitoe:  
1929 Society of Economic Geologists Special Publication 16, p. 361–401.
- 1930 Li, X., Yuan, X., and Kind, R., 2007, The lithosphere-asthenosphere boundary beneath the  
1931 western United States: Geophysical Journal International, v. 170, p. 700-710.

- 1932 Lima, R.D., Prior, M.G., Stockli, D.F. and Hayman, N.W., 2018, Protracted heating of the  
1933 orogenic crust in Death Valley, California, USA: *Geology*, v. 46, p. 315-318.
- 1934 Liu, S. and Currie, C.A., 2016, Farallon plate dynamics prior to the Laramide orogeny:  
1935 Numerical models of flat subduction: *Tectonophysics*, v. 666, p. 33-47.
- 1936 Long, S.P. and Kohn, M.J., 2020, Distributed ductile thinning during thrust emplacement: A  
1937 commonly overlooked exhumation mechanism: *Geology*, v. 48, p. 368-373.
- 1938 Long, S.P. and Soignard, E., 2016, Shallow-crustal metamorphism during Late Cretaceous  
1939 anatexis in the Sevier hinterland plateau: Peak temperature conditions from the Grant  
1940 Range, eastern Nevada, USA: *Lithosphere*, v. 8, p. 150-164.
- 1941 Long, S.P., Thomson, S.N., Reiners, P.W. and Di Fiori, R.V., 2015, Synorogenic extension  
1942 localized by upper-crustal thickening: An example from the Late Cretaceous  
1943 Nevadaplano: *Geology*, v. 43, p. 351-354.
- 1944 Lund Snee, J.E., Miller, E.L., Grove, M., Hourigan, J.K., and Konstantinou, A., 2016, Cenozoic  
1945 paleogeographic evolution of the Elko Basin and surrounding region, northeast Nevada:  
1946 *Geosphere*, v. 12, p. 464-500.
- 1947 Lund, K., Beard, S.L., and Colgan, J.P., 2014, Shrimp U-Pb dating of zircon reveals Oligocene,  
1948 Late Cretaceous, and Late Jurassic ages in Troy granite, east-central Nevada: *Geological*  
1949 *Society of America Abstracts with Programs*, v. 46, no. 5, p. 30.
- 1950 Luth, W.C., Jahns, R.H., and Tuttle, O.F., 1964, The granite system at pressures 4–10 kilobars:  
1951 *Journal of Geophysical Research*, v. 69, p. 759–773.
- 1952 MacCready, T., Snoke, A.W., Wright, J.E. and Howard, K.A., 1997, Mid-crustal flow during  
1953 Tertiary extension in the Ruby Mountains core complex, Nevada: *Geological Society of*  
1954 *America Bulletin*, v. 109, p. 1576-1594.

- 1955 Mahood, G.A., Nibler, G.E. and Halliday, A.N., 1996, Zoning patterns and petrologic processes  
 1956 in peraluminous magma chambers: Hall Canyon pluton, Panamint Mountains, California:  
 1957 Geological Society of America Bulletin, v. 108, p. 437-453.
- 1958 Mallery, C., Barth, A., Roldan-Quintana, J., Haxel, G., Wooden, J., and Jacobson, C., 2018, A  
 1959 geochemical model of the origin of the Pan Tak Granite, the granite of Presumido Peak,  
 1960 and the granite of Sierra San Juan during the Laramide orogeny, southern Arizona and  
 1961 northern Sonora: Geological Society of America Annual Meeting, no. 315.
- 1962 Marvin, R.F., Zartman, R.E., Obradovich, J.D., and Harrison, J.E., 1984, Geochronometric and  
 1963 lead isotope data on samples from the Wallace 1 degrees by 2 degrees Quadrangle,  
 1964 Montana and Idaho: United States Geological Survey Miscellaneous Field Studies Map,  
 1965 MF-1354-G.
- 1966 Mattinson, C.G., Colgan, J.P., Metcalf, J.R., Miller, E.L. and Wooden, J.L., 2007, Late  
 1967 Cretaceous to Paleocene metamorphism and magmatism in the Funeral Mountains  
 1968 metamorphic core complex, Death Valley, California, *in*, Cloos, M., Carlson, W.D.,  
 1969 Gilbert, M.C., Liou, J.G., and Sorenson, S.S., eds., Convergent margin terranes and  
 1970 associated regions: a tribute to W.G. Ernst: Geological Society of America Special Paper,  
 1971 v. 419, p. 205-223.
- 1972 May, D.J. and Haxel, G., 1980, Reconnaissance bedrock geologic map of the Sells quadrangle.  
 1973 Pima County, Arizona: US Geological Survey Miscellaneous Field Studies Map MF-  
 1974 1166, scale, 1:62,500.
- 1975 McFarlane, D.N., 1981, Oreana tungsten-bearing pegmatite and related Rocky Canyon stock,  
 1976 Pershing County, Nevada: University of Nevada, Reno, MS thesis.
- 1977 McGrew, A.J. and Snee, L.W., 1994,  $^{40}\text{Ar}/^{39}\text{Ar}$  thermochronologic constraints on the

1978 tectonothermal evolution of the northern East Humboldt Range metamorphic core  
1979 complex, Nevada: *Tectonophysics*, v. 238, p. 425-450.

1980 McGrew, A.J., Peters, M.T., and Wright, J.E., 2000, Thermobarometric constraints on the  
1981 tectonothermal evolution of the East Humboldt Range metamorphic core complex,  
1982 Nevada: *Geological Society of America Bulletin*, v. 112, p. 45-60.

1983 Meijer, A., 2014, The Pinal Schist of southern Arizona: A Paleoproterozoic forearc complex  
1984 with evidence of spreading ridge–trench interaction at ca. 1.65 Ga and a Proterozoic arc  
1985 obduction event: *Geological Society of America Bulletin*, v. 126, p. 1145-1163.

1986 Miller, C.F. and Barton, M.D., 1990, Phanerozoic plutonism in the Cordilleran interior, USA, *in*  
1987 Kay, S.M. and Rapela, C.W., eds., *Plutonism from Antarctica to Alaska: Geological*  
1988 *Society of America Special Paper*, v. 241, p. 213-231.

1989 Miller, C.F. and Bradfish, L.J., 1980, An inner Cordilleran belt of muscovite-bearing plutons:  
1990 *Geology*, v. 8, p. 412-416.

1991 Miller, C.F. and Wooden, J.L., 1994, Anatexis, hybridization and the modification of ancient  
1992 crust: Mesozoic plutonism in the Old Woman Mountains area, California: *Lithos*, v. 32,  
1993 p. 111-133.

1994 Miller, C.F., 1985, Are strongly peraluminous magmas derived from pelitic sedimentary  
1995 sources?: *The Journal of Geology*, v. 93, p. 673-689.

1996 Miller, C.F., McDowell, S.M. and Mapes, R.W., 2003, Hot and cold granites? Implications of  
1997 zircon saturation temperatures and preservation of inheritance: *Geology*, v. 31, p. 529-  
1998 532.

1999 Miller, C.F., Stoddard, E.F., Bradfish, L.J., and Dollase, W.A., 1981, Composition of plutonic  
2000 muscovite: Genetic implications: *Canadian Mineralogist*, v. 19, p. 25–34.

- 2001 Miller, C.F., Wooden, J.L., Bennett, V.C., Wright, J.E., Solomon, G.C., and Hurst, R.W., 1990b,  
2002 Petrogenesis of the composite peraluminous-metaluminous Old Woman-Piute range  
2003 batholith, southeastern California: isotopic constraints, *in*, Anderson, J.L., ed., The  
2004 Nature and Origin of Cordilleran Magmatism: Geological Society of America Memoir, v.  
2005 174, p. 99-109.
- 2006 Miller, D.M., Hoisch, T.D. and Busby, C., 1995, Jurassic tectonics of northeastern Nevada and  
2007 northwestern Utah from the perspective of barometric studies, *in*, Miller, D.M. and  
2008 Busby, C., eds., Jurassic Magmatism and Tectonics of the North American Cordillera,  
2009 Geological Society of America Special Paper, v. 299, p. 267-294.
- 2010 Miller, D.M., Nakata, J.K. and Glick, L.L., 1990, K-Ar ages of Jurassic to Tertiary plutonic and  
2011 metamorphic rocks, northwestern Utah and northeastern Nevada: U.S. Geological Survey  
2012 Bulletin, no. 1906.
- 2013 Miller, E.L. and Gans, P.B., 1989, Cretaceous crustal structure and metamorphism in the  
2014 hinterland of the Sevier thrust belt, western US Cordillera: *Geology*, v. 17, p. 59-62.
- 2015 Miller, E.L., Dumitru, T.A., Brown, R.W. and Gans, P.B., 1999, Rapid Miocene slip on the  
2016 Snake Range–Deep Creek range fault system, east-central Nevada: Geological Society of  
2017 America Bulletin, v. 111, p. 886-905.
- 2018 Miller, E.L., Konstantinou, A., and Strickland, A., 2012, Comment on Geodynamics of  
2019 synconvergent extension and tectonic mode switching: Constraints from the Sevier-  
2020 Laramide orogen by Michael L. Wells et al.: *Tectonics*, v. 31, 3p.
- 2021 Miller, F.K., Clark, L.D. and Engels, J.C., 1975, Geology of the Chewelah-Loon Lake area,  
2022 Stevens and Spokane Counties, Washington: U.S. Geological Survey Professional Paper  
2023 806, 50p.



- 2024 Miller, J.S., Glazner, A.F. and Crowe, D.E., 1996, Muscovite-garnet granites in the Mojave  
2025 Desert: Relation to crustal structure of the Cretaceous arc: *Geology*, v. 24, p. 335-338.
- 2026 Miller, J.S., Glazner, A.F., Farmer, G.L., Suayah, I.B. and Keith, L.A., 2000, A Sr, Nd, and Pb  
2027 isotopic study of mantle domains and crustal structure from Miocene volcanic rocks in  
2028 the Mojave Desert, California: *Geological Society of America Bulletin*, v. 112, p. 1264-  
2029 1279.
- 2030 Miller, M.G. and Friedman, R.M., 1999, Early Tertiary magmatism and probable Mesozoic  
2031 fabrics in the Black Mountains, Death Valley, California: *Geology*, v. 27, p. 19-22.
- 2032 Milliard, A.K., Ressel, M.W., Henry, C.D., Ricks, C., and Loptien, G., 2015, Spatial and  
2033 temporal constraints on Carlin-type gold mineralization at the Pequop Mountains  
2034 footwall to the Ruby Mountain-East Humboldt metamorphic core complex, *in*, Pennell,  
2035 W.M. and Garside, L.J., *New Concepts and Discoveries: Geological Society of Nevada*  
2036 *Symposium*, v. 1, p. 895-923.
- 2037 Misch, P. and Hazzard, J.C., 1962, Stratigraphy and metamorphism of Late Precambrian rocks in  
2038 central northeastern Nevada and adjacent Utah: *AAPG Bulletin*, v. 46, p. 289-343.
- 2039 Molnar, P., England, P. and Martinod, J., 1993, Mantle dynamics, uplift of the Tibetan Plateau,  
2040 and the Indian monsoon: *Reviews of Geophysics*, v. 31, p. 357-396.
- 2041 Monger, J.W.H., Price, R.A., and Tempelman-Kluit, D.J., 1982, Tectonic accretion and the  
2042 origin of the two major metamorphic and plutonic belts in the Canadian Cordillera:  
2043 *Geology*, v. 10, p. 70-75.
- 2044 Moye, F.J., Hackett, W.R., Blakley, J.D., and Snider, L.G., 1988, Regional geologic setting and  
2045 volcanic stratigraphy of the Challis volcanic field, central Idaho. *Guidebook to the*  
2046 *geology of central and southern Idaho: Idaho Geological Survey Bulletin*, v. 27, p. 87-97.

- 2047 Moynihan, D.P. and Pattison, D.R.M., 2013, Barrovian metamorphism in the central Kootenay  
2048 Arc, British Columbia: petrology and isograd geometry: *Canadian Journal of Earth*  
2049 *Sciences*, v. 50, p. 769-794.
- 2050 Nabelek, P.I., 2019, Petrogenesis of leucogranites in collisional orogens: Geological Society,  
2051 London, Special Publications, v. 491, p. 179-207.
- 2052 Naney, M. T. 1983, Phase equilibria of rock-forming ferromagnesian silicates in granitic  
2053 systems: *American Journal of Science*, v. 283, p. 993–1033.
- 2054 Nelson, J.L., Colpron, M. and Israel, S., 2013, The cordillera of British Columbia, Yukon, and  
2055 Alaska: tectonics and metallogeny, *in*, Colpron, M., Bissig, T., Rusk, B.G., and  
2056 Thompson, J.F.H., eds., *Tectonics, Metallogeny, and Discovery: The North American*  
2057 *Cordillera and Similar Accretionary Settings: Society of Economic Geologists Special*  
2058 *Publication*, v. 17, p. 53-109.
- 2059 Norlander, B.H., Whitney, D.L., Teyssier, C., and Vanderhaeghe, O. 2002, Partial melting and  
2060 decompression of the Thor-Odin Dome, Shuswap metamorphic core complex, Canadian  
2061 Cordillera: *Lithos*, v. 61, p. 103-125.
- 2062 Nourse, J.A., Anderson, T.H. and Silver, L.T., 1994, Tertiary metamorphic core complexes in  
2063 Sonora, northwestern Mexico: *Tectonics*, v. 13, p. 1161-1182.
- 2064 Nourse, J.A., Jacques-Ayala, C., González-León, C.M. and Roldan-Quintana, J., 1995, Jurassic-  
2065 Cretaceous paleogeography of the Magdalena region, northern Sonora, and its influence  
2066 on the positioning of Tertiary metamorphic core complexes, *in*, Jacques-Ayala, C.,  
2067 Gonzalez-Leon, C.M., and Roldan-Quintana, J., eds., *Studies on the Mesozoic of Sonora*  
2068 *and adjacent areas: Geological Society of America Special Paper*, v. 301, p. 59-78.
- 2069 O'Neill, J.M., Lonn, J.D., Lageson, D.R., and Kunk, M.J., 2004, Early Tertiary Anaconda

2070 metamorphic core complex, southwestern Montana: Canadian Journal of Earth Sciences,  
2071 v. 41, p. 63-72.

2072 Parker, D.F., Ren, M., Adams, D.T., Tsai, H. and Long, L.E., 2012, Mid-Tertiary magmatism in  
2073 western Big Bend National Park, Texas, USA: Evolution of basaltic source regions and  
2074 generation of peralkaline rhyolite: Lithos, v. 144, p. 161-176.

2075 Parrish, R.R., Carr, S.D. and Parkinson, D.L., 1988, Eocene extensional tectonics and  
2076 geochronology of the southern Omineca Belt, British Columbia and Washington:  
2077 Tectonics, v. 7, p. 181-212.

2078 Patiño Douce, A.E., 2005, Vapor-absent melting of tonalite at 15–32 kbar: Journal of Petrology,  
2079 v. 46, p. 275–290.

2080 Patiño-Douce, A.E. and Beard, J.S., 1995, Dehydration-melting of biotite gneiss and quartz  
2081 amphibolite from 3 to 15 kbar: Journal of Petrology, v. 36, p. 707-738.

2082 Patiño-Douce, A.E. and Beard, J.S., 1996, Effects of P, f(O<sub>2</sub>) and Mg/Fe ratio on dehydration  
2083 melting of model metagreywackes: Journal of Petrology, v. 37, p. 999-1024.

2084 Patiño-Douce, A.E. and Harris, N., 1998, Experimental constraints on Himalayan anatexis:  
2085 Journal of Petrology, v. 39, p. 689-710.

2086 Patiño-Douce, A.E., 1996, Effects of pressure and H<sub>2</sub>O content on the compositions of primary  
2087 crustal melts: Earth and Environmental Science Transactions of the Royal Society of  
2088 Edinburgh, v. 87, p. 11-21.

2089 Patiño-Douce, A.E., 1999, What do experiments tell us about the relative contributions of crust  
2090 and mantle to the origin of granitic magmas?: Geological Society, London, Special  
2091 Publication, v. 168, p. 55-75.

2092 Patiño-Douce, A.E., Humphreys, E.D. and Johnston, A.D., 1990, Anatexis and metamorphism in

2093 tectonically thickened continental crust exemplified by the Sevier hinterland, western  
2094 North America: *Earth and Planetary Science Letters*, v. 97, p. 290-315.

2095 Pease, V., Foster, D., Wooden, J., O'Sullivan, P., Argent, J. and Fanning, C., 1999, The Northern  
2096 Sacramento Mountains, southwest United States. Part II: Exhumation history and  
2097 detachment faulting: *Geological Society, London, Special Publications*, v. 164, p. 199-  
2098 238.

2099 Peterman, E.M., Hourigan, J.K. and Grove, M., 2014, Experimental and geologic evaluation of  
2100 monazite (U–Th)/He thermochronometry: Catnip Sill, Catalina Core Complex, Tucson,  
2101 AZ: *Earth and Planetary Science Letters*, v. 403, p. 48-55.

2102 Peto, P., 1976, An experimental investigation of melting reactions involving muscovite and  
2103 paragonite in the silica-undersaturated portion of the system  $K_2O-Na_2O-Al_2O_3-SiO_2-$   
2104  $H_2O$ : *Progress in Experimental Petrology*, v. 3, p. 41-45.

2105 Porter, R., Hoisch, T. and Holt, W.E., 2017, The role of lower-crustal hydration in the tectonic  
2106 evolution of the Colorado Plateau: *Tectonophysics*, v. 712, p. 221-231.

2107 Premo, W.R., Castiñeiras, P. and Wooden, J.L., 2008, SHRIMP-RG U-Pb isotopic systematics of  
2108 zircon from the Angel Lake orthogneiss, East Humboldt Range, Nevada: Is this really  
2109 Archean crust?: *Geosphere*, v. 4, p. 963-975.

2110 Prince, C., Harris, N. and Vance, D., 2001, Fluid-enhanced melting during prograde  
2111 metamorphism: *Journal of the Geological Society*, v. 158, p. 233-241.

2112 Prior, M.G., Stockli, D.F. and Singleton, J.S., 2016, Miocene slip history of the Eagle Eye  
2113 detachment fault, Harquahala Mountains metamorphic core complex, west-central  
2114 Arizona: *Tectonics*, v. 35, p. 1913-1934.

2115 Rapp, R.P. and Watson, E.B., 1995, Dehydration melting of metabasalt at 8–32 kbar:

2116 implications for continental growth and crust-mantle recycling: *Journal of Petrology*, v.  
2117 36, p. 891-931.

2118 Rapp, R.P., Watson, E.B. and Miller, C.F., 1991, Partial melting of amphibolite/eclogite and the  
2119 origin of Archean trondhjemites and tonalites: *Precambrian Research*, v. 51, p. 1-25.

2120 Rehrig, W.A. and Reynolds, S., 1980, Geologic and geochronologic reconnaissance of a  
2121 northwest-trending zone of metamorphic core complexes in southern and western  
2122 Arizona: *Geological Society of America Memoir*, v. 153, p. 131-157.

2123 Rey, P.F., Teyssier, C. and Whitney, D.L., 2009, Extension rates, crustal melting, and core  
2124 complex dynamics: *Geology*, v. 37, p. 391-394.

2125 Reynolds, S. J., Wood, Steven E., and Pearthree, Philip A., Field, John J., 2002, Geologic Map of  
2126 the White Tank Mountains, Central Arizona: Arizona Geological Survey Digital  
2127 Geologic Map DGM-14, map scale 1:24,000.

2128 Richard, S.M., Fryxell, J.E. and Sutter, J.F., 1990, Tertiary structure and thermal history of the  
2129 Harquahala and Buckskin Mountains, west central Arizona: Implications for denudation  
2130 by a major detachment fault system: *Journal of Geophysical Research: Solid Earth*, v. 95,  
2131 p. 19973-19987.

2132 Richard, S.M., Spencer, J.E., Ferguson, C.A., and Pearthree, P.A., 1999, Geologic map of the  
2133 Picacho Mountains and Picacho Peak, Pinal County, southern Arizona. Arizona  
2134 Geological Survey Open File Report, OFR-99-18, 43p.

2135 Rivers, T., Ketchum, J., Indares, A., and Hynes, A., 2002, The high pressure belt in the Grenville  
2136 Province: architecture, timing and exhumation: *Canadian Journal of Earth Sciences*, v.  
2137 39, p. 867–893.

2138 Roldán-Quintana, J., 1991, Geology and chemical composition of the Jaralito and Aconchi

2139 batholiths in east-central Sonora, México, *in*, Perez-Segura, E. and Jacques-Ayala, C.,  
2140 eds., Studies of Sonoran Geology: Geological Society of America Special Paper, v. 254,  
2141 p. 69-80.

2142 Rosenberg, C.L. and Handy, M.R., 2005, Experimental deformation of partially melted granite  
2143 revisited: implications for the continental crust: *Journal of metamorphic Geology*, v. 23,  
2144 p. 19-28.

2145 Rudnick, R.L., 1992, Restites, Eu anomalies and the lower continental crust: *Geochimica et*  
2146 *Cosmochimica Acta*, v. 56, p. 963-970.

2147 Runyon, S.E., Seedorff, E., Barton, M.D., Steele-MacInnis, M., Lecumberri-Sanchez, P., and  
2148 Mazdab, F.K., 2019, Coarse muscovite veins and alteration in porphyry systems: *Ore*  
2149 *Geology Reviews*, v. 113.

2150 Saleeby, J., 2003, Segmentation of the Laramide slab—Evidence from the southern Sierra Nevada  
2151 region: *Geological Society of America Bulletin*, v. 115, p. 655-668.

2152 Sawyer, E.W., 1987, The role of partial melting and fractional crystallization in determining  
2153 discordant migmatite leucosome compositions: *Journal of Petrology*, v. 28, p. 445-473.

2154 Scaillet, B., Pichavant, M. and Roux, J., 1995, Experimental crystallization of leucogranite  
2155 magmas: *Journal of Petrology*, v. 36, p. 663-705.

2156 Schwindinger, M., Weinberg, R.F. and Clos, F., 2019, Wet or dry? The difficulty of identifying  
2157 the presence of water during crustal melting: *Journal of Metamorphic Geology*, v. 37, p.  
2158 339-358.

2159 Seedorff, E., Barton, M.D., Gehrels, G.E., Valencia, V.A., Johnson, D.A., Maher, D.J., Stavast,  
2160 W.J., and Marsh, T.M., 2019, Temporal evolution of the Laramide arc: U-Pb  
2161 geochronology of plutons associated with porphyry copper mineralization in east-central

2162 Arizona: Geological Society of America. Field Guide, v. 55, p. 369-400.

2163 Seedorff, E., Barton, M.D., Stavast, W.J. and Maher, D.J., 2008, Root zones of porphyry  
2164 systems: Extending the porphyry model to depth: *Economic Geology*, v. 103, p. 939-956.

2165 Seedorff, E., Dilles, J.H., Proffett, J.M., Einaudi, M.T., Zurcher, L., Stavast, W.J.A., Johnson,  
2166 D.A., and Barton, M.D., 2005, Porphyry deposits: Characteristics and origin of hypogene  
2167 features, in Hedenquist, J.W., Thompson, J.F.H., Goldfarb, R.J., and Richards, J.P., eds.,  
2168 *Economic Geology 100th Anniversary Volume*, p. 251-298.

2169 Sevigny, J.H. and Parrish, R.R., 1993, Age and origin of late Jurassic and Paleocene granitoids,  
2170 Nelson Batholith, southern British Columbia: *Canadian Journal of Earth Sciences*, v. 30,  
2171 p. 2305-2314.

2172 Shafiqullah, M., Damon, P.E., Lynch, D.J., Reynolds, S.J., Rehrig, W.A. and Raymond, R.H.,  
2173 1980, K-Ar geochronology and geologic history of southwestern Arizona and adjacent  
2174 areas. *Studies in western Arizona: Arizona Geological Society Digest*, v. 12, p. 201-260.

2175 Shawe, D.R., Marvin, R.F., Andriessen, P.A.M., Mehnert, H.H. and Merritt, V.M., 1986, Ages of  
2176 igneous and hydrothermal events in the Round Mountain and Manhattan gold districts,  
2177 Nye County, Nevada: *Economic Geology*, v. 81, pp. 388-407.

2178 Siégel, C., Bryan, S.E., Allen, C.M. and Gust, D.A., 2018, Use and abuse of zircon-based  
2179 thermometers: a critical review and a recommended approach to identify antecrystic  
2180 zircons: *Earth-Science Reviews*, v. 176, p. 87-116.

2181 Silver, L.T. and Chappell, B.W., 1988, The Peninsular Ranges Batholith: an insight into the  
2182 evolution of the Cordilleran batholiths of southwestern North America: *Earth and  
2183 Environmental Science Transactions of the Royal Society of Edinburgh*, v. 79, p. 105-  
2184 121.

2185 Silverberg, D.S., 1990, The tectonic evolution of the Pioneer metamorphic core complex, south-  
2186 central Idaho: Massachusetts Institute of Technology, Ph.D. dissertation.

2187 Singleton, J.S., 2015, The transition from large-magnitude extension to distributed dextral  
2188 faulting in the Buckskin-Rawhide metamorphic core complex, west-central Arizona:  
2189 *Tectonics*, v. 34, p. 1685-1708.

2190 Singleton, J.S., Stockli, D.F., Gans, P.B. and Prior, M.G., 2014, Timing, rate, and magnitude of  
2191 slip on the Buckskin-Rawhide detachment fault, west central Arizona: *Tectonics*, v. 33, p.  
2192 1596-1615.

2193 Sizemore, T., Wielicki, M.M., Çemen, I., Stockli, D., Heizler, M. and Robinson, D., 2019,  
2194 Structural evolution of central Death Valley, California, using new thermochronometry of  
2195 the Badwater turtleback: *Lithosphere*, v. 11, p. 436-447.

2196 Sola, A.M., Hasalová, P., Weinberg, R.F., Suzaño, N.O., Becchio, R.A., Hongn, F.D. and  
2197 Botelho, N., 2017, Low-P melting of metapelitic rocks and the role of H<sub>2</sub>O: Insights from  
2198 phase equilibria modelling: *Journal of Metamorphic Geology*, v. 35, p. 1131-1159.

2199 Solar, G.S. and Brown, M., 2001, Petrogenesis of migmatites in Maine, USA: possible source of  
2200 peraluminous leucogranite in plutons?: *Journal of Petrology*, v. 42, p. 789-823.

2201 Solomon, G.C. and Taylor Jr, H.P., 1989, Isotopic evidence for the origin of Mesozoic and  
2202 Cenozoic granitic plutons in the northern Great Basin: *Geology*, v. 17, p. 591-594.

2203 Spencer, J.E., Isachsen, C.E., Ferguson, C.A., Richard, S.M., Skotnicki, S.J., Wooden, J., and  
2204 Riggs, N.R., 2003, U-Pb isotope geochronologic data from 23 igneous rock units in  
2205 central and southeastern Arizona: Arizona Geological Survey Open File Report, OFR-03-  
2206 08, 40p.

2207 Spencer, J.E. and Reynolds, S.J., 1990, Relationship between Mesozoic and Cenozoic



2208 tectonic features in west central Arizona and adjacent southeastern California: *Journal of*  
2209 *Geophysical Research: Solid Earth*, v. 95, p. 539-555.

2210 Stevens, G. and Clemens, J.D., 1993, Fluid-absent melting and the roles of fluids in the  
2211 lithosphere: a slanted summary?: *Chemical Geology*, v. 108, p. 1-17.

2212 Stevens, G., Clemens, J.D. and Droop, G.T., 1997, Melt production during granulite-facies  
2213 anatexis: experimental data from “primitive” metasedimentary protoliths: *Contributions*  
2214 *to Mineralogy and Petrology*, v. 128, p. 352-370.

2215 Stevens, G., Villaros, A., and Moyen, J.F., 2007, Selective peritectic garnet entrainment as the  
2216 origin of geochemical diversity in S-type granites: *Geology*, v. 35, p. 9-12.

2217 Stevens, L.M., Baldwin, J.A., Cottle, J.M. and Kylander-Clark, A.R.C., 2015, Phase equilibria  
2218 modelling and LASS monazite petrochronology: P–T–t constraints on the evolution of  
2219 the Priest River core complex, northern Idaho: *Journal of Metamorphic Geology*, v. 33, p.  
2220 385-411.

2221 Stevens, L.M., Baldwin, J.A., Crowley, J.L., Fisher, C.M. and Vervoort, J.D., 2016. Magmatism  
2222 as a response to exhumation of the Priest River complex, northern Idaho: Constraints  
2223 from zircon U–Pb geochronology and Hf isotopes. *Lithos*, 262, pp.285-297.

2224 Stewart, J. H., 1980, *Geology of Nevada: Nevada Bureau of Mines and Geology Special*  
2225 *Publication*, v. 4, 136p.

2226 Stewart, J.H., McKee, E.H., and Stager, H.K., 1977, *Geology and mineral deposits of Lander*  
2227 *County, Nevada: Nevada Bureau of Mines and Geology Bulletin*, v. 88, 106p.

2228 Stewart, J.H., McManamin, M.A., and Morales-Ramirez, J.M., 1984, Upper Proterozoic and  
2229 Cambrian rocks in the Caborca region, Sonora, Mexico - Physical stratigraphy,  
2230 biostratigraphy, paleocurrent studies, and regional relations: U.S. Geological Survey

- 2231 Professional Paper 1309, 36p.
- 2232 Strickland, A., Miller, E.L., Wooden, J.L., Kozdon, R. and Valley, J.W., 2011, Syn-extensional  
2233 plutonism and peak metamorphism in the Albion–Raft River–Grouse Creek metamorphic  
2234 core complex: *American Journal of Science*, v. 311, p. 261-314.
- 2235 Sylvester, A.G., Ortel, G., Nelson, C.A. and Christie, J.M., 1978, Papoose Flat pluton: A granitic  
2236 blister in the Inyo Mountains, California: *Geological Society of America Bulletin*, v. 89,  
2237 p. 1205-1219.
- 2238 Syracuse, E.M., van Keken, P.E., and Abers, G.A., 2010, The global range of subduction zone  
2239 thermal models: *Physics of the Earth and Planetary Interiors*, v. 183, p. 73-90.
- 2240 Terrien, J., 2012, *The Role of Magmatism in the Catalina Metamorphic Core Complex, Arizona:  
2241 Insights from Integrated Thermochronology, Gravity and Aeromagnetic Data*: Syracuse  
2242 University, Ph.D. Dissertation.
- 2243 Teyssier, C. and Whitney, D.L., 2002, Gneiss domes and orogeny: *Geology*, v. 30, p. 1139-1142.
- 2244 Thompson, A.B. and Connolly, J.A., 1995, Melting of the continental crust: some thermal and  
2245 petrological constraints on anatexis in continental collision zones and other tectonic  
2246 settings: *Journal of Geophysical Research: Solid Earth*, v. 100, p. 15565-15579.
- 2247 Thompson, A.B., 1983, Fluid-absent metamorphism: *Journal of the Geological Society*, v. 140,  
2248 p. 533–547.
- 2249 Valencia-Moreno, M., Ruiz, J., Barton, M.D., Patchett, P.J., Zürcher, L., Hodkinson, D.G. and  
2250 Roldán-Quintana, J., 2001. A chemical and isotopic study of the Laramide granitic belt of  
2251 northwestern Mexico: Identification of the southern edge of the North American  
2252 Precambrian basement: *Geological Society of America Bulletin*, v. 113, p. 1409-1422.
- 2253 van der Molen, I. and Paterson, M.S., 1979, Experimental deformation of partially-melted

- 2254 granite: Contributions to Mineralogy and Petrology, v. 70, p. 299-318.
- 2255 Vanderhaeghe, O. and Teyssier, C., 1997, Formation of the Shuswap metamorphic core complex  
2256 during late-orogenic collapse of the Canadian Cordillera: role of ductile thinning and  
2257 partial melting of the mid-to lower crust: Geodinamica Acta, v. 10, p. 41-58.
- 2258 Vanderhaeghe, O. and Teyssier, C., 2001, Partial melting and flow of orogens: Tectonophysics,  
2259 v. 342, p. 451-472.
- 2260 Vanderhaeghe, O., 2009, Migmatites, granites and orogeny: Flow modes of partially-molten  
2261 rocks and magmas associated with melt/solid segregation in orogenic belts:  
2262 Tectonophysics, v. 477, p. 119-134.
- 2263 Vanderhaeghe, O., Teyssier, C., and Wysoczanski, R., 1999, Structural and geochronological  
2264 constraints on the role of partial melting during the formation of the Shuswap  
2265 metamorphic core complex at the latitude of the Thor-Odin dome, British Columbia:  
2266 Canadian Journal of Earth Science, v. 36, p. 917-943.
- 2267 Vanderhaeghe, O., Teyssier, C., McDougall, I., and Dunlap, W.J., 2003, Cooling and  
2268 exhumation of the Shuswap Metamorphic Core Complex constrained by  $^{40}\text{Ar}/^{39}\text{Ar}$   
2269 thermochronology: Geological Society of America Bulletin, v. 115, p. 200-216.
- 2270 Vielzeuf, D. and Montel, J.M., 1994, Partial melting of metagreywackes. Part I. Fluid-absent  
2271 experiments and phase relationships: Contributions to Mineralogy and Petrology, v. 117,  
2272 p. 375-393.
- 2273 Vielzeuf, D. and Schmidt, M.W., 2001, Melting relations in hydrous systems revisited:  
2274 application to metapelites, metagreywackes and metabasalts: Contributions to  
2275 Mineralogy and Petrology, v. 141, p. 251-267.
- 2276 Villaros, A., Laurent, O., Couzinié, S., Moyen, J.F. and Mintrone, M., 2018, Plutons and domes:

2277 the consequences of anatectic magma extraction—example from the southeastern French  
2278 Massif Central: *International Journal of Earth Sciences*, v. 107, p. 2819-2842.

2279 Vogl, J.J., Foster, D.A., Fanning, C.M., Kent, K.A., Rodgers, D.W. and Diedesch, T., 2012,  
2280 Timing of extension in the Pioneer metamorphic core complex with implications for the  
2281 spatial-temporal pattern of Cenozoic extension and exhumation in the northern US  
2282 Cordillera: *Tectonics*, v. 31.

2283 Wallace, C.A., Lidke, D.J., Elliott, J.E., Desmarais, N.R., Obradovich, J.D., Lopez, D.A., Zarske,  
2284 S.E., Heise, B.A., Blaskowski, M.J., and Lean, J.S., 1992, Geologic map of the  
2285 Anaconda-Pintlar Wilderness and contiguous roadless area, Granite, Deer Lodge,  
2286 Beaverhead, and Ravalli counties, western Montana: U.S. Geological Survey  
2287 Miscellaneous Field Studies Map 1633-C.

2288 Watson, E.B. and Harrison, T.M., 1983, Zircon saturation revisited: temperature and  
2289 composition effects in a variety of crustal magma types: *Earth and Planetary Science*  
2290 *Letters*, v. 64, p. 295-304.

2291 Watts, K.E., John, D.A., Colgan, J.P., Henry, C.D., Bindeman, I.N., and Schmitt, A.K., 2016,  
2292 Probing the volcanic–plutonic connection and the genesis of crystal-rich rhyolite in a  
2293 deeply dissected supervolcano in the Nevada Great Basin: source of the Late Eocene  
2294 Caetano Tuff: *Journal of Petrology*, v. 57, p. 1599-1644.

2295 Webster, E.R., Pattison, D. and DuFrane, S.A., 2017, Geochronological constraints on  
2296 magmatism and polyphase deformation and metamorphism in the southern Omineca Belt,  
2297 British Columbia: *Canadian Journal of Earth Sciences*, v. 54, p. 529-549.

2298 Weinberg, R.F. and Hasalová, P., 2015, Water-fluxed melting of the continental crust: A review:  
2299 *Lithos*, v. 212, p. 158-188.

2300 Weinberg, R.F., 2016, Himalayan leucogranites and migmatites: nature, timing and duration of  
2301 anatexis. *Journal of Metamorphic Geology*, v. 34, p. 821-843.

2302 Wells, M.L. and Hoisch, T.D., 2008, The role of mantle delamination in widespread Late  
2303 Cretaceous extension and magmatism in the Cordilleran orogen, western United States:  
2304 *Geological Society of America Bulletin*, v. 120, p. 515-530.

2305 Wells, M.L. and Hoisch, T.D., 2012, Reply to comment by E.L. Miller et al. on Geodynamics of  
2306 synconvergent extension and tectonic mode switching: Constraints from the Sevier-  
2307 Laramide orogen: *Tectonics*, v. 31.

2308 Wells, M.L., Hoisch, T.D., Cruz-Uribe, A.M. and Vervoort, J.D., 2012, Geodynamics of  
2309 synconvergent extension and tectonic mode switching: Constraints from the Sevier-  
2310 Laramide orogen: *Tectonics*, v. 31.

2311 Wells, M.L., Spell, T.L., Grove, M., 2002, Late Cretaceous intrusion and extensional exhumation  
2312 of the Cadiz Valley batholith, Iron Mountains, southeastern California: *Geological*  
2313 *Society of America Annual Meeting, Abstracts with Programs*.

2314 Whitehouse, M.J., Stacey, J.S. and Miller, F.K., 1992, Age and nature of the basement in  
2315 northeastern Washington and northern Idaho: isotopic evidence from Mesozoic and  
2316 Cenozoic granitoids: *The Journal of Geology*, v. 100, p. 691-701.

2317 Whitmeyer, S.J. and Karlstrom, K.E., 2007, Tectonic model for the Proterozoic growth of North  
2318 America: *Geosphere*, v. 3, p. 220-259.

2319 Whitney, D.L., Paterson, S.R., Schmidt, K.L., Glazner, A.F. and Kopf, C.F., 2004, Growth and  
2320 demise of continental arcs and orogenic plateaux in the North American Cordillera: From  
2321 Baja to British Columbia, *in* Grocott, J., McCaffrey, K.J.W., Taylor, G., and Tikoff, B.,  
2322 eds., *Vertical coupling and decoupling in the lithosphere*: Geological Society, London,

- 2323 Special Publication, v. 227, p. 167-175.
- 2324 Whitney, D.L., Teyssier, C. and Fayon, A.K., 2004b, Isothermal decompression, partial melting  
2325 and exhumation of deep continental crust: Geological Society, London, Special  
2326 Publications, v. 227, p. 313-326.
- 2327 Whitney, D.L., Teyssier, C. and Vanderhaeghe, O., 2004, Gneiss domes and crustal flow, *in*,  
2328 Whitney, D.L., Teyssier, C., and Siddoway, C.S., eds., Gneiss domes in orogeny:  
2329 Geological Society of America Special Paper, v. 380, p. 15-34.
- 2330 Whitney, D.L., Teyssier, C., Rey, P., and Buck, W.R., 2013, Continental and oceanic core  
2331 complexes: Geological Society of America Bulletin, v. 125, p. 273-298.
- 2332 Wolfram, L.C., Weinberg, R.F., Nebel, O., Hamza, K., Hasalová, P., Míková, J., and Becchio,  
2333 R., 2019, A 60-Myr record of continental back-arc differentiation through cyclic melting:  
2334 Nature Geoscience, v. 12, p. 215-219.
- 2335 Wong, M.S. and Gans, P.B., 2008, Geologic, structural, and thermochronologic constraints on  
2336 the tectonic evolution of the Sierra Mazatán core complex, Sonora, Mexico: New insights  
2337 into metamorphic core complex formation: Tectonics, v. 27.
- 2338 Wong, M.S., Gans, P.B. and Scheier, J., 2010, The  $^{40}\text{Ar}/^{39}\text{Ar}$  thermochronology of core  
2339 complexes and other basement rocks in Sonora, Mexico: Implications for Cenozoic  
2340 tectonic evolution of northwestern Mexico. Journal of Geophysical Research: Solid  
2341 Earth, v. 115.
- 2342 Wong, M.S., O'Brien, H.P., Bunting, K.C., and Gans, P.B., 2011,  $^{40}\text{Ar}/^{39}\text{Ar}$  K-feldspar  
2343 thermochronology of the Harcuvar core complex, western Arizona: New insight into the  
2344 timing of extension and degree of footwall tilt: Geological Society of America Annual  
2345 Meeting, Abstracts with Programs, v. 43, p. 53.

2346 Wooden, J.L., Kistler, R.W., and Tosdal, R.M., 1999, Strontium, lead, and oxygen isotopic data  
2347 for granitoid and volcanic rocks from the northern Great Basin and Sierra Nevada,  
2348 California, Nevada and Utah: U.S. Geological Survey Open-File Report 99-569, 20p.

2349 Wright, J.E. and Haxel, G., 1982, A garnet-two-mica granite, Coyote Mountains, southern  
2350 Arizona: Geologic setting, uranium-lead isotopic systematics of zircon, and nature of the  
2351 granite source region: Geological Society of America Bulletin, v. 93, p. 1176-1188.

2352 Wright, J.E. and Snoke, A.W., 1993, Tertiary magmatism and mylonitization in the Ruby-East  
2353 Humboldt metamorphic core complex, northeastern Nevada: U-Pb geochronology and Sr,  
2354 Nd, and Pb isotope geochemistry: Geological Society of America Bulletin, v. 105, p. 935-  
2355 952.

2356 Wright, J.E. and Wooden, J.L., 1991, New Sr, Nd, and Pb isotopic data from plutons in the  
2357 northern Great Basin: Implications for crustal structure and granite petrogenesis in the  
2358 hinterland of the Sevier thrust belt: Geology, v. 19, p. 457-460.

2359 Wust, S.L., 1986, Regional correlation of extension directions in Cordilleran metamorphic core  
2360 complexes: Geology, v. 14, p. 828-830.

2361 Wyld, S.J., 2002, Structural evolution of a Mesozoic backarc fold-and-thrust belt in the US  
2362 Cordillera: New evidence from northern Nevada: Geological Society of America  
2363 Bulletin, v. 114, p. 1452-1468.

2364 Wyllie, P.J. and Wolf, M.B., 1993, Amphibolite dehydration-melting: sorting out the solidus:  
2365 Geological Society, London, Special Publications, v. 76, p. 405-416.

2366 Wyllie, P.J., 1977, Crustal anatexis: an experimental review: Tectonophysics, v. 43, p. 41-71.

2367 Yardley, B.W. and Barber, J.P., 1991, Melting reactions in the Connemara Schists: the role of  
2368 water infiltration in the formation of amphibolite facies migmatites: American

2369 Mineralogist, v. 76, p. 848-856.  
2370 Yonkee, W.A. and Weil, A.B., 2015, Tectonic evolution of the Sevier and Laramide belts within  
2371 the North American Cordillera orogenic system: Earth-Science Reviews, v. 150, p. 531-  
2372 593.  
2373 Zen, E.A., 1986, Aluminum enrichment in silicate melts by fractional crystallization: some  
2374 mineralogic and petrographic constraints: Journal of Petrology, v. 27, p. 1095-1117.  
2375 Zen, E.A., 1988, Phase Relations of Peraluminous Granitic Rocks and Their Petrogenetic  
2376 Implications: Annual Review of Earth and Planetary Sciences, v. 16, p. 21–51.

2377

2378

2379 **Figure and Table Captions**

2380

2381 Fig. 1: Overview map of the North American Cordilleran Anatectic Belt (CAB). Feature  
2382 locations were compiled from previously published works including core complexes (Rehrig and  
2383 Reynolds, 1980; Armstrong, 1982; Wust, 1986; Roldán-Quintana, 1991; Nourse et al., 1994;  
2384 1995; Foster and John, 1999; Miller et al., 1999; Foster et al., 2001; 2007; 2010; Vanderhaeghe  
2385 et al., 2003; Laberge and Pattison, 2007; Kruckenberg et al., 2008; Howard et al., 2011;  
2386 Konstantinou et al., 2013; Hoisch et al., 2014; Singleton et al., 2015; Stevens et al., 2016; Lee et  
2387 al., 2017; Gottardi et al., 2020), Sevier thrust belt and Laramide deformation front (Yonkee and  
2388 Weil, 2015; Fitz-Díaz et al., 2018), and  $^{87}\text{Sr}/^{86}\text{Sr}_i$  isopleths (Armstrong 1988; Kistler and  
2389 Anderson, 1990; Miller et al., 2000; Valencia-Moreno et al., 2001). CAB locations, data, and  
2390 data sources presented in Table 1 and Supplementary File 2. Map projection: UTM, NAD 83  
2391 Zone 12N.



2392

2393 Fig. 2: A comparison between the A) North American Cordilleran Anatectic Belt (CAB) and the  
2394 B) Himalayan leucogranite belt, both shaded orange and shown at the same scale. Blue polygons  
2395 are metamorphic core complexes in the CAB and leucogranite bodies in the Himalaya (Whitney  
2396 et al., 2013; Kohn, 2014).

2397

2398 Fig. 3: A) Cordilleran Anatectic Belt (CAB) rocks (blue circles) are silica-rich ( $\text{SiO}_2 > 70$  wt. %) and peraluminous with aluminum saturation indices (ASI) of ca. 1.0-1.3. Silica-rich,  
2399 and peraluminous compositions can also be generated from originally metaluminous intrusive rocks  
2400 with protracted fractional crystallization or assimilation as represented by the Chemehuevi  
2401 Mountains plutonic suite, California (orange squares; John and Wooden, 1990) and the White  
2402 Creek batholith, Kootenay arc, British Columbia (red diamonds; Brandon and Lambert, 1993).  
2403 B.) A down-plunge cross-section view of the Chemehuevi Mountains plutonic suite shows zoned  
2404 or nested intrusive rocks with increasing ASI toward the center (modified from John, 1988; John  
2405 and Wooden, 1990), which is not observed in CAB intrusive suites. Data and data sources are  
2406 presented in Supplementary File 2.

2408

2409 Fig. 4: Pairs of unaltered and hydrothermally altered intrusive rocks from the southern U.S.  
2410 Cordillera that display elevated Rb/Sr and peraluminosity as a result of hydrothermal alteration,  
2411 ASI = aluminum saturation index. Cordilleran Anatectic Belt rocks (blue polygons) generally  
2412 have  $\text{ASI} < 1.3$ . Data and data sources are presented in Supplementary File 2.

2413

2414 Fig. 5. Cordilleran Anatectic Belt rocks (blue circles) generally plot as granite on a normative

2415 Ab–An–Or ternary diagram and overlap with metasedimentary melt compositions for water-  
2416 absent dehydration melting experiments (Patiño Douce and Beard, 1995; Patiño Douce and  
2417 Harris, 1998; Patiño Douce, 2005) rather than water-excess melting experiments (Conrad et al.,  
2418 1988; Patiño Douce and Harris, 1998). Data and data sources are presented in Supplementary  
2419 File 2.

2420

2421 Fig. 6: The majority of Cordilleran Anatectic Belt (CAB) rocks (blue circles) have compositions  
2422 consistent with peraluminous leucogranite melts produced by experimental melting of mica-rich  
2423 metasedimentary rocks (shaded blue) rather than amphibolite (black outline). CAB rock  
2424 compositions are also largely distinct from S-type granite and Cordilleran granite. The  
2425 Chemehuevi Mountains plutonic suite (orange squares; John and Wooden, 1990) and White  
2426 Creek batholith (red diamonds; Brandon and Lambert, 1993) are shown for comparison.  
2427 Compositional fields are from Patiño-Douce (1999). Data and data sources are presented in  
2428 Supplementary File 2.

2429

2430 Fig. 7. The North American Cordilleran Anatectic Belt (CAB) crosses many Proterozoic to  
2431 Archean basement provinces/terranes. The northern and central CAB overlaps with areas where  
2432 Proterozoic rocks are present in the Cordilleran passive margin sequence (Miogeocline), which  
2433 has been proposed as one possible protolith. Metasedimentary rocks from the Mesoproterozoic  
2434 Belt-Purcell Basin and Paleoproterozoic Pinal Basin have also been proposed as possible  
2435 protoliths. The inferred edge of North American basement is based on the position of the  
2436  $^{87}\text{Sr}/^{86}\text{Sr}_i = 0.706$  isopleth (Fig. 1). Map projection: UTM, NAD 83 Zone 12N.

2437

2438 Fig. 8. A histogram and kernel density estimate (red curve) of zircon saturation temperatures  
2439 (Watson and Harrison, 1983) for rocks in the Cordilleran Anatectic Belt (CAB). The uncertainty  
2440 of the average is based on the standard deviation ( $1\sigma$ ). Data and data sources are presented in  
2441 Supplementary File 2. A kernel density estimate (blue curve) shows the maximum (peak)  
2442 temperatures in migmatite within the CAB as reported by previous studies (Table 1).

2443  
2444 Fig. 9: A plot of age vs. latitude for crystallization ages of rocks in the Cordilleran Anatectic Belt  
2445 (CAB; green rectangles), rapid exhumation/cooling ages for the Cordilleran metamorphic core  
2446 complexes (blue squares), and timing for the onset of extension in the core complexes (red  
2447 circles) (Table 1). Most major core complexes are labelled for reference. Data and data sources  
2448 are presented in Supplementary Files 1 and 2.

2449  
2450 Fig. 10: A) Time-temperature and B) pressure-temperature (P-T) diagrams for the Ruby-East  
2451 Humboldt metamorphic core complex (modified from Henry et al., 2011) used to illustrate  
2452 periods of rapid cooling and near-isothermal decompression in the Cordilleran core complexes in  
2453 general. Rapid cooling is chiefly identified using thermochronology (AHe = apatite U-Th/He,  
2454 AFT = apatite fission track, ZFT = zircon fission track) whereas periods of near-isothermal  
2455 decompression are not well-resolved or recorded at all by thermochronometers and may have  
2456 occurred up to several 10s of Myr prior to rapid exhumation.

2457  
2458 Fig. 11: Melt reactions for metasedimentary protoliths showing solidus curves for water-present  
2459 melting (Stevens and Clemens, 1993), muscovite dehydration melting (Patiño Douce and Harris,  
2460 1998; P76 = Peto, 1976), biotite dehydration melting (Vielzeuf and Montel, 1994), and

2461 amphibole dehydration melting (Wyllie and Wolf, 1993). The range of calculated zircon  
2462 saturation temperatures (ZST) from the Cordilleran Anatectic Belt is shown in blue and  
2463 presented in Fig. 8.

2464  
2465 Fig. 12: A) Cordilleran Anatectic Belt (CAB) rocks (blue circles) plot along Rb/Sr vs. Sr trends  
2466 consistent with water-absent muscovite dehydration melting and fractional crystallization of  
2467 plagioclase. Black arrows show trends produced by melting experiments and red arrows show  
2468 trends expected from crystallization of the phase listed (modified from Inger and Harris, 1993).  
2469 B) Strongly positive ( $> 3$ ) Eu anomalies were suggested by Prince et al. (2001) to distinguish  
2470 water-excess melting. Feldspar-rich cumulate rocks may also have positive Eu anomalies, but  
2471 can be recognized by their low total REE (Rudnick, 1992). Data and data sources are presented  
2472 in Supplementary File 2.

2473  
2474 Fig. 13: An isobaric (5 kbar) temperature- $X_{H_2O}$  assemblage diagram for a quartz- and muscovite-  
2475 rich metasedimentary rock from the Pinal Schist that illustrates differences between water-  
2476 absent, water-deficient, and water-excess melting. Constructed using *Perple\_X* (Connolly,  
2477 2005). See text for modeling details. Average zircon saturation temperatures calculated for the  
2478 Cordilleran Anatectic Belt are shaded red (Fig. 8).

2479  
2480  
2481 Table 1:  
2482 Summary of details for locations in the North American Cordilleran Anatectic Belt. Data  
2483 Sources: 1 = Sevigny and Parrish (1993); 2 = Armstrong (1991); 3 = Crowley et al., 2001; 4 =

2484 Crowley et al., 2008); 5 = Norlander et al. (2002); 6 = Carr, 1992; 7 = Holk and Taylor (1997); 8  
2485 = Holk and Taylor (2000); 9 = Vanderhaeghe et al. (1999); 10 = Vanderhaeghe et al. (2003); 11  
2486 = Hinchey et al. (2006); 12 = Leclair et al. (1993); 13 = Brandon and Lambert (1993); 14 =  
2487 Brandon and Lambert (1994); 15 = Brandon and Smith (1994); 16 = Spear and Parrish (1996);  
2488 17 = Spear (2004); 18 = Gordon et al. (2008); 19 = Laberge and Pattinson (2007); 20 = Cubley  
2489 and Pattinson (2012); 21 = Cubley et al. (2013); 22 = Carlson et al. (1991); 23 = Hansen and  
2490 Goodge (1998); 24 = Kruckenberg et al. (2008); 25 = Doughty and Price (1999); 26 = Stevens et  
2491 al. (2015); 27 = Stevens et al. (2016); 28 = Whitehouse et al. (1992); 29 = Asmerom et al.  
2492 (1988); 30 = Guevara (2012); 31 = Foster (2007); 32 = Doughty and Chamberlain (2007); 33 =  
2493 Foster and Raza (2002); 34 = Gaschnig et al. (2010); 35 = Gaschnig et al. (2011); 36 = Foster et  
2494 al. (2001); 37 = King and Valley (2001); 38 = Wallace et al. (1992); 39 = Foster et al. (2010); 40  
2495 = Silverberg (1990); 41 = Vogl (2012); 42 = Lee and Marvin (1981); 43 = Miller et al. (1990);  
2496 44 = Wright and Wooden (1991); 45 = Wooden et al. (1999); 46 = McGrew and Snee (1994); 47  
2497 = Lee et al. (2003); 48 = Howard et al. (2011); 49 = Henry et al. (2011); 50 = Hallet and Spear  
2498 (2014); 51 = Hallet and Spear (2015); 52 = Barton (1987); 53 = Evan et al. (2015); 54 = Lee et  
2499 al. (2017); 55 = Lee and Christiansen (1983); 56 = King et al. (2004); 57 = Gotlieb et al. (2017);  
2500 58 = Miller et al. (1999); 59 = Fryxell (1988); 60 = Lund et al. (2014); 61 = Long and Soignard  
2501 (2016); 62 = Applegate et al. (1992); 63 = Holm and Dokka (1991); 64 = Mattinson et al. (2007);  
2502 65 = Sizemore et al. (2019); 66 = Lima et al. (2018); 67 = Mahood et al. (1996); 68 = Miller and  
2503 Wooden (1994); 69 = Bryant and Wooden (2008); 70 = Wong et al. (2011); 71 = DeWitt and  
2504 Reynolds (1990); 72 = Singleton et al. (2014); 73 = Isachsen et al. (1999); 74 = Prior et al.  
2505 (2016); 75 = Richard et al. (1990); 76 = Shaw and Gilbert (1990); 77 = Shafiqullah et al. (1980);  
2506 78 = Gottardi et al. (2018); 79 = Spencer et al. (2003); 80 = S. Scoggin (unpublished); 81 = Long

2507 et al. (1995); 82 = Creasey et al. (1977); 83 = J. Chapman (unpublished); 84 = Fornash et al.  
2508 (2013); 85 = Fayon et al. (2000); 86 = Terrien (2012); 87 = Peterman et al. (2014); 88 = Davis et  
2509 al. (2019); 89 = Ducea et al. (2020); 90 = G. Haxel (unpublished); 91 = Wright and Haxel  
2510 (1982); 92 = Gottardi et al. (2020); 93 = C. Pridmore (unpublished); 94 = Arnold (1986); 95 =  
2511 Goodwin and Haxel (1990); 96 = Anderson et al. (1980); 97 = Mallery et al. (2018); 98 = Wong  
2512 et al. (2010); 99 = Roldán-Quintana (1991); 100 = González-León et al. (2011); 101 = González-  
2513 Becuar et al. (2017); 102 = Wong and Gans (2008).  
2514